Entry Mechanism of Natural Killer Cell derived Granzyme B into Target Cells

Dissertation

submitted to the

Faculty of Chemistry and Chemical Biology

at the Technische Universität Dortmund, Germany

for the degree of

Doctor of Natural Sciences

Thesis by	Nora Bruning (born in Vechta)
Referees	Prof. Dr. Carsten Watzl Prof. Dr. Dr. Philipp Zimmer

Meiner Familie

Table of contents

Acknowledgements

First and foremost, I want to thank Prof. Dr. Carsten Watzl. I am sincerely grateful for the opportunity to continue this project in your group after my Master's thesis. Thank you for listening to my countless questions, your encouragement and scientific advice.

I also thank Prof. Dr. Dr. Philipp Zimmer for taking responsibility as referee of this thesis.

Moreover, I would like to thank Dr. Stefano Maffini and Dr. Rosemarie Marchan for being part of my thesis advisory committee and for all the helpful discussions and ideas.

Special thanks to all past and present members of the Watzl research group. You have accompanied me in good and difficult times over the last 5 years. I have learned a lot from you, both on a professional level and through quite 'interesting' discussions of private matters during lunch breaks – it was always fun!

Katharina Belgasmi	Luca Kröll	Michèle Saretzki
Vivian Bönnemann	Estefanía Martínez- Albert	Elena Schwendich
Peter Bröde	Sarah Metzler	Doris Teutsch
Silvia Capellino	Jens Niemann	Sina Trebing
Maren Claus	Martin Obholzer	Doris Urlaub
Anke Flegel	Lea Picard	Isabel Uhlenbrock
Leonie Fleige	Julian Pretel	Karolin Wieber
Defne Göcener	Sarah Recknagel	Sabine Wingert
Mia Juditzki	Mina Sandusky	Natalie Wolfsdorff
Nicole Klaschik		

Finally, I want to thank my family and friends. You have been my biggest supporters and made this time much more bearable. Thank you for your endless motivation, for always believing in me, having my back and celebrating even the smallest progress with me.

Abstract

During elimination of virally infected or malignant cells, NK cells release lytic granules. These contain perforin and granzyme B (GrzB), which synergistically trigger apoptosis of affected cells. However, despite intensive research, the mechanism by which GrzB traverses membrane barriers to gain access to the target cell cytosol is controversial. Two main entry models have been described: I) perforin pores in the plasma membrane (PM) act as passageways for GrzB to allow direct diffusion into the cytosol or II) target cells internalize GrzB via an endocytic mechanism followed by a release from endosomes. Yet, mutual exclusivity is not necessarily a given; both pathways could also support each other.

To investigate how GrzB enters target cells during NK cell-mediated cytotoxicity, we developed fluorescent localization reporters that can detect GrzB activity in living cells. We can localize these reporters at the PM, the endoplasmic reticulum (ER), or other intracellular compartments of target cells. Therefore, it becomes possible to assess the GrzB entry site over time using live cell imaging. Using the NK cell line NK92 or different human primary NK cells as effectors and HeLa cells as targets, we could observe a predominant GrzB activity at the PM of target cells; but low GrzB activity was also detected at the ER. This could indicate either a mutual supportive role of both pathways or diffusion of GrzB from the PM to the ER. However, we did not observe GrzB activity at mitochondria arguing against general diffusion of GrzB. By reducing the amount of active perforin with concanamycin A (CMA), we were able to show that the preferential entry through PM pores is independent of the available amount of perforin. However, in the absence of perforin, no GrzB activity was detectable in target cells, confirming the essential role of perforin for GrzB to enter target cells. Taken together, our results demonstrate that during NK cell-mediated killing GrzB enters HeLa directly via the PM. Additionally, cell death occurs before GrzB activity reaches intracellular compartments demonstrating that critical GrzB substrates are in vicinity of the PM. However, we found differences between target cells. K562 were almost exclusively killed without GrzB, while we found rare events in MDA-MB #468 cells where GrzB was predominantly delivered via the endocytic pathway, which may be enhanced by altering membrane tension.

Zusammenfassung

Bei der Eliminierung von virusinfizierten oder bösartigen Zellen setzen NK-Zellen lytische Granula frei. Diese enthalten Perforin und GrzB, die synergistisch die Apoptose der betroffenen Zellen auslösen. Trotz intensiver Forschung ist der Mechanismus umstritten, über den GrzB die Membranbarrieren überwindet, um in das Zytosol der Zielzellen zu gelangen. Zwei Haupteintrittsmodelle sind beschrieben worden: I) Perforin Poren in der PM fungieren als Durchgang für GrzB, um eine direkte Diffusion in das Zytosol zu ermöglichen, oder II) Zielzellen internalisieren GrzB über einen endozytischen Mechanismus, gefolgt von einer Freisetzung aus Endosomen. Die gegenseitige Exklusivität ist jedoch nicht unbedingt gegeben; beide Wege könnten sich auch gegenseitig unterstützen.

Um zu untersuchen, wie GrzB während der NK-Zell-vermittelten Zytotoxizität in die Zielzellen gelangt, haben wir fluoreszente Lokalisierungsreporter entwickelt, die die Aktivität von GrzB in lebenden Zellen nachweisen können. Wir können diese Reporter an der PM, dem ER oder anderen intrazellulären Kompartimenten der Zielzellen lokalisieren. Daher ist es möglich, die GrzB-Eintrittsstelle über die Zeit mittels Bildgebung lebender Zellen zu beurteilen. Bei Verwendung der NK-Zelllinie NK92 oder verschiedener humaner primärer NK-Zellen als Effektorzellen und HeLa-Zellen als Zielzellen konnten wir eine hauptsächliche GrzB-Aktivität an der PM der Zielzellen beobachten; aber eine geringe GrzB-Aktivität wurde auch am ER festgestellt. Dies könnte entweder auf eine sich gegenseitig unterstützende Rolle beider Wege oder auf eine Diffusion von GrzB von der PM zum ER hindeuten. Wir haben jedoch keine GrzB-Aktivität an Mitochondrien beobachtet, was gegen eine allgemeine Diffusion von GrzB spricht. Indem wir die Menge an aktivem Perforin mit CMA reduzierten, konnten wir außerdem zeigen, dass der bevorzugte Eintritt durch die PM-Poren unabhängig von der verfügbaren Perforinmenge ist. In Abwesenheit von Perforin war jedoch keine GrzB-Aktivität nachweisbar, was die Bedeutung von Perforin für den Eintritt von GrzB in die Zielzellen bestätigt. Zusammengefasst zeigen unsere Ergebnisse, dass GrzB während der NK-Zell-vermittelten Abtötung direkt über die PM in HeLa eindringt. Zudem tritt der Zelltod ein, bevor die GrzB-Aktivität intrazelluläre Kompartimente erreicht, was zeigt, dass sich kritische GrzB-Substrate in der Nähe der PM befinden. Allerdings fanden wir Unterschiede zwischen Zielzellen. K562-Zellen wurden fast ausschließlich ohne GrzB abgetötet, während wir bei MDA-MB #468-Zellen seltene Ereignisse feststellten, bei denen GrzB überwiegend über Endozytose übertragen wurde, was eventuell durch Änderung der Membranspannung erhöht werden kann.

1. Introduction

The continuous protection of our body against foreign or self-harms is ensured by a variety of cells and modulatory components of the immune systems' innate and adaptive branches (Alam, 1998). One of these is the natural killer (NK) cell, which was discovered in 1975 (Kiessling et al., 1975).

1.1 Natural killer (NK) cells

The lymphoid NK cell is categorized into the innate branch of the immune system as it lacks a rearranged antigen receptor, although developing in the bone marrow from the same progenitor cell as T and B cells (Colucci et al., 2003, Watzl, 2014). NK cells circulate in peripheral blood, but can also reside in lymphoid tissues such as spleen, bone marrow and lymph nodes or non-lymphoid tissues like liver and lung (Westermann and Pabst, 1992). Within the peripheral blood, most NK cells can be characterized as cytotoxic, $CD16^{+}$ $CD56^{dim}$, whereas the remaining are the less mature, mainly cytokine-producing $CD16^{-}$ $CD56^{bright}$ NK cells (Melsen et al., 2016, Vivier et al., 2008). Yet, both subgroups can exert either of the two main effector functions – cytokine production and cytotoxicity – depending on stimulus (Melsen et al., 2016, Fauriat et al., 2010, Beziat et al., 2011).

NK cells are mainly involved in the early phase of clearing viral infections and fighting cancer development (Jost and Altfeld, 2013, Vivier et al., 2008, Watzl, 2014). During such, they are regulated by specific cytokines like (IL)-12, -15, -18 and type I interferons (IFNs), generated by other immune cells e.g. dendritic cells. In response, NK cells proliferate, produce cytokines and become primed to increase their responsiveness for activation. As cytokine producers, NK cells themselves influence other immune cells by secreting e.g. granulocyte-macrophage colony-stimulating factor (GM-CSF), tumor necrosis factor (TNF)-α and IFN-γ (Vivier et al., 2008, Walzer et al., 2005). Moreover, activation of NK cells is a prerequisite for their cytotoxic effector function. In general, NK cell activation is regulated by tightly balanced signals from germline encoded receptors of activating and inhibiting nature (Watzl and Long, 2010, Watzl, 2003) (figure 1). Usually, when NK cells engage healthy cells, they receive inhibiting signals via the interaction of NK cell inhibitory receptors with MHC class I ligands. However, stressors like transformations or infections can cause the affected cells to reduce or loose MHC class I. The resulting loss of the inhibitory signal, which would usually suppress signals from activating receptors, shifts the balance and

enables NK cells to get activated, known as missing-self recognition (Ljunggren and Kärre, 1990, Kärre et al., 1986, Watzl, 2003). Conversely, stressed cells can also exhibit an upregulation of activating ligands (induced-self theory). The now dominant activation signals outweigh the inhibitory signaling, which also leads to the activation of NK cells (Watzl, 2003).

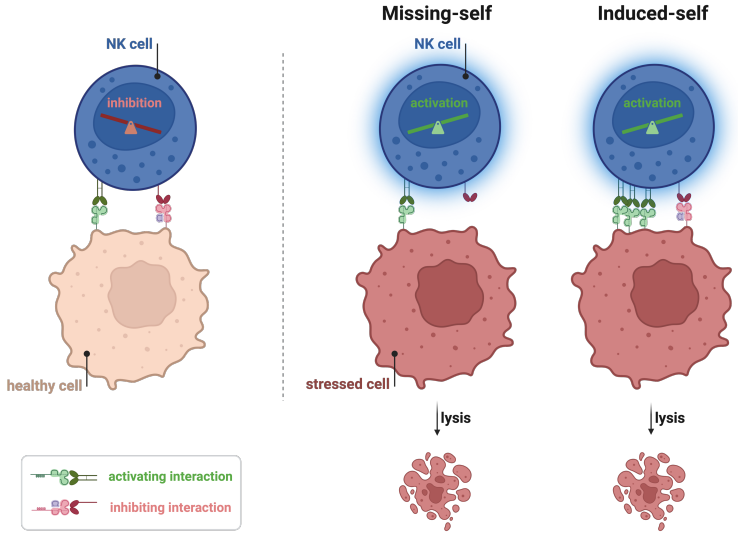

Figure 1: NK cell activation is regulated by a balance between inhibiting and activating signaling. Healthy cells are protected from NK cell lysis by the interaction of MHC class I with NK cell inhibiting receptors, which block possible activating signaling. However, infected or malignant cells downregulate MHC class I (missing-self) or increase activating ligand expression (induced-self), which tilt the balance towards NK cell activation (figure based on (Watzl, 2003, Raulet and Vance, 2006)).

As a precautionary measure to safely trigger activation, two different activating receptor types must be engaged by a potential target cell. However, this does not apply to cytokine-primed NK cells, which allow activation by a single activating receptor type and to the antibody dependent cellular cytotoxicity (ADCC)-mediator CD16, which can activate NK cells on its own (Watzl, 2014). Either way, once successfully activated, NK cells can proceed with their cytotoxic mechanisms.

1.2 NK cell cytotoxicity

NK cells are equipped with a diverse set of weapons and can choose between two main cytotoxic mechanisms to induce target cell death – death receptor (DR)-mediated or lytic granule-mediated cytotoxicity (figure 2). The former is triggered by NK cells expressing DR ligands like TNF, TRAIL and FasL (CD95L) on their surface which interact with their respective receptors TNF-R1/-R2, TRAIL-R1/-R2 and Fas (CD95) on target cells (Prager and Watzl, 2019). After receptor activation, the adaptor protein Fas-associated death domain (FADD) recruits procaspase-8 and -10 to form a death-inducing signaling complex (DISC). In the following, proteolytically activated Caspase-8 and -10 cleave various proteins like other caspases or BID, resulting in apoptotic

death of the target cell (Peter and Krammer, 2003, Prager and Watzl, 2019). The induction of death by DR is a rather slow process with a time resolution of 1 to 2 hours (Li et al., 2014, Prager et al., 2019, Prager and Watzl, 2019). Furthermore, the DR-mediated cytotoxicity has been demonstrated to emerge in two scenarios: I) In the context of serial killing NK cells (Prager et al., 2019) – a process that describes the sequential killing of multiple targets by a single NK cell (Bhat and Watzl, 2007). During such, DRs activation was predominantly found in late and final killing events. II) NK cells, whose lytic granule-mediated cytotoxicity was impaired by depleting the key mediator perforin, only killed once and via DRs (Prager et al., 2019). When not compromised, NK cells mainly use their much faster killing mechanism during early killing events – exocytosis of lytic granules (Prager et al., 2019). Lytic granules combine features of lysosomes and secretory granules and provide a dense core in which proteins such as granulysin, perforin and granzymes are safely stored (Burkhardt et al., 1990, Burkhardt et al., 1989, Groscurth et al., 1987). These proteins are responsible for the killing during lytic granule-mediated cytotoxicity (Prager and Watzl, 2019). NK cells secrete about 10 % of their lytic granules repertoire per kill, with just 2 to 4 lytic granules sufficing to kill the target cell which underlines the efficiency of this pathway (Gwalani and Orange, 2018). In the following chapters, we will focus on the lytic granule-mediated cytotoxicity and, particularly, on perforin and granzyme B (GrzB).

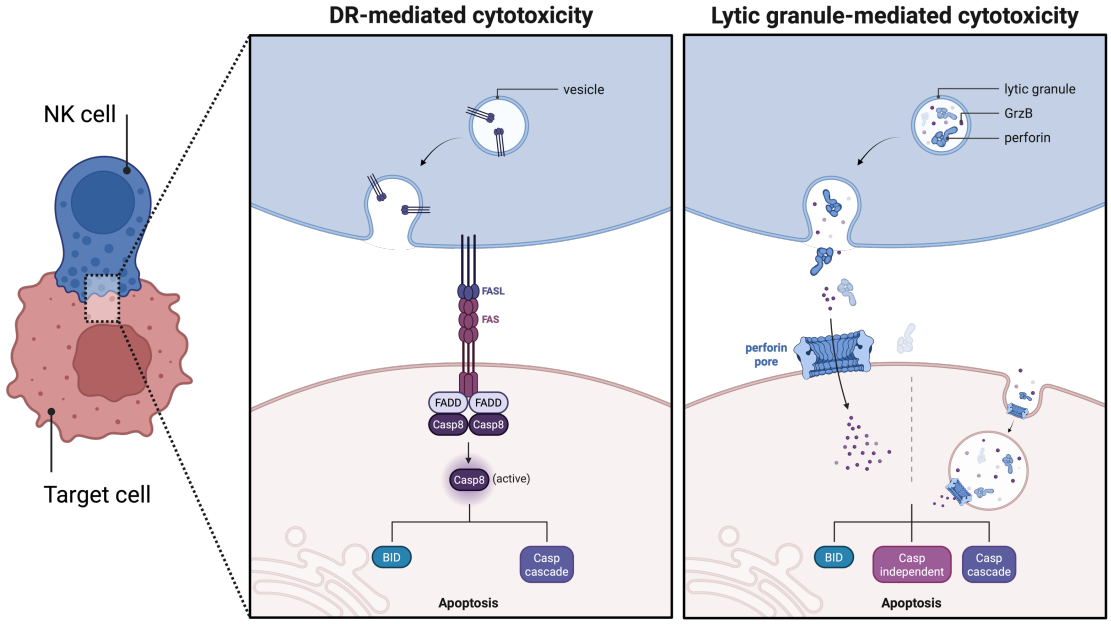

Figure 2: Cytotoxic mechanisms of NK cells. NK cells engage DR or secrete lytic granules to induce target cell death. DR-mediated cytotoxicity: DR ligands on the NK cell surface interact with DR on target cells inducing apoptosis-signaling pathways. For simplicity, only the FasL/Fas interaction and Caspase-8 (Casp8) are shown (left). Lytic-granule mediated cytotoxicity: Lytic granules containing perforin and GrzB are secreted. Perforin forms pores allowing GrzB to enter the target cells' cytosol. GrzB induces apoptosis e.g. caspase-dependent, -independent or by cleaving BID (right). (Illustration simplified and based on Prager and Watzl, 2019, perforin pore structure is according to Law et al., 2010).

1.2.1 Function of perforin and GrzB

Perforin

Perforin belongs to the membrane attack complex/perforin/cholesterol-dependent cytolysin (MACPF/CDC) superfamily (Reboul et al., 2016) and its crystal structure reveals 3 domains: a N-terminal conserved MACPF domain, an epidermal growth factor (EGF)-like domain and a C-terminal C2 domain (Law et al., 2010, Ivanova et al., 2022). Perforins' cytotoxic ability relies on pore formation in a pH and Ca^{2+}-dependent manner (Voskoboinik et al., 2005, Praper et al., 2010). In the presence of Ca^{2+}, the C2 domains of perforin monomers bind to membranes (Voskoboinik et al., 2005), which is not affected by pH (Praper et al., 2010, Hodel et al., 2025). Perforin monomers start to oligomerize and form short prepores (Leung et al., 2017). While not yet inserted, conformational changes within the MACPF domain result in β-hairpins inserting into the membrane (Ivanova et al., 2022, Law et al., 2010, Leung et al., 2017). This is presumably due to exposure to neutral pH which may allow the formation of stabilizing hydrogen bonds (Hodel et al., 2025). Following insertion, which transits the prepore to a pore state, other oligomer assemblies are recruited to form large, open arc-shaped or closed ring-like structures (Leung et al., 2017, Praper et al., 2011). The mature pore contains a transmembrane β-barrel motif with a diameter of 10 – 20 nm (around 19 – 24 monomers), which would allow other molecules or proteins, like granzymes, to traverse membrane barriers (Law et al., 2010, Ivanova et al., 2022, Leung et al., 2017, Praper et al., 2011).

Granzyme B

The human NK cells' repertoire of cytotoxic weapons comprises a group of 5 different granzyme (Grz) variants – GrzA, B, H, K and M – with most knowledge focusing on GrzA and B. As serine proteases, Grz mediate their cytotoxic ability by proteolytically cleaving a variety of proteins (Prager and Watzl, 2019). Here, we focus on GrzB.

GrzBs' ideal tetrapeptide recognition motif has been demonstrated to be IEPD (positions P4 – P1 upstream of cleavage site). While amino acids in positions P4 – P2 may deviate, GrzB hydrolyzes peptide bonds strictly after an aspartic acid residue in P1, a preference also known for caspases (Thornberry et al., 1997). Variations of this tetrapeptide motif are present e.g. in procaspases-3, -7, -8 and -10 (Fischer et al., 2003, Earnshaw et al., 1999, Thornberry et al., 1997), marking them as potential targets. GrzB has been shown to directly cleave these procaspases, hence initiates

caspase-dependent apoptosis (Andrade et al., 1998, Adrain et al., 2005). Besides, GrzB can even trigger apoptotic death independently from activation of initiator and executioner caspases by directly cleaving their substrates (Andrade et al., 1998). These include proteins which are involved in the DNA damage pathway, e.g. NuMa, DNA-PKcs, PARP-1, or are important in the pro-apoptotic mitochondrial pathway like BID (Andrade et al., 1998, Chowdhury and Lieberman, 2008, Waterhouse et al., 2005, Sutton et al., 2000).

1.2.2 Biogenesis and storage of perforin and GrzB

Given the cytolytic activities of perforin and granzymes, NK cells are forced to establish safety measures to prevent self-induced damage, especially during perforin/Grz synthesis and sorting to lytic granules. Protection against perforin might involve its expression as an inactive precursor (Prager and Watzl, 2019). In this inactive version the membrane binding C2 domain contains a short sequence at its C-terminal end. This short sequence is modified with a N-linked glycosylation which supposedly hinders membrane binding when perforin traffics through endoplasmic reticulum (ER) and Golgi network (Uellner et al., 1997, House et al., 2017). Perforin is transferred from the Golgi network to lytic granules, which decisively involves lysosome-associated membrane protein 1, LAMP1 (CD107a) (Krzewski et al., 2013). During transfer, perforin might also be bound to and kept inactive by the ER chaperone calreticulin (Fraser et al., 1998, Fraser et al., 2000, Andrin et al., 1998, Prager and Watzl, 2019). Inside lytic granules, perforin is converted into its shorter, mature version (Uellner et al., 1997). Proteolytic cleavage of inactive perforin has been shown to be mediated by cathepsin L, which, however, might not be exclusively responsible for the cleavage (House et al., 2017, Konjar et al., 2010).

GrzB is also produced as an inactive precursor (zymogen) (figure 3). In its pre-pro form, GrzB is N-terminally linked to an inhibitory dipeptide and a terminal signal peptide for the ER, the latter being removed upon translation into the ER lumen (Jenne and Tschopp, 1988, Prager and Watzl, 2019). Subsequently, the pro-GrzB form arrives at the cis-Golgi network. While traversing the Golgi, pro-GrzB acquires a mannose-6-phospate (M6P) modification, which enables further transport to lytic granules via the M6P-receptor (MPR) pathway (Griffiths and Isaaz, 1993). Whether M6P is removed in the acidic environment of lytic granules upon arrival or remains bound to GrzB is uncertain (Prager and Watzl, 2019). Finally, cathepsins, like cathepsin H and C,

separate GrzB from its inhibitory dipeptide and render GrzB active (D'Angelo et al., 2010).

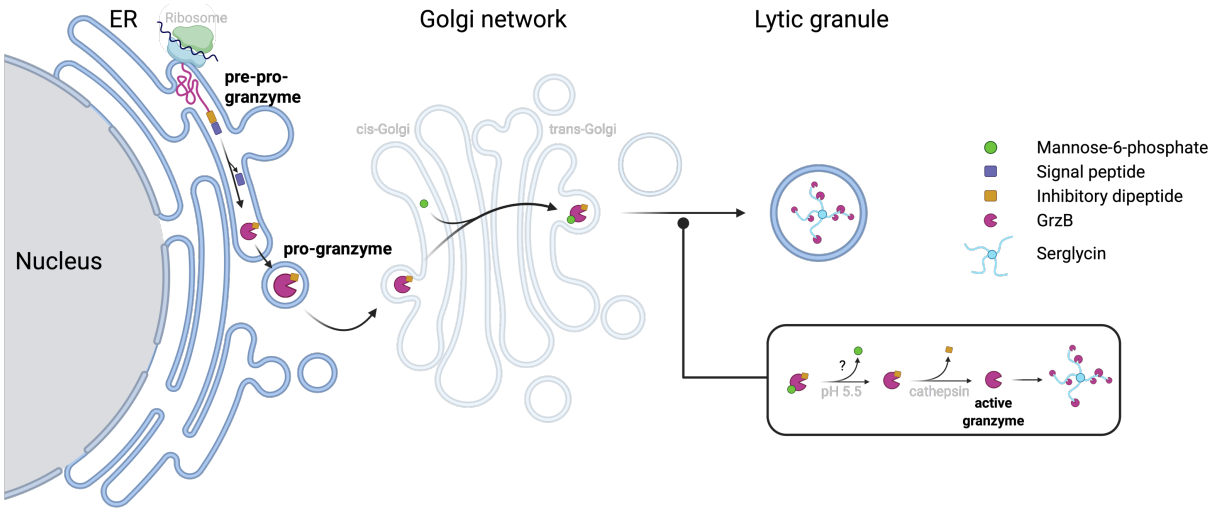

Figure 3: Biogenesis of GrzB. Granzyme B undergoes various processing steps to reach its active form. First, GrzB is translated as a nascent pre-pro-enzyme, containing an inhibitory dipeptide and a signal peptide, the latter of which is cleaved inside the ER. In its still inactive pro-form, GrzB traverses the Golgi network. The acquisition of a mannose-6-phosphate (M6P) modification enables sorting to lytic granules. Upon arrival, M6P may be removed by the low pH. Moreover, cathepsins remove the inhibitory dipeptide, hence activating GrzB. To avoid self-directed damage, the large proteoglycan serglycin scavenges GrzB into a complex. (Illustration modified according to Prager and Watzl, 2019).

The storage of highly cytotoxic, active cargo also requires safety precautions. The lytic granules' acidic environment of pH 5.5 (Burkhardt et al., 1990) interferes with perforin pore formation (Praper et al., 2010, Hodel et al., 2025). Additionally, a large chondroitin sulfate proteoglycan, named serglycin, plays a crucial role in storing perforin and granzymes (Masson et al., 1990, Sutton et al., 2016, Grujic et al., 2005). It is suggested that the negatively charged sidechains of serglycin scavenge the cationic surface of GrzB and form a tight complex in low pH environments (Raja et al., 2002). Since neutralizing the pH within lytic granules has been shown to induce degradation of mature perforin, presumably mediated by GrzB or cathepsin L, proteases might act as a backup protection mechanism against perforin (Kataoka et al., 1997, Domagala et al., 2025).

1.2.3 Release of perforin and GrzB – degranulation

Perforin and GrzB are released during the directed exocytosis of lytic granules (degranulation) into a tightly sealed cleft between NK cells and target cells, commonly referred to as immune synapse (IS). To generate this immune synapse, NK cells progress through a multitude of sequential steps, which can be categorized into three

main stages – initiation/recognition, effector and termination stage (Orange, 2008, Mace et al., 2014).

Following an initial contact, the NK cell adheres to its potential target cell via different receptors. The engagement of activating receptors induces initial activating signals, which activate the integrin LFA-1 to enhance adhesion by reorganizing the NK cells' actin cytoskeleton. This reorganization establishes the firm connection between NK cell and target cell and thus initiates the formation of an immune synapse (Orange, 2008, Bryceson et al., 2009, Mace et al., 2009, Mace et al., 2010, Mace et al., 2014). Early in this initiation/recognition stage, the microtubule motor protein complex dynein-dynactin transports lytic granules in minus-end direction towards the microtubule organizing center (MTOC) at which they converge (Mentlik et al., 2010, James et al., 2013). If activating signals dominate over inhibitory ones, the NK cell is successfully activated and the commitment towards killing (effector stage) induces further structural changes regarding the filamentous actin (F-actin) network (Orange, 2008, Mace et al., 2014). F-actin has been shown to accumulate throughout the now mature IS (Rak et al., 2011). Subsequently, the converged lytic granules and MTOC polarize towards the plasma membrane (PM) region facing the IS (Mace et al., 2014) (figure 4).

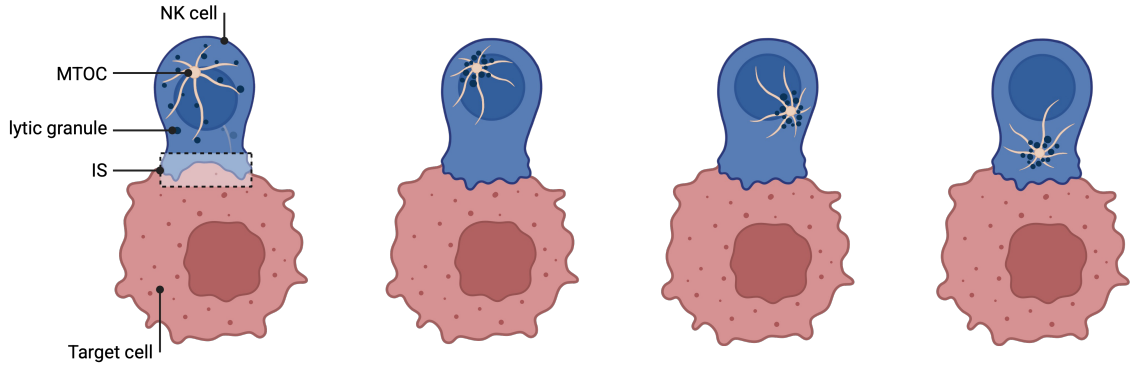

Figure 4: Lytic granule movement during degranulation. After the initial contact between NK and target cell, lytic granules are transported along microtubules towards the MTOC at which they converge. Subsequently, lytic granules and MTOC polarize towards IS (simplified illustration based on Orange, 2008, Mace et al., 2014)

Driven by Myosin IIA (Sanborn et al., 2009), lytic granules navigate through channels in the F-actin mesh to reach the PM (Rak et al., 2011). Upon arrival, lytic granules undergo docking, priming and fusion with the PM, involving MUNC13-4, Rab27a and SNAREs (Mace et al., 2014). Following fusion, Serglycin, GrzB as well as perforin are secreted into the synaptic cleft (Metkar et al., 2002, Raja et al., 2005, Masson et al., 1990). Upon exposure to the pH neutral environment and increased Ca^{2+} concentration within the IS, perforin exerts its pore forming function (as described above), while GrzB

is released from serglycin (Raja et al., 2005) and enters target cells with the help of perforin to induce target cell death (chapter 1.3).

In the following, the NK cell cytotoxicity enters the final/termination stage (Mace et al., 2014). After successful target cell death, the NK cell is able to disengage from the target cell, presumably driven by downregulation of receptors/ligands on NK and target cell sides (Anft et al., 2020) which might disturb the maintenance of the IS (Netter et al., 2017). Henceforth, the NK cell can progress to a new target and might even perform serial killing of several targets, but this is only mediated by the minority of NK cells (Bhat and Watzl, 2007, Prager et al., 2019).

1.2.4 Protection against perforin and GrzB during degranulation

Although perforin and GrzB are present in the IS, killing occurs unidirectionally (Kupfer et al., 1986, Lopez et al., 2013a). Several protection mechanisms against perforin were proposed which may contribute to prevent the self-inflicted damage of NK cells. CD107a, which is co-residing in lytic granule membranes, is exposed to the cell surface alongside perforin and GrzB secretion (Alter et al., 2004, Bryceson et al., 2005). Manipulating CD107a levels – i.e. deletion/reduction (NK cells) or overexpression (target cells) – have been shown to increase NK cell deaths or protect target cells during killing, respectively. In addition, perforin was less capable of binding the cell membrane in the presence of CD107a, which presumably hinders perforin from inserting its C2 domain into the PM (Cohnen et al., 2013). During degranulation, the protease cathepsin reaches the cell surface and might mediate the inactivation of perforin (Balaji et al., 2002), however, to a questionable extent (Baran et al., 2006). Moreover, other studies rather emphasized the role of highly ordered, dense lipid membranes accompanied by negative charge, which are brought to the IS upon degranulation as a protective shield (Li and Orange, 2021, Rudd-Schmidt et al., 2019a). Recently, the mechanical softness of cytotoxic T lymphocytes (CTLs) has been proposed as another possibility to avoid perforin-mediated self-lysis (Zhou et al., 2024). Complementing these protection mechanisms, leaked or misdirected GrzB can be specifically and irreversibly inactivated by Serpin B9 (or proteinase inhibitor 9), a cytosolic protein expressed by NK cells (Sun et al., 1996, Bird et al., 1998, Ida et al., 2003, Hirst et al., 2003).

1.3 Perforin and GrzB synergy – entry mechanisms of GrzB into target cells

Upon secretion, the formation of a perforin pore in the target cell PM is capable to induce necrotic death on its own, however, target cells also die by apoptosis, e.g. due to the combined action of perforin and GrzB (Voskoboinik et al., 2006, Backes et al., 2018). As outlined before (chapter 1.2.1), GrzB induces target cell apoptosis by proteolytically cleaving key proteins within the target cell. Hence, GrzB must reach the target cell cytosol. Over the decades, many different hypotheses on GrzB delivery mechanisms were postulated and highly discussed but mainly toggled between two models – plasma membrane (PM) pores and endocytic uptake (Trapani and Smyth, 2002, Voskoboinik et al., 2015, Prager and Watzl, 2019, Spicer et al., 2022).

Within the PM pore model, perforin pores are described as passageways for Grz to directly enter the target cell cytosol (Froelich et al., 1996, Trapani et al., 1998) (figure 5, left). The exclusivity of this model was challenged quickly by an early, endocytic uptake model: Using isolated GrzB (fluorescently labeled or unlabeled), GrzB uptake by target cells has been shown to occur independent of perforin but apoptosis induction required its presence (Froelich et al., 1996, Shi et al., 1997, Pinkoski et al., 1998). Hence, perforin was suggested to release endocytosed GrzB from endosomal vesicles, which was termed “facilitated access” (Froelich et al., 1996, Trapani et al., 1998). Additionally, a delivery of small proteins across PM pores was observed only at high concentrations of isolated perforin (Browne et al., 1999). On this basis, a coordinated link between PM pores and endocytosis/facilitated access (or endosomolysis) was proposed which could depend on available perforin concentration during early and late degranulation events (dose-dependent hypothesis). Accordingly, high perforin concentrations might favor PM pore delivery while endocytosis of GrzB would rather be enabled at sublytic perforin concentrations, respectively (Browne et al., 1999) – a concentration which only induces minimal lytic death on its own (Browne et al., 1999, Keefe et al., 2005). However, the release of endocytosed GrzB into the cytosol was shown to require the prior simultaneous addition of perforin (Shi et al., 2005, Keefe et al., 2005). In the following, a revised endocytic uptake model was established (Keefe et al., 2005, Thiery et al., 2010, Thiery et al., 2011) (figure 5, right): In the presence of sublytic perforin concentration and during CTL attack, a transient Ca^{2+} influx was observed, presumably enabled by small perforin pores. Driven by this influx, target cells respond with a membrane repair program to avoid being osmotically lysed by perforin (Keefe et al., 2005). While resealing these lesions, Perforin and GrzB are internalized via clathrin-

and dynamin-dependent endocytosis (Thiery et al., 2010). Thereupon, GrzB and perforin accumulate in large EEA1^{+} endosomes (gigantosomes) (Thiery et al., 2010, Thiery et al., 2011, Keefe et al., 2005) from which GrzB is gradually released, presumably enabled by perforin pore-mediated lysis of the gigantosome (Thiery et al., 2011).

Although the largest doubt regarding the PM pore model was related to the inability to deliver small dyes such as propidium iodide (PI) (Metkar et al., 2002, Keefe et al., 2005, Lopez et al., 2013b, Voskoboinik et al., 2015), a PI influx directly at the contact site between CTL or NK cell and target cell has been demonstrated (Lopez et al., 2013a, Lopez et al., 2013b). In that regard, it has been shown that although HeLa cells resealed their membrane within 80 seconds after NK cell contact, a small dose of GrzB sufficing in apoptosis induction reached the cell cytosol within this time frame. This provided support for the PM pore model in a physiologically relevant setting (Lopez et al., 2013b). Moreover, the PM pore model was strengthened by other studies showing that pores are large enough to enable GrzB transfer (Kurschus et al., 2008, Law et al., 2010, Stewart et al., 2014, Ivanova et al., 2022). In addition, arc-shaped channels were suggested to mediate GrzB delivery across the PM while closed, ring-shaped pores trigger the membrane repair (Metkar et al., 2015).

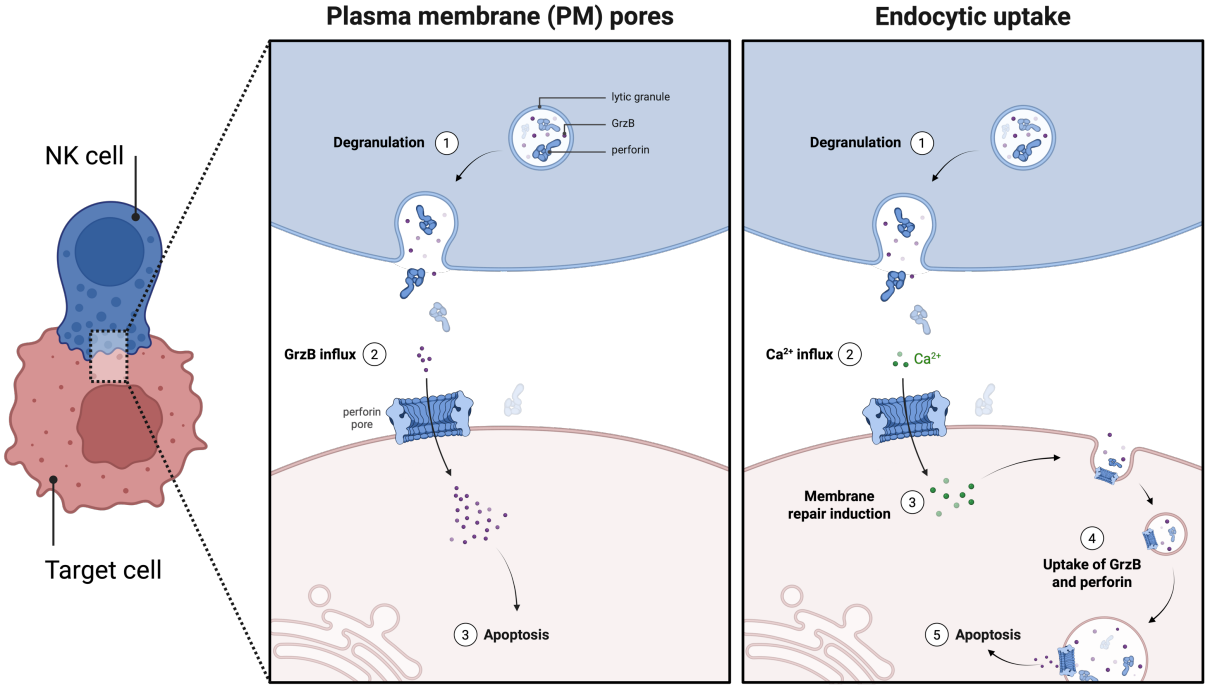

Figure 5: Proposed GrzB uptake mechanisms into target cells. After secretion into the immune synapse, GrzB and perforin synergistically induce target cell death. The proposed two main mechanisms of GrzB delivery into the target cell either describe the direct passaging of GrzB via perforin PM pores (modified according to Trapani and Smyth, 2002) (left) or a multistep endocytic uptake of perforin and GrzB by a perforin pore-triggered membrane repair mechanism (modified according to Thiery et al., 2011) (right).

Some alternative/extended mechanisms regarding endocytic uptake have been proposed along the way. A GrzB-receptor was considered to be a contributing factor to induce endocytic uptake (Pinkoski et al., 1998). Given GrzBs' M6P modification during trafficking to lytic granules (Griffiths and Isaaz, 1993), a potential role of the cation-independent (CI) MPR on target cells was described (Motyka et al., 2000). Target cells overexpressing CI MPR showed higher susceptibility to GrzB induced apoptosis and blocking CI MPR – GrzB interaction impaired GrzB uptake (Motyka et al., 2000, Veugelers et al., 2004). Yet, GrzB was still taken up by receptor negative target cells or target cells whose underlying dynamin-dependent endocytic machinery was inhibited (Trapani et al., 2003, Dressel et al., 2004, Veugelers et al., 2004). Hence, other forms of endocytosis, e.g. pinocytosis, were emphasized in addition to receptor-mediated entry (Trapani et al., 2003). Moreover, instead of being taken up as a free protein, GrzB endocytic uptake was thought to occur while in complex with serglycin (Metkar et al., 2002, Galvin et al., 1999, Veugelers et al., 2004). However, upon showing that GrzB is not taken up while in complex with serglycin (Raja et al., 2005), it was rather believed that GrzB is released from serglycin by binding to proteoglycans on target cells depending on charge and subsequently endocytosed (Bird et al., 2005, Raja et al., 2005). In that regard, a possible role of heparan sulfate proteoglycans was proposed (Kurschus et al., 2005, Shi et al., 2005).

Although the PM pore model is currently the popular model for GrzB to gain access to the target cell cytosol (Nüssing et al., 2022, Spicer et al., 2022, Lopez et al., 2013b) it does not confirm its exclusivity (Prager and Watzl, 2019). Moreover, most research on GrzB delivery was conducted using isolated proteins and non-physiological conditions, which has been criticized (Catalfamo and Henkart, 2003, Voskoboinik et al., 2015). Few exceptions also used effector cells for target cell killing and visualized GrzB uptake either by using e.g. I) an NK cell line modified to express EGFP-labeled GrzB (Thiery et al., 2011), II) an NK cell line in combination with an exogenously added larger variant of GrzB (Kurschus et al., 2008) or III) indirectly by PI influx during live cell imaging of human and mice NK or CTLs with HeLa target cells (Lopez et al., 2013b).

1.4 Fluorescent localization reporter (FLR)

Previously, GrzB activity inside living cells was analyzed using cleavable sensors. These sensors covered a broad range of techniques like fluorescence quenching (Packard et al., 2007), Förster resonance energy transfer (FRET) (Choi and Mitchison, 2013, Zhu et al., 2016), cleavage inducible luminescence (Li et al., 2014, Vrazo et al.,

2015) or fluorescence (Bednar et al., 2023) and fluorescence redistribution (Liesche et al., 2018, Prager et al., 2019, Bönnemann, 2023, Bruning et al., 2023), to name a few. Among these, fluorescent localization reporters (FLRs) were advantageous for the simultaneous comparison of GrzB vs. other protease activities within single living target cells (Liesche et al., 2018, Prager et al., 2019, Bönnemann, 2023). Initially, FLRs were developed to determine the spatial Caspase-8 activity inside single living target cells after triggering apoptosis (Beaudouin et al., 2013). They offer a simple concept: The overall assembly of FLRs comprises 3 building blocks with (I) a localization domain which connects via (II) a linking sequence to (III) a fluorescent protein (figure 6). Importantly, the linker contains a proteolytic target enabling protease specific cleavage.

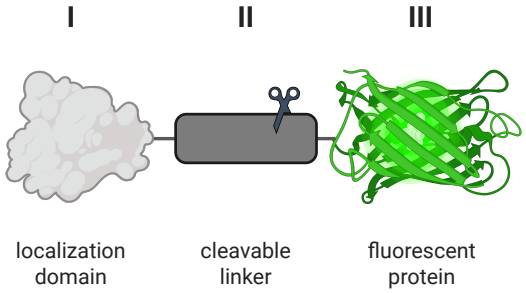

Figure 6: Assembly of a fluorescent localization reporter (FLR). FLRs consist of a localization domain directing the construct to a specific organelle or site within cells. The protease specific cleavable linker connects the localization domain with a fluorescent protein (Beaudouin et al., 2013).

The function of FLRs is also straightforward. While intact, the localization domain binds the FLR to a specific site or organelle in the target cell, resulting in a locally confined fluorescent signal. However, protease-mediated cleavage of the linker separates fluorescent protein and localization domain. Once set free, the fluorescent protein distributes visibly and quantifiably within the cell until reaching an equilibrium (Beaudouin et al., 2013, Liesche et al., 2018).

Until now, nuclear export signaling (NES) localization domain containing FLRs have provided valuable insights into the cytotoxic mechanism of NK cells (Liesche et al., 2018, Prager et al., 2019, Bönnemann, 2023). When comparing the activities of GrzB and Caspase-8 (as proxy for DR killing), serial killing NK cells preferably utilize GrzB for early but engage DRs during last kills (Prager et al., 2019). Additionally, this FLR construct also provided insights into cytolytic functions of ammonia treated NK cells, which demonstrated a reduced GrzB but upregulated DR killing compared to control NK cells (Domagala et al., 2025). Moreover, FLRs adapted to distinguish GrzB from GrzA-, K-, M- or H-mediated deaths underlined the dominant role of GrzB over other

granzymes in NK cells (Bönnemann, 2023). However, the application of FLRs is not restricted to NK cell research and has already been extended to analyze cytotoxic mechanisms of other immune cells. ILC3 mostly killed via death receptors (Siegler et al., 2022), while γδ T cells killed via GrzB or death receptors (Sandoz et al., 2023).

Since the FLR system can be modified in any way, it is a powerful tool to analyze protease activities offering versatile insights. Changing the localization domain can provide information about spatial activities, while modifying the linker is useful to analyze other proteases. Moreover, FLRs also report on the kinetics of protease-mediated deaths. As mentioned above, not just one but two different proteases (or the same protease but spatially at different sites) can be analyzed and compared simultaneously within a single living cell using two different fluorescent proteins (Beaudouin et al., 2013, Liesche et al., 2018). However, handling two FLR constructs could be at the expense of equal FLR expression levels within a single cell. Therefore, comparability is ensured by a viral *Thosea asigna* (T2A) sequence, which acts as a connective bridge between two individual FLRs at DNA level and mediates a self-induced co-translational separation (Daniels et al., 2014) (figure 7).

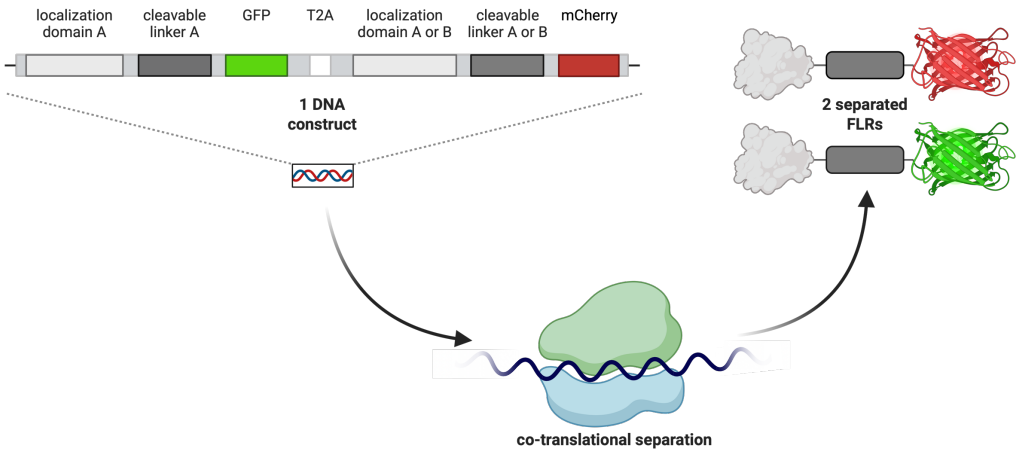

Figure 7: FLRs can be modified individually. Thus, two identical or different localization domains or cleavable linker can be combined. At DNA level, two FLRs are connected via a viral T2A sequence to ensure equimolar expression. Upon translation, the FLRs are separated from each other.

Hence, the opportunity to generate differently located FLRs will aid in assessing the two main GrzB entry mechanism into target cells during NK cell mediated cytotoxicity in parallel and in a physiological relevant setting.

2. Aim of the thesis

During NK cell cytotoxicity, GrzB is delivered to the cytosol of target cells to initiate the apoptotic cascade. Despite detailed analysis, however, it is controversial which entry mechanism – PM pores vs. endocytic uptake – is used by GrzB and whether these mechanisms are mutually supportive or exclusive. With the fluorescent localization reporter (FLR) system at hand, we have the ability to analyze the GrzB delivery from a different angle by localizing GrzB activity within target cells during NK cell-mediated killing. To tackle the main proposed entry mechanisms, GrzB specific tandem FLRs localized at PM and ER have already been generated and analyzed in first experiments in a previous work (Bruning, 2020). After expanding and deepening the establishment of our FLR system for GrzB activity, covering controls like the use of GrzB KO NK cells and non-cleavable FLRs, this study aims to investigate the possible co-existence of GrzB entry via PM pores and GrzB internalization. Henceforth, we want to answer the following three questions: I) does the entry depend on the NK cell activation state, II) does the entry mechanism depend on the perforin concentration and III) does the entry depend on the target cell itself? Therefore, we plan the use of NK cells from different sources like the NK cell line NK92 and human primary NK cells. Moreover, the titration of isolated lytic granules will help us to mimic different perforin availabilities. Since most of our previous research was based on HeLa target cells, we also plan to transfect other adherent or suspension target cells. This study will contribute to a better understanding which delivery mechanism is preferably used by GrzB.

3. Material and Methods

3.1 Materials

3.1.1 Chemicals and Reagents

Name	Source
2-Mercaptoethanol (2-ME)	Sigma Aldrich (St. Louis, MO, USA)
7-AAD Viability Staining Solution	BioLegend (San Diego, CA, USA)
AcOH	Carl Roth (Karlsruhe, Germany)
Annexin V - FITC	BioLegend (San Diego, CA, USA)
BD FACSFlow Sheath Fluid	BD Bioscience (Franklin Lakes, NJ, USA)
BioTracker™ 405 Blue Mitochondria Dye	Merck Millipore (Burlington, MA, USA)
Bovine serum albumin (BSA)	Carl Roth (Karlsruhe, Germany)
Bromophenol blue	Sigma Aldrich (St. Louis, MO, USA)
$CaCl_2$	AppliChem (Darmstadt, Germany)
Collagen (rat tail)	Roche (Basel, Switzerland)
DAPI	Life Technologies (Carlsbad, CA, USA)
DMSO	Sigma Aldrich (St. Louis, MO, USA)
Dynabeads® Untouched™ Human NK cells kit	Invitrogen (Waltham, MA, USA)
EDTA	Carl Roth (Karlsruhe, Germany)
Fetal calf serum (FCS)	Gibco® by Life Technologies, Thermo Fisher Scientific (Waltham, MA, USA)
Formaldehyde (FA)	Carl Roth (Karlsruhe, Germany)
Geneticin (G418)	Gibco® by Life Technologies, Thermo Fisher Scientific (Waltham, MA, USA)
Glycerol	MERCK (Darmstadt, Germany)
Glycin	AppliChem (Darmstadt, Germany)
Hepes	Carl Roth (Karlsruhe, Germany)
Horse serum	PAN-Biotech (Aidenbach, Germany)
Human IL-2 (recombinant)	NIH Cytokine Repository (Frederick, MD, USA)
Human IL-21 (recombinant)	Miltenyi Biotec (Bergisch Gladbach, Germany)
Human IL-15 (recombinant)	PAN-Biotech (Aidenbach, Germany)
KCl	AppliChem (Darmstadt, Germany)
KH_2PO_4	
Lipofectamine 2000	Life Technologies (Carlsbad, CA, USA)
Lysosome Isolation Kit (LYSISO1 Kit)	Sigma Aldrich (St. Louis, MO, USA)
MeOH	Carl Roth (Karlsruhe, Germany)
NaCl	
NaF	Sigma Aldrich (St. Louis, MO, USA)
$Na_2HPO_4 \cdot 2H_2O$	AppliChem (Darmstadt, Germany)
NaN_3	Carl Roth (Karlsruhe, Germany)
Na_3VO_4	Sigma Aldrich (St. Louis, MO, USA)
NEAA (MEM NEAA, 100X)	Gibco® by Life Technologies, Thermo Fisher Scientific (Waltham, MA, USA)
Paraformaldehyde (PFA)	Sigma Aldrich (St. Louis, MO, USA)
Penicillin-Streptomycin (P-S)	Gibco® by Life Technologies, Thermo Fisher Scientific (Waltham, MA, USA)
Phenylmethanesulfonyl fluoride (PMSF)	Sigma Aldrich (St. Louis, MO, USA)
Polybrene	Sigma Aldrich (St. Louis, MO, USA)
Poly-L-Lysine solution	
Precision Plus Protein™ All Blue Standard 250 kDa – 10 kDa	Bio-Rad (Hercules, CA, USA)
Protease inhibitor cocktail (LYSISO1-Kit)	Sigma Aldrich (St. Louis, MO, USA)

Puromycin (10 mg/ml)	Thermo Fisher Scientific (Waltham, MA, USA)
SDS	Carl Roth (Karlsruhe, Germany)
Skimmed milk powder	Sucofin
Sodium pyruvate (100mM, 100X)	Gibco® by Life Technologies, Thermo Fisher Scientific (Waltham, MA, USA)
Sucrose (LYSISO1 Kit)	Sigma Aldrich (St. Louis, MO, USA)
SuperSignal West Dura Chemiluminescence Signal	Thermo Fisher Scientific (Waltham, MA, USA)
Tris	Carl Roth (Karlsruhe, Germany)
Tris-HCl	
Trypan blue	Thermo Fisher Scientific (Waltham, MA, USA)
TrypLE™ Express™ Enzyme (1X)	Gibco® by Life Technologies, Thermo Fisher Scientific (Waltham, MA, USA)
Tween-20	Carl Roth (Karlsruhe, Germany)
Zombie NIR™ Fixable Viability Kit	BioLegend (San Diego, CA, USA)

3.1.2 Buffers and Solutions

Name	Ingrediencies / Source
Annexin V binding buffer (AVBB), 10X	1.4 M NaCl 25 mM $CaCl_2$ 0.1 M Hepes (0.2 µm sterile filtered) pH 7.4 for 1X: dilution in ddH_2O
BD FACS™ Permeabilizing Solution 2	BD Bioscience (Franklin Lakes, NJ, USA)
Blocking buffer	<u>Microscopy:</u> DPBS 2 % (w/v) BSA <u>Western blot:</u> PBS-T 5 % (w/v) milk powder
CASYton	OLS® OMNI Life Science (Bremen, Germany)
Coating solution	Collagen 0.2 % (v/v) AcOH
	Poly-L-Lysine:ddH_2O (1:10)
Dissociation buffer	Gibco® by Life Technologies, Thermo Fisher Scientific (Waltham, MA, USA)
DPBS (1X)	
Dynal buffer	DPBS (1X) 0.1 % (w/v) BSA 2 mM EDTA
Extraction buffer (5X) (LYSISO1)	Sigma-Aldrich (St. Louis, MO, USA)
FA fixing solution	FACS buffer 2% (v/v) FA
FACS buffer	DPBS (1X) 2 % (v/v) FCS
Freezing solution	FCS 10 % (v/v) DMSO
HB buffer	250 mM Sucrose 10 mM Hepes 0.3 mM EDTA ddH_2O; pH = 7.3

Lysis buffer (pH 7.3)	20 mM Tris-HCl (pH 7.4) 150 mM NaCl 10 % (v/v) Glycerin 0.5 % (v/v) Triton X-100 2 mM EDTA 10 mM NaF pH = 7.3 <u>freshly added:</u> 1 mM PMSF 1 mM Na_3VO_4
NuPAGE® MOPS SDS Running Buffer (20X)	Thermo Fisher Scientific (Waltham, MA, USA) dilution in ddH_2O (refer to running buffer)
5X RSB (reducing sample buffer)	10 % (w/v) SDS 25 % (v/v) 2-ME 0.1 % (w/v) bromophenol blue 50 % (v/v) glycerol 0.3125 mM Tris-HCl ddH_2O; pH = 6.8
Optiprep dilution buffer (20X) (LYSISO1)	Sigma-Aldrich (St. Louis, MO, USA) for 1X: dilution in ddH_2O
Pancoll Lymphocyte Separation Medium	PAN-Biotech (Aidenbach, Germany)
PBS (10X)	1.37 M NaCl 81 mM KCl 27 mM $Na_2HPO_4 \cdot 2H_2O$ 15 mM KH_2PO_4 ddH_2O; pH = 7.4
PBS-T	1X PBS (10X) 0.05 % (v/v) Tween-20 ddH_2O; pH = 7.4
PBS-T-NaCl	1X PBS (10X) 0.05 % (v/v) Tween-20 0.5 M NaCl ddH_2O; pH = 7.3
PFA fixing solution (4 %)	DPBS 4 % (w/v) PFA <u>Microscopy:</u> 4 % PFA fixing solution <u>FACS staining:</u> 4 % PFA fixing solution:FACS Buffer (1:1)
Running buffer (SDS-PAGE)	1X MOPS SDS Running Running Buffer (20X) ddH_2O; pH = 7.3
Staining solution (western blot, primary antibodies)	PBS-T 5 % (w/v) BSA 0.1 % (w/v) NaN_3
Transfer buffer (western blot)	20 % (v/v) MeOH 24 mM Tris 129 mM Glycin ddH_2O; pH = 7.3

3.1.3 Inhibitors

Name	Target	solvent	concentration	Source
(S)-4'-nitro-Blebbistatin	Myosin II	DMSO	50 µM	Cayman Chemical (Ann Arbor, MI, USA)
Concanamycin A (CMA)	V-type H^+-ATPase Inhibitor	DMSO	50 nM (stock: 0.25 mM)	Santa Cruz Biotechnology, Inc. (Dallas, TX, USA)

3.1.4 Cell culture media

Name	Source	Additives
Alpha-MEM	Gibco® by Life Technologies, Thermo Fisher Scientific (Waltham, MA, USA)	12.5 % (v/v) Horse serum (heat inactivated) 12.5 % (v/v) FCS (heat inactivated) 1 % (v/v) P-S 50 µM 2-ME
DMEM		10 % (v/v) FCS (heat inactivated) 1 % (v/v) P-S
DMEM (MDA-MB #468)		10 % (v/v) FCS (heat inactivated) 1 % (v/v) P-S 1 % (v/v) Sodium pyruvate 1 % (v/v) NEAA
IMDM		10 % (v/v) FCS (heat inactivated) 1 % (v/v) P-S
IMDM w/o Phenol red		10 % (v/v) FCS (heat inactivated) 1 % (v/v) P-S
IMDM GlutaMAX™		10 % (v/v) FCS (heat inactivated) 1 % (v/v) P-S
Opti-MEM™ GlutaMAX™		-
RPMI 1640		10 % (v/v) FCS (heat inactivated) 1 % (v/v) P-S

3.1.5 Vectors

The initial fluorescent localization reporter (FLR) constructs were kindly provided by Dr. Joël Beaudouin and Dr. Clarissa Liesche (Beaudouin et al., 2013, Liesche et al., 2018). These were further modified by Mina Sandusky in our lab. Tandem FLRs for GrzB activity (short: GrzB reporter) are under control of a CMV promotor. GFP-EEA1 wt was purchased from Addgene (Watertown, MA, USA) and was a gift from Silvia Corvera (Addgene plasmid # 42307; http://n2t.net/addgene:42307; RRID:Addgene_42307)(Lawe et al., 2000). It was subcloned into our GrzB reporter containing pEGFP backbone and further modified by Mina Sandusky.

GrzB reporter in pEGFP backbone (geneticin (G418) resistance):

Short name	Protein (reading from N to C terminus)	Source
$PM^{mGFP}ER^{mC}$ GrzB Reporter	MyrSnap2-VGPD'FGR-mGFP-T2A-Calnexin-VGPD'FGR-mCherry	Constructs kindly provided by Mina Sandusky (IfADo, Germany)
$PM^{mC}ER^{mGFP}$ GrzB Reporter	MyrSnap2-VGPD'FGR-mCherry-T2A-Calnexin-VGPD'FGR-mGFP	
$PM^{mC}ER^{mGFP, non-cl.}$ GrzB Reporter	MyrSnap2-VGPD'FGR-mCherry-T2A-Calnexin-AAAAFGR-mGFP	

$ER^{mGFP}Mito^{mC}$ GrzB Reporter	Calnexin-VGPD'FGR-mGFP-T2A-MitoNEET-VGPD'FGR-mCherry	Constructs kindly provided by Mina Sandusky (IfADo, Germany)
$PM^{mC}EE^{mGFP}$ GrzB Reporter	MyrSnap1-VGPD'FGR-mCherry-T2A-mGFP-VGPD'FGR-EEA1	

GrzB reporter in pBabe vector backbone (puromycin resistance):

Short name	Protein (reading from N to C terminus)	Source
$PM^{mC}ER^{mGFP}$ GrzB Reporter	MyrSnap2-VGPD'FGR-mCherry-T2A-Calnexin-VGPD'FGR-mGFP	Construct kindly provided by Mina Sandusky (IfADo, Germany)

FLR building blocks	Amino acid sequence (reading from N to C terminus)
AAAAFGR	VDGG**AAAAFGR**GGG
Calnexin (short)	*M*EGK…DGH(1-24) GGG GAA…RKPRRE(443-573) (UniProtKB P27824)
EEA1	*M*LRR…NDLQG(1-1411) (UniProtKB Q15075)
mGFP	*M*VSKGE…DELYK (Heim et al., 1995)
mCherry	*M*VSKGE…DELYK (Shaner et al., 2004)
MitoNEET (short)	*M*SLT…KDHRN(1-41) (UniProtKB Q9NZ45) (additionally coupled to Snap)
Myr (MyrPalm)	*M*GCIKSKRKDNLNDDE (Zacharias et al., 2002)
Snap	DKD…PAG (Keppler et al., 2004); New England Biolabs (Frankfurt am Main, Germany)
T2A	EGRGSLLTCGDVEENPG'P (Daniels et al., 2014)
VGPD'FGR	TGGG**VGPD'FGR**GGG

(*M* = start codon; cleavage site marked by ')

CD48 in pBabe backbone (puromycin resistance):

	Source
CD48	(Claus et al., 2016)

3.1.6 Cells

Cell name	Genome editing	Origin	Culture medium
HeLa	-	Cervical cancer cell line	DMEM (3.1.4)
	$CD48^+$		DMEM (3.1.4) + puromycin (1 µg/ml)
	$CD48^+$ $PM^{mGFP}ER^{mC}$ GrzB Reporter$^+$		DMEM (3.1.4) + puromycin (1 µg/ml) + G418 (1 mg/ml)
	$CD48^+$ $PM^{mC}ER^{mGFP}$ GrzB Reporter$^+$		
	$CD48^+$ $PM^{mC}ER^{mGFP, non-cl.}$ GrzB Reporter$^+$		
	$CD48^+$ $ER^{mGFP}Mito^{mC}$ GrzB Reporter$^+$		
	$CD48^+$ $PM^{mC}EE^{mGFP}$ GrzB Reporter$^+$		DMEM (3.1.4)

K562	-	Chronic myeloid leukemia (CML)	IMDM (3.1.4)
	$CD48^+$		IMDM (3.1.4) + puromycin (1 µg/ml)
	$PM^{mC}ER^{mGFP}$ GrzB Reporter$^+$		
K562 (Feeder cells, 30 Gy irradiated)	mbIL15-41BBL		IMDM (3.1.4)
	mbIL15-41BBL-mbIL21		
MDA-MB #468	-	Breast cancer cell line	DMEM for MDA (3.1.4)
	$PM^{mC}ER^{mGFP}$ GrzB Reporter$^+$		DMEM for MDA (3.1.4) + puromycin (1 µg/ml)
NK92	-	malignant non-Hodgkin lymphoma (human) NK cell line	Alpha-MEM (3.1.4) + IL-2 (100 U/ml)
	GrzB KO generated by Dr. Vivian Bönnemann (Bönnemann, 2023)		
NKL	-	NK cell leukemia	RPMI 1640 (3.1.4) + IL-2 (100 U/ml)
Phoenix-AMPHO (amphotropic virus producing)	constructs for viral gag-pol and envelope protein production	Human embryonic kidney (HEK 293T)	DMEM (3.1.4)
Primary human NK cell	-	Whole blood/buffy coats (healthy humans)	IMDM GlutaMAX™ (3.1.4) + (see 3.2.2)

3.1.7 Antibodies

Primary Antibodies

Antigen (clone)	Conjugate	Origin	Dilution	Source
CD56 (NCAM16.2)	BV421	Mouse	1:200	BioLegend (San Diego, CA, USA)
CD107a (H4A3)	PE-Cy5	Mouse	1:100	BD Bioscience (Franklin Lakes, NJ, USA)
GM130 (D6B1)	-	Rabbit	1:3000	Cell Signaling Technology (Danvers, MA, USA)
Golgin-97 (D8P2K)	-	Rabbit	1:100	
GrzB (GB11)	AF647	Mouse	1:200	BioLegend (San Diego, CA, USA)
GrzB (M3304B06)	-	Mouse	1:500	
LAMP1 (D2D11)	-	Rabbit	1:200	Cell Signaling Technology (Danvers, MA, USA)
PDI (C81H6)	-	Rabbit	1:200	
Perforin (dG9)	FITC	Mouse	1:100	BioLegend (San Diego, CA, USA)
Perforin (Pf344)	-	Mouse	1:1000	Mabtech AB (Stockholm, Sweden)

Secondary Antibodies

Antigen (clone)	Conjugate	Origin	Dilution	Source
Goat anti Rabbit IgG	AF405	Goat	1:600 (in blocking buffer for microscopy)	Abcam (Cambridge, UK)
Goat anti mouse	HRP	Goat	1:10000 (in blocking buffer for western blot)	Dianova (Hamburg, Germany)

3.1.8 Devices

Device	Name	Source
Cell counter	CASY Cell Counter & Analyzer	OLS® OMNI Life Science (Bremen, Germany)
Cell disruption (with nitrogen)	4639 cell disruption vessel; 45 ml	PARR Instrument company (Moline, IL, USA)
Cell sorter	BD FACSAria™ Fusion (+ biosafety cabinet)	BD Bioscience (Franklin Lakes, NJ, USA)
Centrifuge	Heraeus Multifuge 3 S-R	Thermo Fisher Scientific (Waltham, MA, USA)
	Heraeus Megafuge 40R	
	Heraeus Fresco 21 centrifuge	
	Eppendorf centrifuge 5910Ri	Eppendorf (Hamburg, Germany)
	Sorvall WX+ ultra series Centrifuge equipped with: - Rotor: SW41 Ti (41000 rpm)	Thermo Fisher Scientific (Waltham, MA, USA) Beckman Coulter (Brea, CA, USA)
Clean bench	HERA Safe 2020	Thermo Fisher Scientific (Waltham, MA, USA)
Cool Cell® freezing container		Biozym Scientific GmbH (Hessisch Oldendorf, Germany)
Film-developer system	CD1000	Agfa (Mortsel, Belgium)
Flow cytometer	BD LSRFortessa®	BD Bioscience (Franklin Lakes, NJ, USA)
	Cytek® Aurora 5L 16UV-16V-14B-10YG-8R	Cytek Bioscience Inc. (Fremont, CA, USA)
Gel electrophoresis device	PowerEase 500 Power supply + WorkOut 2.5	Thermo Fisher Scientific (Waltham, MA, USA)
Heating block	Thermomixer comfort	Eppendorf (Hamburg, Germany)
Incubator	HERAcell240i CO_2 Incubator	Thermo Fisher Scientific (Waltham, MA, USA)
Magnetic particle concentrator	Dynal MPC® - 50	Dynal Biotech (Oslo, Norway)
Microscope equipped with: - Heating device - Heating Insert - Incubator - CO_2 module - Temperature module - Camera - LED light source - Objective	Axio Observer 7 Heating Device Humidity S1 Heating Insert P Lab-Tek™ S1 Incubator PM 2000 RBT CO_2 Module S Temp Module S Axiocam 506 mono Colibri 7 Plan-Apochromat 40x/1.4 oil DIC(UV)VIS-IR	Carl Zeiss Microscopy (Jena, Germany) PeCon GmbH (Erbach, Germany) PeCon GmbH PeCon GmbH PeCon GmbH Carl Zeiss Microscopy Carl Zeiss Microscopy Carl Zeiss Microscopy

Microscope	EVOS® FL Auto Imaging System	Thermo Fisher Scientific (Waltham, MA, USA)
<u>equipped with:</u>		
- Incubator	EVOS™ Onstage Incubator	Thermo Fisher Scientific
- LED light source	EVOS™ LED Cube, DAPI	Thermo Fisher Scientific
	EVOS™ LED Cube, GFP	Thermo Fisher Scientific
	EVOS™ LED Cube, RFP	Thermo Fisher Scientific
- Objective	PlanApoN 60x/1.42 oil	Olympus (Shinjuku, Tokyo prefecture, Japan)
Microscope	Mica WideFocal Live Cell	Leica Microsystems (Wetzlar, Germany)
<u>equipped with:</u>		
- Incubator	Mica-CO_2-Incubator	Okolab s.r.l. (Pozzuoli NA, Italy)
	Mica-CO_2-Incubator-sensor-module	
	Mica-CO_2-Incubator-HM	Okolab s.r.l.
	Mica-CO_2-Incubator-valve-kit	Okolab s.r.l.
	Mica-water-bottle-cap	Okolab s.r.l.
	Mica-water-pump	Okolab s.r.l.
- LED/Laser	365nm, 470nm, 555nm, 625nm/	Leica Microsystems
	405nm, 488nm, 561nm, 638nm	Leica Microsystems
- Detection unit	widefield and confocal detection unit for FluoSync™	Leica Microsystems
- Objective	HC PL APO 40x/1.1 water motCORR CS2	Leica Microsystems
	HC PL APO 63x/1.2 water motCORR CS2	Leica Microsystems
Pellet pestle motor	Pellet pestle® cordless motor	Kimble Chase Life Science (Vineland, NJ, USA)
RTCA analyzer	xCELLigence RTCA DP	Agilent Technologies (Santa Clara, CA, USA)
Tank blotter	Xcell IITM Blot Module	Invitrogen (Waltham, MA, USA)
Ultrasonic cleaner		JSP

3.1.9 Software

Software	Full name/version	Source
Flow cytometry analysis software	FlowJo v 10	FlowJo, LLC, Ashland, USA
Flow cytometry software	BD FACSDiva™ software	BD Bioscience (Franklin Lakes, NJ, USA)
	SpectroFlo®	Cytek Bioscience Inc. (Fremont, CA, USA)
GraphPad Prism	GraphPad Prism V10	GraphPad Software, Inc (La Jolla, CA, USA)
Illustrations	BioRender App	BioRender (Toronto, Canada)
Image analysis	ImageJ 1.54	Wayne Rasband and contributors (NIH, Maryland, MD, USA)

Imaging software	ZEN 2.6 pro (blue edition)	Carl Zeiss Microscopy (Jena, Germany)
	EVOS fl auto	Thermo Fisher Scientific (Waltham, MA, USA)
	Leica Application Suite X (LAX)	Leica Microsystems (Wetzlar, Germany)
RTCA analyzer software	RTCA software 2.0	Agilent Technologies (Santa Clara, CA, USA)

3.1.10 General material

Material	Description	Source
6-well plate		Greiner Bio-One (Kremsmünster, Austria)
12-well plate		Greiner Bio-One (Kremsmünster, Austria)
96-well plate	TC Microwell 96 U Nunclon™ Delta Surface	Thermo Fisher Scientific (Waltham, MA, USA)
	Nunc™ 96-Well Polystyrene Conical Bottom MicroWell™	
CASY cups	Cups for automated cell counter	OLS® OMNI Life Science (Bremen, Germany)
Cell culture flask	Nunc™ EasYFlask™ 25 cm^2 NunclonTM Delta Surface	Thermo Fisher Scientific (Waltham, MA, USA)
	Nunc™ EasYFlask™ 75 cm^2 NunclonTM Delta Surface	
Cell strainer	pore size 100 µm	Sarstedt (Nümbrecht, Germany)
CL-XPosure™ Film	18 x 24 cm	Thermo Fisher Scientific (Waltham, MA, USA)
Cryovials	CRYO.S™ PP, with screw cap, sterile	Greiner Bio-One (Kremsmünster, Austria)
Ibidi slide	ibiTreat, µ-slide 8-well	ibidi GmbH (Gräfelfing, Germany)
NuPAGE® 4 – 12 % Bis-Tris gel	1.0 mm, 12-well	Thermo Fisher Scientific (Waltham, MA, USA)
PVDF membrane		MERCK (Darmstadt, Germany)
Pellet pestle®	Pellet pestle (1.5 ml)	Kimble Chase Life Science (Vineland, NJ, USA)
Reaction tubes	0.5 – 2 ml	Sarstedt (Nümbrecht, Germany)
RTCA analyzer slides	E-Plate 16 PET	Agilent Technologies (Santa Clara, CA, USA)
Ultra-Clear™ Centrifuge tubes	13 x 51 mm	Beckman Coulter (Brea, CA, USA)

3.2 Methods

3.2.1 Isolation of primary human NK cells

Peripheral blood mononuclear cells (PBMCs) were isolated from buffy coats (provided by Deutsches Rotes Kreuz Hagen or Blutbank Dortmund) or whole blood of healthy donors according to standard procedure. Briefly, blood was collected and carefully layered onto Human Pancoll Lymphocyte Separation Medium (LSM) followed by centrifugation (25 min, 1082 x *g*) without brake. Afterwards, the PBMC layer was extracted and washed with DPBS three times. Then, NK cells were negatively selected using the Dynabeads® Untouched™ Human NK cells kit (3.1.1) according to manufacturer's protocol. Freshly isolated NK cells were stained for CD3 and CD56 to determine purity by flow cytometry (above 90 % $CD3^-CD56^+$). If fresh NK cells (resting NK cells) were required for experiments, they were rested overnight (37 °C, 5 % CO_2) with low dose of IL-15 (0.5 ng/ml). Otherwise, NK cells were expanded (3.2.2).

3.2.2 Cultivation of NK cells

Isolated NK cells were seeded at a density of 1-2 x 10^6 cells/ml in IMDM GlutaMax™ (3.1.4) together with 30 Gy irradiated K562 mbIL15-41BBL feeder cells (3.1.6) at a ratio of 2:1 (NK:K562) in 96-well U bottom plates (3.1.10). The culture was supplemented with recombinant IL-2 (200 U/ml) as well as IL-21 (100 ng/ml). After a few days, spent medium was replaced with fresh medium/IL-2. One week after isolation, NK cells were restimulated by diluting the culture to a density of 1 x 10^6 cells/ml and addition of fresh feeder cells (2:1) as well as fresh IL-2 (200 U/ml). Subsequently, if NK cell density exceeded 3 x 10^6 cells/ml, they were diluted to a density of 1.5-2 x 10^6 cells/ml with fresh medium supplemented with IL-2 (100 U/ml). Otherwise, spent medium was replaced with fresh medium and IL-2 (100 U/ml). After two weeks, IL-15 (2.5 ng/ml) was added as well.

During this work, K562 mbIL15-41BBL feeder cells were replaced with K562 mbIL15-41BBL-mbIL21 feeder cells. Consequently, supplementation with recombinant IL-21 was not necessary. On restimulation day, NK cells were diluted to a density of 1 x 10^6 cells/ml and supplemented with fresh IL-2 (200 U/ml) without addition of fresh feeder cells. Moreover, NK cells were cultured without addition of recombinant IL15.

Pre-activated NK cells were always used at the earliest 3 and at the latest 5 weeks after isolation.

3.2.3 Cultivation of cell lines

Cell lines (3.1.6) were maintained in appropriate growth medium (3.1.4; 3.1.6) at 37 °C and 5 % CO_2 in tissue culture flasks. Passaging was performed periodically three times per week.

Suspension cell lines (K562, NK92, NKL) were split to a concentration of 0.3 x 10^6/ml. After passaging, NK92 and NKL cell cultures were supplemented with 100 U/ml IL-2.

Once adherent cell lines (HeLa, MDA-MB #468, Phoenix-AMPHO) had reached a confluency of about 80 %, spent growth medium was removed and the cell monolayer was washed gently with DPBS. Depending on further steps, cells were brought into suspension differently: I) TrypLE™ Express™ Enzyme was used for regular cell passaging. II) Dissociation buffer was added if cells were required for further experiments. After complete detachment, cells were resuspended in fresh growth medium and split depending on growth speed (table 1).

Table 1: Splitting ratios of adherent cell lines (3.1.6)

Cell line	Splitting ratio
HeLa and transduced/transfected variants	1:10 – 1:20
Phoenix-AMPHO	1:10
MDA-MB #468 and transduced variant	1:3

Cells transduced with pBabe-CD48 or pBabe-GrzB reporter vector were selected by addition of puromycin (1 µg/ml); Cells transfected with the pEGFP-GrzB reporter vector were selected by addition of G418 (1 mg/ml).

3.2.4 Transduction

Stable modification of target cells to express CD48 or the $PM^{mC}ER^{mGFP}$ GrzB reporter (pBabe backbone) was achieved using the retrovirus-producing Phoenix-AMPHO system. HeLa cells were transduced retrovirally to express CD48. MDA-MB #468 and K562 cells were transduced retrovirally to express $PM^{mC}ER^{mGFP}$ GrzB reporter.

2 x 10^6 Phoenix-AMPHO cells were grown in 3 ml appropriate growth medium in T25 tissue culture flasks (3.1.10). The next day, Phoenix-AMPHO were transfected with vectors (pBabe backbone; 3.1.5). The transfection mixture was prepared as follows: (A) 237.5 µl OptiMEM™ and 12.5 µl Lipofectamine 2000 as well as (B) 240 µl OptiMEM™ and 10 µl DNA (CD48: 18.8 µg, GrzB reporter: 10.3 µg) were incubated separately for 5 min. Afterwards, (A) and (B) were mixed, incubated for 20 min and added to cells dropwise. After 24 h, the medium was replaced with 2.5 ml fresh growth

medium of the cells to be transduced (3.1.6). The supernatant was collected the following day, carefully ensuring that Phoenix-AMPHO cells were not transferred. 0.5 x 10^6 cells (HeLa, MDA-MB #468 or K562) were seeded in the retrovirus containing supernatant in a 12-well plate and supplemented with 5 µg/ml polybrene (3.1.1) followed by centrifugation (1251 x *g*, 1.5 h, 30 °C) and overnight incubation. The medium was replaced with fresh growth medium and on the subsequent day, puromycin (0.5 µg/ml) was added for selection. Transduced cells were expanded and frozen for storage. Additionally, transduced MDA-MB #468 and K562 cells were sorted (3.1.6).

3.2.5 Transfection

Modification of HeLa $CD48^+$ with different GrzB reporter constructs based on pEGFP backbone was achieved by transient transfection.

Transfection in 6-well plates

0.25 x 10^6 HeLa $CD48^+$ cells were seeded in 2 ml medium (3.1.6) into a 6-well plate. On the next day, medium was replaced with 800 µl fresh medium. For preparation of the transfection mixture, (A) 100 µl OptiMEM™ and 3 µl Lipofectamine 2000 as well as (B) 100 µl OptiMEM™ and 1 µl DNA (approx. 1 – 2 µg DNA, depending on construct) were incubated separately for 5 min. Subsequently, (A) and (B) were mixed and incubated for 15 min followed by dropwise addition to cells. After overnight incubation, medium was replaced with fresh growth medium and the following day, cells expressing the GrzB reporter were selected using G418 (1 mg/ml). Additionally, cells were expanded for cell sorting (3.2.6).

Transfection in ibidi slides ($PM^{mC}EE^{mGFP}$ GrzB reporter construct)

The transient transfection of HeLa $CD48^+$ cells with the $PM^{mC}EE^{mGFP}$ GrzB reporter construct was performed similarly as described above:

On the first day, 2 x 10^4 HeLa $CD48^+$ cells were seeded in 200 µl medium (3.1.6) into ibidi slides (3.1.10) and rested overnight (37 °C, 5 % CO_2). The medium was carefully replaced with 160 µl fresh medium and the transfection mixture was prepared (table 2):

Table 2: Transfection steps ($PM^{mC}EE^{mGFP}$ GrzB reporter construct)

Step 1	Step 2	Step 3	Step 4	Step 5
(A) 20 µl OptiMEM™ + 0.6 µl Lipofectamine 2000	5 min incubation	Mixing of (A) and (B)	15 min incubation	Addition to cells
(B) 20 µl OptiMEM™ + 0.2 µl (0.3 µg) DNA	5 min incubation			

After 24 h, the medium was replaced with 200 µl fresh growth medium. On the fourth day, the slide was prepared for microscopy experiments by carefully replacing medium with 170 µl IMDM without phenol red (3.1.4; 3.2.14).

3.2.6 Cell sorting

Sorting of GrzB reporter expressing cells ($mGFP^+mCherry^+$) was performed in Dynal buffer and using the BD FACSAria™ Fusion (3.1.8). High purity of double positive cells was achieved by using the sort precision mode “4-way purity”. After sorting, the cells were expanded and cryopreserved. All GrzB reporter transduced or transfected variants of MDA-MB #468, K562 and HeLa $CD48^+$ (except $PM^{mC}EE^{mGFP}$ GrzB reporter cells) were sorted at least once or until a stable expression of reporter was achieved.

3.2.7 Isolation of lytic granules

The LYSISO 1 kit (3.1.1) was used for isolating NK cell lytic granules. Each step was performed with pre-cooled buffers/devices at 4 °C. NKL or pre-activated NK cells ($1.1 – 1.3 \times 10^9$) were harvested, washed twice with DPBS and disrupted by nitrogen cavitation using 1000 psi for 5 min (NKL cells) or 500 psi for 1 min (pre-activated NK cells). Subsequently, the crude lysosomal fraction (CLF) was separated from intact cells and nuclei by differential centrifugation: centrifugation at low speed (1000 x *g*, 10 min) was performed twice. The supernatant was transferred to a fresh tube and centrifugation at medium speed (20000 x *g*, 20 min) yielded the CLF containing pellet. The CLF was resuspended in 800 µl extraction buffer (3.1.2) using a pellet pestle (3.1.8) and further prepared for gradient centrifugation as shown in table 3 (left). The different OptiPrep™ density gradient medium solutions (8, 12, 16, 22.5 and 27 % OptiPrep™) were prepared according to manufacturer’s instructions. Next, the OptiPrep™ step gradient was layered starting with 27 % OptiPrep™ at the bottom and 8 % OptiPrep™ at the top of Ultra-Clear™ Centrifuge tubes (3.1.10; table 3 (right)).

Table 3: Left: Preparation of CLF sample for step gradient. Right: OptiPrep™ step gradient.

CLF sample (19 % OptiPrep™)	Volume
OptiPrep™	0.505 ml
OptiPrep™ dilution buffer	0.275 ml
CLF	0.8 ml

	OptiPrep™	Volume
top	8 %	1.5 ml
	12 %	1.5 ml
	16 %	1.5 ml
	19 %	1.5 ml
	22 %	1.5 ml
bottom	27 %	1.5 ml

Then, the gradient was placed carefully into a SW41 Ti rotor (3.1.8) and lytic granules were separated from other organelles by centrifugation for 4-5 h at 150000 x *g* using the Sorvall WX+ ultra series centrifuge (3.1.8; brake was switched off). Afterwards, six fractions were extracted by aspiration (approx. 1 ml) from the top of the gradient, diluted with HB buffer (3.1.2) and pelleted by centrifugation at 21100 x *g* for 30 min. The fractions were resuspended in HB buffer and stored at – 80 °C.

3.2.8 Western Blot (lytic granules)

The six fractions (3.2.7) as well as a whole lysate control were analyzed regarding the presence of perforin and GrzB by western blot. First, one hundredth of the NK cell input used for lytic granule isolation (3.2.7) was lysed in 100 µl lysis buffer (3.1.2) for 20 min on ice, followed by a centrifugation at 21100 x *g* for 20 min at 4 °C. Next, 1 µl of the lysate supernatant (whole lysate; WL) or 1 µl of each fraction (3.2.7) was diluted with PBS and RSB buffer (1X; 3.1.2) was added (V_{final} of 15 µl). For denaturation, the samples were heated for 3 min, 95 °C. Then, samples as well as Precision Plus Protein™ All Blue Standard (3.1.1) were loaded on a NuPAGE® 4 – 12 % Bis-Tris gel (3.1.10) and separated for 1 h 15 min at 150 V in running buffer (3.1.2). Afterwards, the separated proteins were transferred to a MeOH pre-activated PVDF membrane for 1 h 30 min at 200 mA in transfer buffer (3.1.2) followed by blocking of the membrane with blocking buffer (3.1.2) for 1 h at rt. The membrane was washed three times with PBS-T (3.1.2) followed by cutting into three sections (first cut: above 75 kDa, second cut: underneath 50 kDa). Subsequently, the membrane sections were treated with primary antibodies (3.1.7; upper section: CD107a; middle section: perforin; lower section: GrzB) in staining solution (3.1.2) overnight at 4 °C. Next, the sections were washed thrice with PBS-T-NaCl (3.1.2), incubated with secondary HRP conjugated antibodies (3.1.7) in blocking buffer (3.1.2) for 1 h at rt and washed repeatedly with PBS-T. The sections were treated with SuperSignal West Dura (3.1.1),

chemiluminescence signal was captured on CL-XPosure™ films (3.1.10) and developed using the film-developer CD1000 (3.1.8).

3.2.9 Flow cytometry based killing assay (lytic granules)

The functionality of isolated lytic granules was evaluated by a flow cytometry based killing assay. Isolated lytic granules (fractions 1 – 6) from NKL or pre-activated NK cell isolation (3.2.7) were sonicated for 10 min using an ultrasonic cleaner (3.1.8). 1 x 10^5 K562 (for NKL granules) or 5 x 10^4 K562 (for pre-act. NK granules) were mixed at a ratio of 1:2, 1:4, 1:8, 1:16 and 1:32 with lytic granules from fractions 1 – 6. The killing assay was performed in IMDM medium (3.1.4) supplemented with 5mM $CaCl_2$ for 2 h at 37 °C, 5 % CO_2. Afterwards, K562 were washed and stained with Annexin V – FITC (1:20; 3.1.1) in AVBB (3.1.2; 1X) for 15 min at rt. 7-AAD (1:100; 3.1.1) was directly added and the samples were immediately measured using the BD LSRFortessa® (3.1.8). For solvent controls, K562 were treated with HB buffer or medium. Additionally, K562 were heat-shocked (70 °C, 5 min) as a positive control for dead cells. The analysis was performed using FlowJo (3.1.9).

3.2.10 Flow cytometry staining of GrzB and perforin

Intracellular levels of GrzB and perforin were determined by flow cytometry using the Cytek® Aurora. The staining comprises 5 steps in the following order: live/dead staining, surface marker staining, fixation, permeabilization, intracellular staining. Between the individual steps, NK cells were washed with FACS buffer and centrifuged at 500 x *g* and rt for 5 min.

Living cells were distinguished from dead cells by staining with Zombie NIR™ Fixable Viability dye (3.1.1; 1:700 in PBS) for 15 min at rt. The surface of NK cells was stained with CD56-BV421 (1:200 in FACS buffer) for 20 min at 4 °C. Cells were fixed in PFA fixing solution (3.1.2) for 10 min at rt and permeabilized using BD FACS™ Permeabilizing Solution 2 (3.1.2; 1:10 in ddH_2O) for 10 min at rt. Perforin and GrzB were stained intracellularly using perforin-FITC (1:100 in FACS buffer) and GrzB-AF647 (1:200 in FACS buffer) for 20 min at 4 °C. Lastly, cells were washed and resuspended in 150 µl FACS buffer (measurement on the same day) or in 150 µl FA fixing solution (measurement on the following day). The analysis was performed using

FlowJo (3.1.9). GrzB and perforin levels were determined by gating on single, living $CD56^+$ NK cells and displayed as background subtracted gMFI.

3.2.11 CMA treatment

Pre-activated NK cells were treated with 50 nM concanamycin A (CMA) for 30, 60 and 180 min or 0.02 % DMSO (180 min) as solvent control (37 °C, 5 % CO_2). Afterwards, NK cells were washed, and 2 x 10^4 NK cells of each condition were prepared for live cell imaging (3.2.14), while the remaining NK cells were stained according to 3.2.10 determine CMA effect on perforin via flow cytometry.

3.2.12 (S)-4'-nitro-Blebbistatin treatment

Real-time cell analysis (RTCA)

The effect of (S)-4'-nitro-Blebbistatin on NK cell killing was determined by impedance measurement using the xCELLigence RTCA DP (3.1.8). RTCA analyzer E-Plate slides (3.1.10) were coated with collagen coating solution (3.1.2) for 30 min at rt. Afterwards, the coating solution was replaced with 50 µl DMEM for MDA (3.1.4) and a baseline measurement was performed. 2 x 10^4 MDA-MB #468 $PM^{mC}ER^{mGFP}$ GrzB Reporter cells (3.2.12) in 50 µl DMEM or 50 µl DMEM containing DMSO or 50 µM (S)-4'-nitro-Blebbistatin (c_{final}) were added followed by impedance measurement every 15 min. After 12 h, (S)-4'-nitro-Blebbistatin or DMSO were washed out by replacing the medium with fresh medium and measurement was continued. After additional 12 h, 2 x 10^4 NK cells (E:T ratio of 1:1) in 10 µl per well were added and the measurement was continued every 15 min for 12 h and then every 30 min for 24 h.

(S)-4'-nitro-Blebbistatin treatment for microscopy

Ibidi slides (3.1.10) were coated with collagen coating solution (3.1.2) for 30 min at rt. Subsequently, 4 x 10^4 MDA-MB #468 $PM^{mC}ER^{mGFP}$ GrzB Reporter were grown in 200 µl DMEM for MDA (3.1.4) or 200 µl DMEM for MDA supplemented with 50 µM (S)-4'-nitro-Blebbistatin or DMSO. After 12 h, (S)-4'-nitro-Blebbistatin or DMSO were washed out by replacing the medium with fresh medium and cells were incubated for additional 12 h. Then, the slide was prepared for microscopy experiments by carefully replacing medium with 170 µl IMDM without phenol red (3.1.4), NK cells were prepared (3.1.14) and live-cell imaging was performed using the MICA WideFocal live cell microscope (3.1.14).

3.2.13 Staining of cell organelles

4 x 10^4 HeLa CD48$^+$ PM^{mGFP}ER^{mC} GrzB reporter cells were grown overnight in ibidi slides. Between individual steps, cells were washed with DPBS (3.1.2). Cells were fixed with 4 % PFA fixing solution (3.1.2) for 10 min at rt and permeabilized using BD FACS™ Permeabilizing Solution 2 (3.1.2; 1:10 in ddH_2O) for 10 min at rt. Subsequently, cells were incubated in blocking buffer (2 % BSA in DPBS, 3.1.2) for 1 h at rt. Nuclei were stained with 4,6-diamidino-2-phenylindole (DAPI, 1:40000 in blocking buffer, 3.1.1) for 10 min at rt followed by a final washing step and imaging. Golgi (GM130 1:3000; Golgin-97 1:100; 3.1.7), Lysosomes (LAMP1 1:200; 3.1.7) and ER (PDI 1:200; 3.1.7) were stained in blocking buffer overnight at 4 °C. On the following day, cells were stained with secondary antibody goat-anti-rabbit AF405 (3.1.7; 1:600 in blocking buffer) for 1 h at 4°C followed by a final washing step and imaging.

Mitochondria staining (live cell)

4 x 10^4 HeLa CD48$^+$ PM^{mGFP}ER^{mC} or ER^{mGFP}Mito^{mC} GrzB reporter cells were grown overnight in ibidi slides and washed once with DPBS the next day. Mitochondria were stained for 15 min with 100 nM BioTracker™ 405 Blue Mitochondria Dye (3.1.1; in IMDM without phenol red) and images were acquired immediately within 15-20 min.

Imaging

Images of GrzB reporter and different organelles were acquired using the confocal mode of MICA WideFocal Live Cell microscope (3.1.8) equipped with a 40x/1.1 water immersion HC PL APO motCORR CS2 objective (3.1.8). mCherry (mC) was excited with laser diode 561 nm, mGFP was excited with laser diode 488 nm. Excitation of DAPI, AF405 and BioTracker™ 405 was realized with laser diode 405 nm.

Alternatively, images of GrzB reporter and mitochondria were acquired using the EVOS® FL Auto Imaging System equipped with a 60x/1.42 oil immersion PlanApoN objective (3.1.8). mCherry (mC) was excited with EVOS™ LED Cube RFP (3.1.8). mGFP was excited with EVOS™ LED Cube GFP (3.1.8). Excitation of BioTracker™ 405 was realized with EVOS™ LED Cube DAPI (3.1.8). Z stacks were acquired and projected by the EVOS fl auto imaging software (3.1.9). Additionally, background was removed using the rolling ball algorithm embedded in ImageJ (https://imagej.nih.gov).

3.2.14 Time-lapse live cell imaging of GrzB reporter cells with NK cells

Preparation of GrzB reporter cells

Adherent GrzB reporter cells (HeLa CD48$^+$ GrzB reporter: 2 x 10^4; MDA-MB #468 PM^{mC}ER^{mGFP} GrzB reporter: 4 x 10^4) were grown in appropriate growth medium (3.1.6) in ibidi slides (3.1.10) overnight. On experiment day, medium was replaced with 150-170 µl IMDM without phenol red (3.1.4). For preparation of K562 PM^{mC}ER^{mGFP} GrzB reporter cells, ibidi slides were coated with Poly-L-Lysin coating solution (3.1.2) for 30 min at rt. The solution was discarded, and the slide was dried overnight. Then, 5 x 10^4 K562 PM^{mC}ER^{mGFP} GrzB reporter cells were seeded in 170 µl IMDM without phenol red. The ibidi slides were placed into the humidified chamber of the microscope.

Preparation of NK cells

Depending on the number of target cells, 2 x 10^4 or 2.5 x 10^4 fresh NK cells, pre-activated NK cells or NK92 cells (wt or GrzB KO) were washed and resuspended in 30 µl IMDM without phenol red (3.1.4). The cells were rested for 30 min at 37 °C, 5 % CO_2 and added to target cells at an NK:Target cell ratio of 1:1 (NK:HeLa CD48$^+$ GrzB reporter cells) or 1:2 (NK:MDA-MB #468 or K562 GrzB reporter cells). Immediately after addition, time-lapse live cell imaging was started.

Time-lapse live cell imaging using the Axio Observer 7 microscope

Time-lapse live cell imaging of all HeLa CD48$^+$ GrzB reporter$^+$ cells (3.1.6) together with different NK cell types was carried out using the Axio Observer 7 microscope (3.1.8) equipped for 37 °C, 5 % CO_2 and humidified incubation. mCherry (mC) was excited with Colibri 7 LED-module 561/filter set 64 HE. mGFP was excited with Colibri 7 LED-module 488/filter set 38 HE. Brightfield images were acquired using TL LED module. Images were acquired every 3 min for 3-5 h with a 40x/1.4 oil immersion Plan-Apochromat objective (3.1.8). GrzB reporter cleavage was analyzed using ImageJ (3.2.16).

Time-lapse live cell imaging using the MICA WideFocal Live Cell microscope

Time-lapse live cell imaging of HeLa CD48$^+$ PM^{mC}EE^{mGFP}, MDA-MB #468 PM^{mC}ER^{mGFP} and K562 PM^{mC}ER^{mGFP} GrzB reporter cells with NK cells was carried out using the MICA WideFocal Live Cell microscope (3.1.8) equipped for humidified incubation at 37 °C and 5 % CO_2. Depending on the target cell line, widefield and/or confocal microscopy was performed (table 4). Widefield microscopy: mCherry (mC) was excited with LED 555 nm, mGFP was excited with LED 470 nm. Confocal

microscopy: mCherry (mC) was excited with laser diode 561 nm, mGFP was excited with laser diode 488 nm. Fluorescence and brightfield images were acquired every 3 min for 3-5 h with a 40x/1.1 water immersion HC PL APO motCORR CS2 objective (3.1.8). Out-of-focus background in widefield imaging was removed using the THUNDER method small volume computational clearing (SVCC) (table 4). GrzB reporter cleavage was analyzed using ImageJ (3.2.16).

Table 4: Imaging techniques and deconvolution methods used for live cell imaging.

Target cell line	Imaging technique	Deconvolution method
HeLa CD48^{+} PM^{mC}EE^{mGFP}	Widefield Confocal	THUNDER: SVCC -
K562 PM^{mC}ER^{mGFP}	Confocal	-
MDA-MB #468 PM^{mC}ER^{mGFP}	Widefield	THUNDER: SVCC

3.2.15 GrzB reporter analysis

The reporter cleavage analysis was performed based on the method already described elsewhere (Beaudouin et al., 2013, Liesche et al., 2018, Bruning et al., 2023) and can be applied to the GrzB reporters used in this work with minor modifications.

Briefly, 16-bit grayscale .tif stacks of mC and mGFP channels were merged, assigned colors (mC – red, mGFP – green) and converted into RGB stacks. Next, numbers were assigned to the killed reporter cells. Subsequently, the brightfield time stack was used to determine the number of NK cells attached to the killed reporter cells. Only target cells in contact with just one NK cell were included in the analysis. Reporter cleavage was measured using 4 different circular regions of interest (ROIs) as depicted exemplarily in figure 8 and the RGB_measure function embedded in ImageJ.

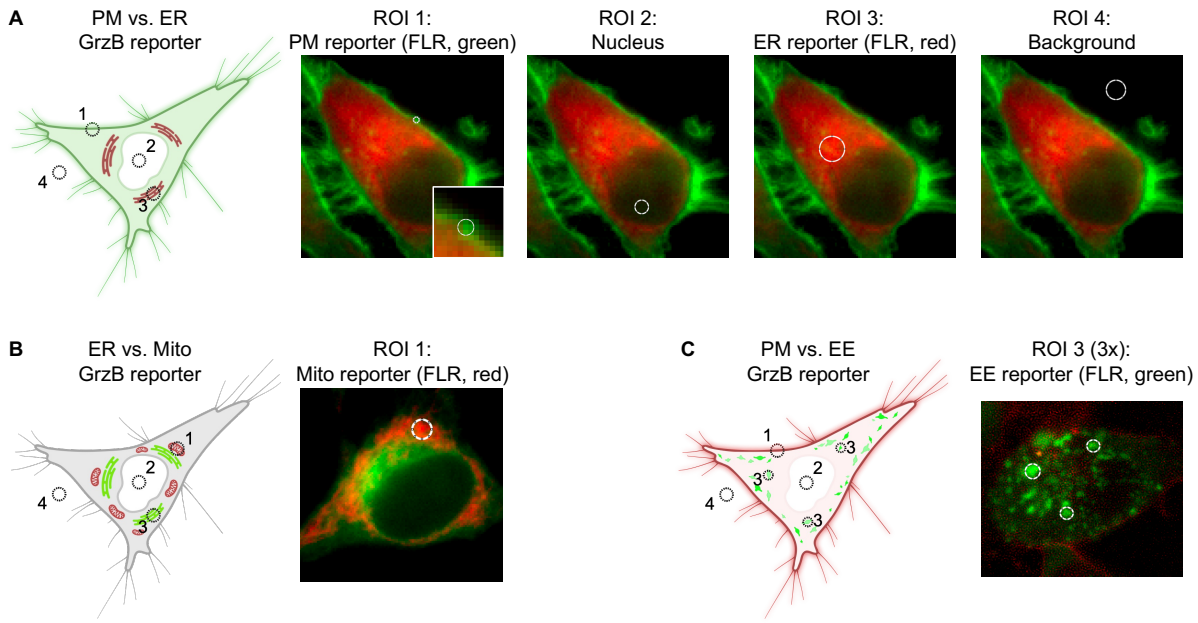

Figure 8: 4 different regions of interest (ROIs) were used to measure reporter cleavage. Schematic representations and representative fluorescence images of different reporter and ROIs. Placements and sizes of ROIs depend on cell morphology and are different for individual cells. Since cells move during live cell imaging, the placement of ROIs was adjusted. **A** PM vs. ER GrzB reporter (here: $PM^{mGFP}ER^{mC}$ GrzB reporter; representative for all other PM vs. ER GrzB reporter variants); ROI 1 = PM reporter (here: fluorescent localization reporter (FLR) connected to mGFP (green)), 2 = nucleus, 3 = ER reporter (here: FLR connected to mC (red)), 4 = background. **B** ER vs. Mito ($ER^{mGFP}Mito^{mC}$) GrzB reporter; ROI 1 = Mito reporter, 2 = nucleus, 3 = ER reporter, 4 = background (for simplicity, only ROI 1 (Mito reporter) is shown. The other ROI are like shown in (**A**)). **C** PM vs. EE ($PM^{mC}EE^{mGFP}$) GrzB reporter; ROI 1 = PM reporter, 2 = nucleus, 3 = EE reporter (3 different ROI; mean was calculated and used for further steps), 4= background (for simplicity, only ROI 3 (3x; EE reporter) is shown. The other ROI are like shown in (**A**)).

The measurement was started three time points before NK cell contact (or from the first time point of the experiment) by running the RGB_measure function. This was continued for each following frame and was stopped one time point before the target cell morphology changed due to death (strong shrinkage, membrane rupture or blebbing). Afterwards, red and green mean intensity values of each ROI were transferred to an Excel spreadsheet. For each time point, background values were subtracted from red or green values of the other ROIs. Then, background subtracted values were normalized and the offset (intact reporter state; average of the first three normalized nuclear intensity values) was subtracted (figure 9):

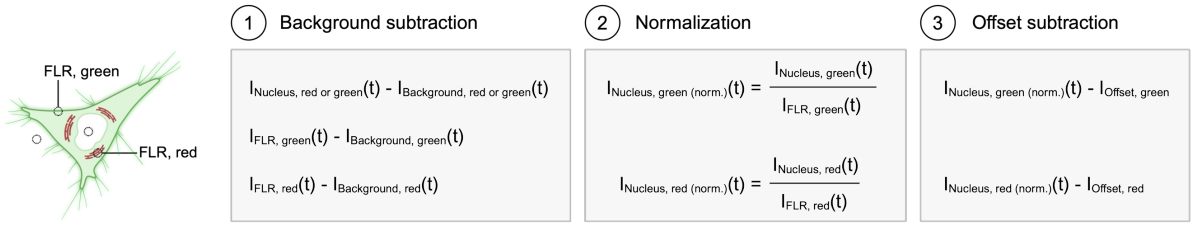

Figure 9: Calculation steps for the reporter cleavage analysis. Schematic representation of a $PM^{mGFP}ER^{mC}$ GrzB reporter cell. For simplicity, the ROI used to measure PM^{mGFP} reporter is depicted as FLR, green. ROI for ER^{mC} reporter measurement = FLR, red. With this simplification, the calculation can be applied easier to GrzB reporters with other localization domains, by defining which FLR is represented by green or red signal. **(1) Background subtraction:** For each time point, red or green intensity values of the background were subtracted from nuclear and FLR intensity values. The background corrected values were used for normalization. **(2) Normalization:** For each time point, nuclear intensity values were divided by corresponding red or green FLR values. This results in normalized red and green nuclear intensities. **(3) Offset subtraction:** the intact reporter state is represented by the offset which is the average of the first three normalized nuclear intensities. The offset value was subtracted from normalized nuclear intensities of each time point.

The resulting relative fluorescence intensity (RFI) of the nucleus was converted into % reporter cleavage. A value of 1 represents even distribution of the reporter within the cell (100 % cleavage). The last measurement – also called time of death (TOD) was set to 0 min and all preceding time points were calculated back. Reporter cleavage is displayed as % over time (mean ± SD) and x axis was cut off at – 45 min.

3.2.16 Statistics

Significant differences in perforin and GrzB levels of different NK cells were analyzed by ordinary one-way ANOVA with Tukey's multiple comparisons test embedded in GraphPad Prism 10 software (3.1.9). Significant differences in perforin and GrzB levels and killing after CMA or DMSO treatment were analyzed by repeated measures (RM) one-way ANOVA with Dunnett's multiple comparisons test (GraphPad Prism 10 software). Significant differences in NK cell killing (area under curve (AUC) values) after (S)-4'-nitro-Blebbistatin or control treatments were analyzed using RM one-way ANOVA with Tukey's multiple comparisons test (GraphPad Prism 10). Data are shown as Mean ± SD. Statistical comparison of the $PM^{mGFP}ER^{mC}$ vs. $PM^{mC}ER^{mGFP}$ GrzB reporter cleavage outcomes was performed in R using the Chi-Squared test. Statistical comparison of reporter cleavage outcomes after (S)-4'-nitro-Blebbistatin vs. control treatments was performed in R using the Cochran-Mantel-Haenszel Chi-Squared test (Agresti, 2002). Statistical significance is indicated by asterisks. ns ($P > 0.05$), * ($P \leq 0.05$), ** ($P \leq 0.01$), *** ($P \leq 0.001$), **** ($P \leq 0.0001$).

4. Results

The successful initiation of apoptosis during granule-mediated NK cell cytotoxicity depends on the transfer of granzymes into the target cell. In this context, the interplay of perforin and GrzB was investigated in depth. Perforin oligomerizes into pores paving the way for GrzB to enter the cytosol of the target cell. Whether this entry occurs directly at the PM (PM pore model) or after membrane repair-induced endocytosis (endocytosis model), however, remains a subject of controversial debate (Prager and Watzl, 2019, Spicer et al., 2022). Both pathways might even have a mutual supportive role with possible dependency on perforin concentration (Browne et al., 1999). Moreover, other contributing factors like NK cell type or the target cell itself may influence the entry mechanism. Based on a previous work (Bruning, 2020), these factors will be analyzed here.

4.1 Development of a fluorescent localization reporter (FLR) system for uncovering the GrzB entry mechanism into target cells

In the past, fluorescent localization reporters (FLRs) have been extensively used to detect and compare the activities of different proteases within target cells during NK cell mediated cytotoxicity (chapter 1.4). Within these studies, cytosolically localized FLRs were sufficient to determine the dominant protease used per kill, but not its specific site of activity. However, decoding the entry mechanism of GrzB into target cells requires a different strategy. Novel tandem FLRs for GrzB activity were designed (Bruning, 2020), which cover the two main GrzB entry models – PM pore entry and endocytic uptake.

4.1.1 $PM^{mGFP}ER^{mC}$ GrzB reporter expressing HeLa $CD48^{+}$ cells show correct localization of PM and ER reporters

To address the PM pore and endocytosis model in parallel, we considered the use of two GrzB specific reporters localized in proximity to the presumed GrzB entry sites in target cells. Once secreted into the immune synaptic cleft, perforin oligomerizes into prepores which insert into the target cell PM as arcs or rings (Metkar et al., 2015). After passing through these pores, GrzB entry could be detected immediately by a PM-localized fluorescent reporter. On the contrary, if GrzB is taken up via endocytosis and released into the target cells' cytosol, a reporter localized at the endoplasmic reticulum (ER) could cover the endocytosis model.

For the assembly of our novel GrzB-specific FLR system, we utilized the existing FLR strategy and its advantages (highlighted in chapter 1.4). To fit our model, we modified the preexisting FLRs' individual building blocks (Bruning, 2020). First, nuclear export signaling (NES) domains were replaced with localization domains for the PM and ER. Previously, FLR constructs with PM or ER localization domains were developed specifically for the characterization of Caspase-8 activity (Beaudouin et al., 2013). Localization of the reporter to the PM was induced by a domain prone to myristoylation and palmitoylation, which was derived from Lyn kinases' N-terminus (Zacharias et al., 2002), whereas a truncated Calnexin, an ER chaperon (Bergeron et al., 1994), directed the FLR towards the ER membrane (Beaudouin et al., 2013). Consequently, we relied on these published localization domains – MyrSnap and Calnexin. The PM localization domain is abbreviated here as MyrSnap, with the term Snap referring to SNAP-tags (Keppler et al., 2004), which are directly coupled to the PM domain. Although included in the construct, its labeling features have not yet been used, hence it can be neglected in our approach. Additionally, we only want to detect activity of GrzB. The sequence VGPD'FGR (short: VGPD), derived from the protein kinase DNA-PKc (Liesche et al., 2018), is targeted by GrzB and its cleavage can indicate a GrzB activity as shown before using other FLRs (Liesche et al., 2018, Prager et al., 2019, Bönnemann, 2023). Hence, VGPD was embedded in both linker sequences of the tandem FLR for GrzB activity. Finally, parallel analysis of the two proposed GrzB entry mechanisms requires the distinction of PM and ER FLRs, which is achieved using different fluorescent proteins (here: PM – mGFP, ER – mCherry). The design of the tandem FLR for GrzB activity (GrzB reporter) construct is outlined schematically in figure 10**A**. Previously, we already transfected HeLa $CD48^+$ successfully with the GrzB reporter construct (Bruning, 2020). Here, we once again generated HeLa $CD48^+$ GrzB reporter cells and expanded the validation of reporter localization. Upon expression, PM and ER reporters are separated successfully and are localized at PM (green) and within the cell, presumably at the ER (red) (figure 10**B**). To qualitatively confirm the correct localization of the FLRs, different organelles were stained (figure 10**C**). Since the transfection efficiency in the population is not 100%, the fluorescence images also show cells without or only low reporter expression, which are nevertheless stained by the immunostaining and dyes. Staining of nucleus (DAPI), cis and trans Golgi network (GM130; Golgin97), lysosomes (LAMP1) and mitochondria (BioTracker 405 Mitochondria) show organelle-specific structures, yet they show a structurally distinct distribution than the ER reporter. Additionally, the reporter cells were stained for protein

disulfide isomerase (PDI), which is an ER localized protein (Noiva and Lennarz, 1992). Although low unspecific nuclear staining was observed, the distribution of strong PDI staining is similar compared to the ER reporter, suggesting that the ER reporter is localized correctly.

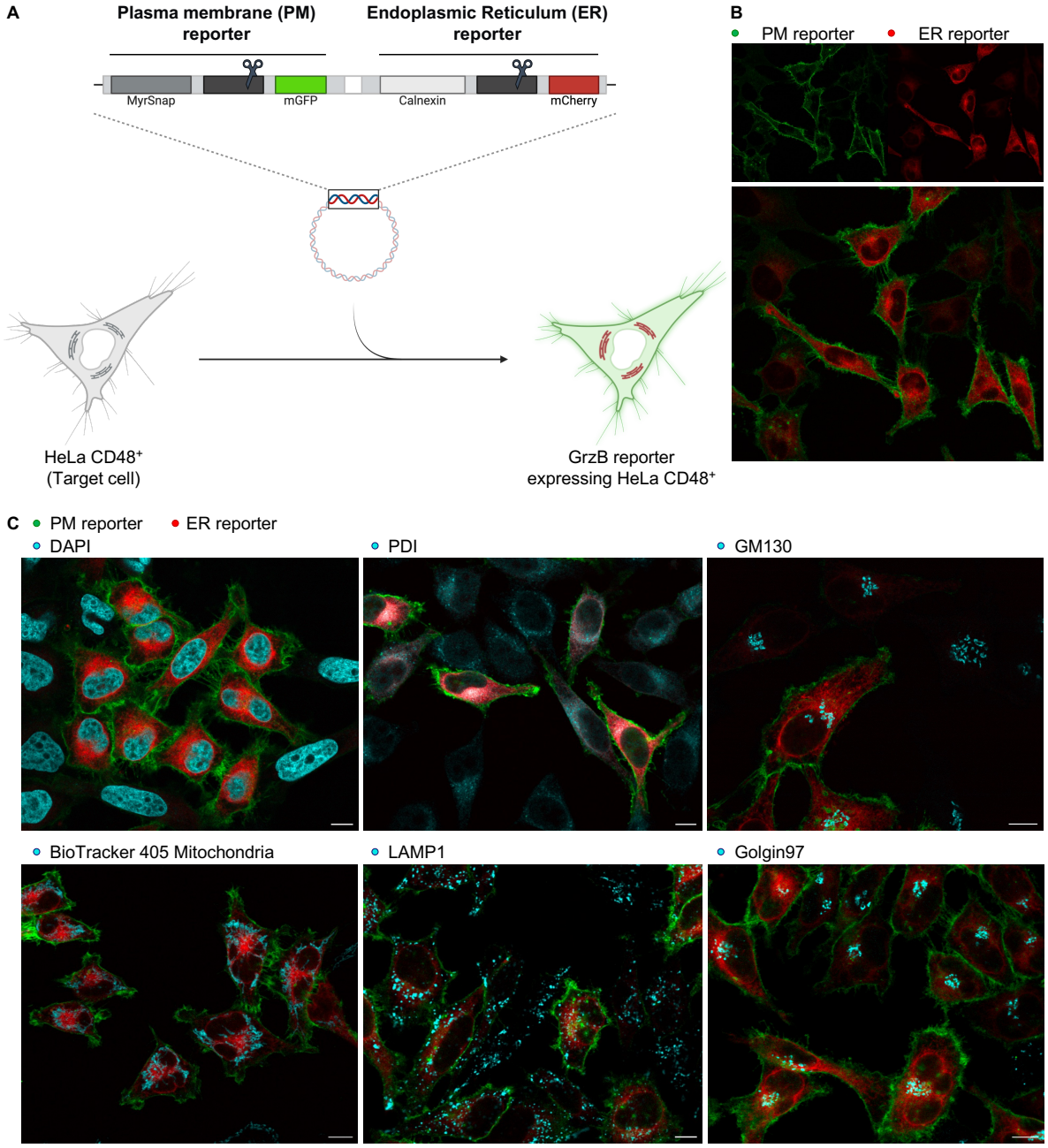

Figure 10: HeLa CD48⁺ PM^{mGFP}ER^{mC} GrzB reporter cells show correct localization of the PM reporter as well as the ER reporter. A schematic design of the PM^{mGFP} vs. ER^{mC} FLR construct for GrzB activity (PM^{mGFP}ER^{mC} GrzB reporter). PM reporter localization domain: Myr. ER reporter localization domain: Calnexin. Dark gray boxes represent the cleavable linker sequence (VGPD'FGR) while scissors symbols indicate GrzB cleavage sites (VGPD'FGR). The white box represents the viral T2A sequence. HeLa CD48⁺ target cells are transfected with the PM^{mGFP}ER^{mC} GrzB reporter construct. **B** Representative images of HeLa CD48⁺ PM^{mGFP}ER^{mC} GrzB reporter cells. PM reporter = green; ER reporter = red. **C** Qualitative confirmation of ER reporter localization. GrzB reporter cells were stained with DAPI (nucleus), BioTracker 405 Mitochondria dye (Mitochondria) or primary antibodies against PDI (ER), GM130 (cis-golgi), LAMP1 (lysosomes) or Golgin97 (trans-golgi) and secondary AF405 conjugated antibody. Merged images: PM reporter (red); ER reporter (green); stained organelles (cyan). Fluorescence images were acquired with 40 x magnification (MICA WideFocal microscope). Scale bars are 10 µm.

4.1.2 NK92 cells induce three different reporter cleavage outcomes in $PM^{mGFP}ER^{mC}$ GrzB reporter cells

After assembling our GrzB reporter system, we wanted to investigate whether the GrzB reporter can detect GrzB activity. To detect GrzB activity at the PM and the ER and thus determine the GrzB entry mechanism, the fluorescence intensity at the PM, the ER and the cytosol/nucleus is measured over time. In the intact state, both FLRs are bound to their specific localization domains with limited distribution within the cell. This state is represented by a high fluorescence signal at the PM (mGFP) and the ER (mCherry) and low cytosolic/nuclear fluorescence signal. As soon as an NK cell engages the reporter cell and executes its cytotoxicity by releasing GrzB, GrzB enters the target cell (Prager and Watzl, 2019). Figure 11**A** depicts a hypothetical scenario of GrzB entry via perforin pores in the PM: Upon binding of the VGPD-containing linker sequence, GrzB cleaves the sequence and thus separates the localization domain and mGFP. The separation enables diffusion of mGFP within the cell, causing a gradual increase of the cytosolic/nuclear mGFP signal, accompanied by a relative decrease in mGFP signal at the PM (Beaudouin et al., 2013). This redistribution indicates the site of GrzB activity and hence an assumption on the GrzB entry site can be made. While the PM reporter is cleaved in this scenario, the ER reporter stays intact until time of death (TOD; last measurement, set to 0 min), indicating an GrzB entry via PM pores. In the context of FLRs, the TOD was described as the time point before the cell morphologically shows death initiation by strong shrinkage and blebbing (Liesche et al., 2018). Previously, this has already been established for our GrzB reporter and is important to minimize measurement artifacts due to strong volume compression (Bruning, 2020).

To investigate whether the FLRs can detect GrzB activity within killed target cells in an experimental setup, NK92 cells were used as effector cells. The NK cell line NK92 preferentially used GrzB during the killing of HeLa $CD48^+$ reporter target cells (Bönnemann, 2023), and provides a simple and fast method to evaluate our GrzB reporter system. After live cell imaging of NK92 cells with HeLa $CD48^+$ $PM^{mGFP}ER^{mC}$ GrzB reporter cells, killing events mediated by a single NK92 cell were categorized into three different cleavage outcomes based on a certain threshold value. The establishment of this threshold value (20 %) is based on a non-cleavable GrzB reporter and will be further specified in chapter 4.1.4.

Individual reporter cells, representative for each outcome, show the reporter distribution of the intact state (first measurement), 0 min (last measurement, TOD) and 3 min after TOD in separate channels (figure 11**B**, left). The quantification of the reporter cleavage is shown as % reporter cleavage over time (figure 11**B**, right). In some cases (19 cells), the PM reporter as well as the ER reporter remained intact during target cell killing and were still localized at their specific localization domains at TOD (0 min). Quantification showed a mean PM reporter cleavage of 9.2 % and for the ER reporter of 5.9 % at TOD. Even beyond TOD (+ 3 min), no reporter redistribution was observed qualitatively (top row, figure 11**B**). In these cells, no GrzB activity was detected by the FLRs (outcome 1) assuming these cells were killed by other mechanisms. However, in all other cases, GrzB activity was detected by the FLRs: In most cases (24 cells), a strong PM reporter redistribution was observed at TOD (80.4 %), starting approximately 9 – 12 min before death (middle row, figure 11**B**). The ER reporter remained intact (11.8 %), thus indicating that GrzB was solely active at the PM (outcome 2). In only a few cases (2 cells), a redistribution of the ER reporter was also observed, although starting with a time delay of around 9 min compared to the PM reporter. Moreover, 33.2 % ER reporter cleavage was observed at TOD whereas the PM reporter reached 117.5 % cleavage (bottom row, figure 11**B**), indicating that despite the additional activity of GrzB at the ER, GrzB activity predominates at the PM (outcome 3). Interestingly, we observed that the mean PM reporter cleavage at TOD was higher in cells categorized into outcome 3 than of cells of outcome 2.

To conclude, our GrzB reporter system enables the detection of GrzB activity at two different sites (PM and ER) within killed target cells. Reporter cells killed with detectable GrzB activity show the main GrzB activity at the PM and if at all only a minor activity at the ER, hence favoring the PM pore entry model.

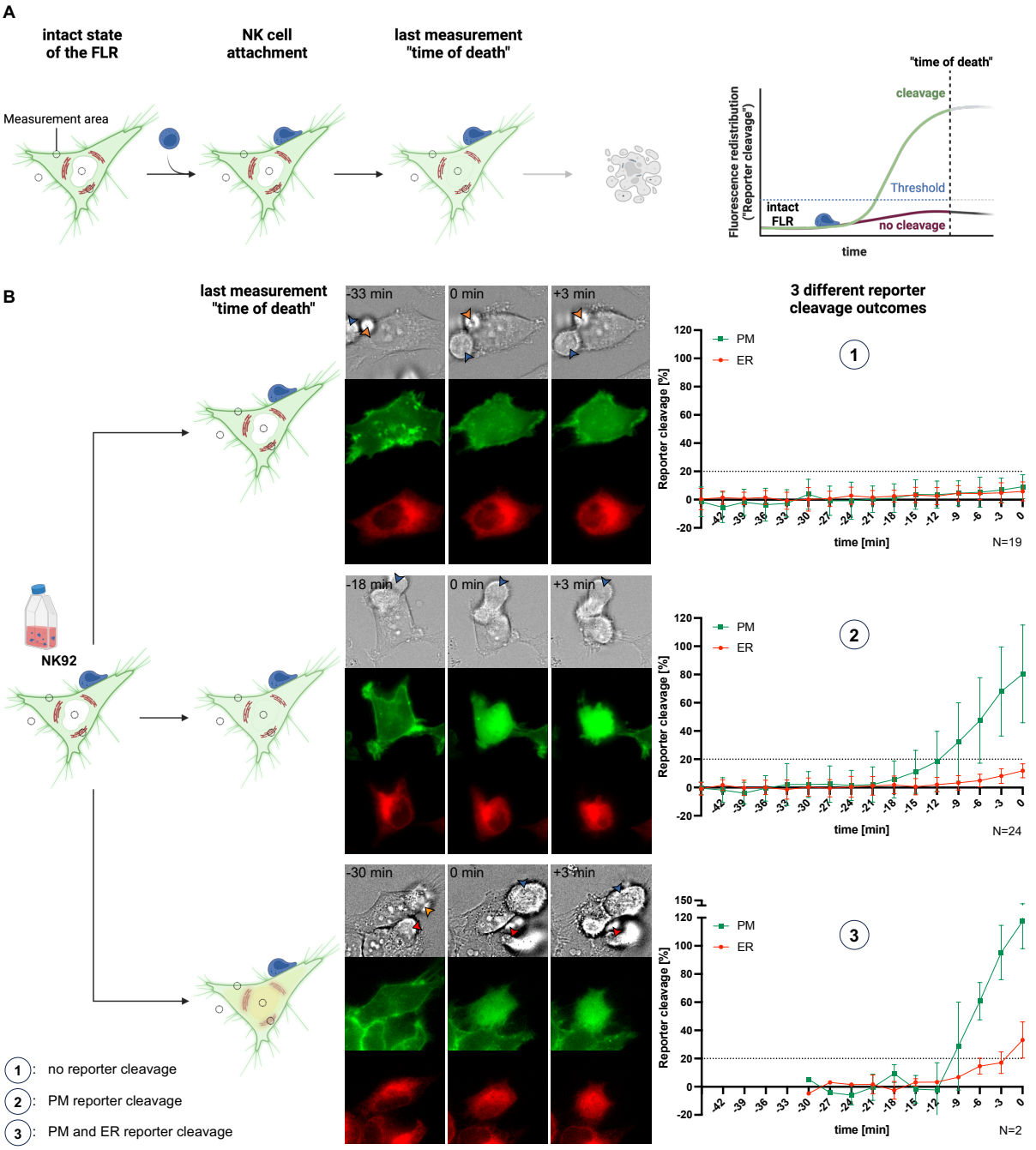

Figure 11: NK92 cell mediated killing of HeLa CD48^{+} PM^{mGFP}ER^{mC} GrzB reporter cells show three different GrzB activity scenarios at time of death (0 min). A Schematic presentation of reporter cleavage and redistribution. **B** Co-culture of NK92 cells with HeLa CD48^{+} PM^{mGFP}ER^{mC} GrzB reporter cells (E:T ratio of 1:1) for 5 h during live cell imaging (3 min image acquisition interval). Three different reporter cleavage outcomes were observed: no reporter cleavage (outcome 1, top row), only PM reporter cleavage (outcome 2, middle row) or cleavage of both FLRs with dominant PM reporter cleavage (outcome 3, bottom row). For each outcome, representative snapshots of a reporter cell killed by an NK92 cell show the reporter distribution at the first measurement time point (intact reporter state), at 0 min (time of death; TOD) and +3 min. PM reporter = green, ER reporter = red. Brightfield images show GrzB reporter cells and NK92 cells (marked by blue arrows); red arrows show NK92 cells in proximity to the killed reporter cell, that do not contribute to the kill; orange arrows indicate cell debris/other non-NK cell particles (left panel). Quantification of PM as well as ER reporter cleavage is presented as reporter cleavage (%) over time with TOD (last measurement) being set to 0 min. Preceding time points (3 min interval) were calculated back (right panel). Pooled data include 6 independent experiments (N = 5 – 11 cells per experiment, N = 46 cells in total) and are shown as Mean ± SD. Images were acquired using the Axio Observer 7, 40 x magnification.

4.1.3 Both FLRs of the PM^{mGFP}ER^{mC} GrzB reporter remain intact in the absence of GrzB

Next, we investigated whether the reporter cleavage is mediated specifically by GrzB alone. Cell death pathways are multistep processes carried out by a variety of endogenous proteases which become active once triggered by internal or external stimuli like death receptors or granzymes (Elmore, 2007). Besides GrzB, four other granzymes can be secreted by human NK cells (Prager and Watzl, 2019). These exogenous as well as endogenous proteases may have the potential to target and cleave the VGPD linker sequence of FLRs.

Previously, much attention has been focused on verifying the protease-specific cleavage of FLR linker sequences by inhibiting GrzB with Serpin B9 or inducing the Caspase-8 cascade via soluble trimerized CD95L (Liesche et al., 2018)or by using NK92 cells which lack GrzB (Bönnemann, 2023). Here, we use NK92 GrzB knockout (KO) cells which provide a simple but valuable control to verify the exclusive GrzB-mediated cleavage of our PM vs. ER GrzB reporter.

The NK92 GrzB KO cells were generated and characterized thoroughly in a previous study (Bönnemann, 2023). For this study, wild type (wt) NK92 and NK92 GrzB KO cells were stained for GrzB and perforin once again (figure 12**A**). As expected, comparison of GrzB levels in wt and KO cells validate the loss of GrzB in GrzB KO cells whereas perforin levels were unaffected by the GrzB KO. To investigate whether the PM and ER reporters are cleaved in the absence of GrzB, live cell imaging of NK92 GrzB KO cells and HeLa CD48^{+} PM^{mGFP}ER^{mC} GrzB reporter cells was performed. Within 5 h, only a few reporter cell deaths were recorded. Without GrzB as a potential weapon targeting the linker sequence, we suggest that the FLRs remain intact regardless of the NK92 GrzB KO cell number contributing to killing. Consequently, reporter cells engaged by more than one NK92 GrzB KO cell were also included in the analysis. Intact localization of PM and ER reporters was detected in killed reporter cells (12 cells) during attachment of NK92 GrzB KO cells until TOD (1.4 % PM reporter cleavage; – 0.6 % ER reporter cleavage). Furthermore, no redistribution of FLRs was observed qualitatively beyond TOD, when reporter cells broke down into apoptotic bodies (figure 12**B**) confirming the specific GrzB-mediated VGPD linker cleavage also in our PM vs. ER reporter context. Additionally, we observed a prolonged time until reporter cells died (mean time from first NK contact until TOD: 209.5 ± 39.3 min), which might hint at death receptor- or granzyme A-mediated killing.

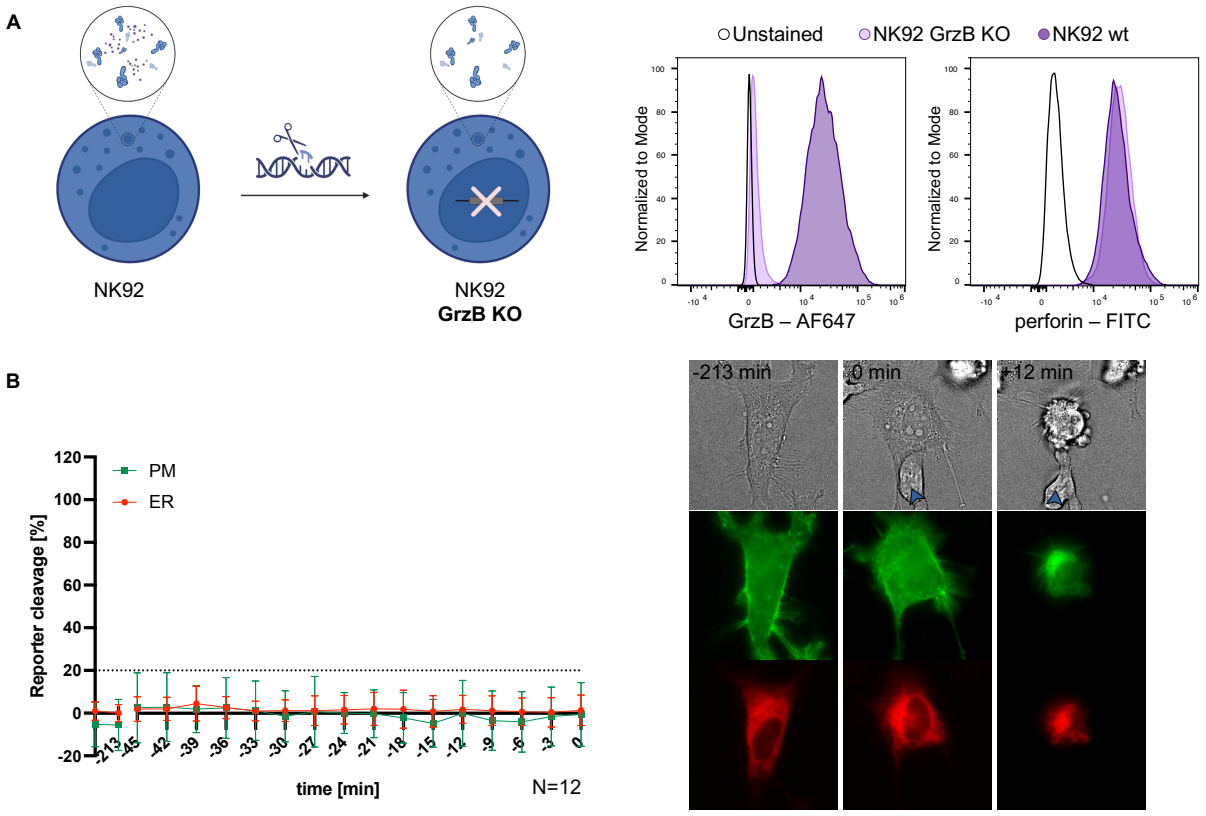

Figure 12: Both FLRs are not cleaved in the absence of GrzB, confirming the specificity for the detection of GrzB activity. A Schematic representation of CRISPR/Cas9-mediated GrzB KO in NK92 (left). Confirmation of GrzB KO in NK92 cells by intracellular flow cytometry staining of GrzB and perforin in NK92 wt and NK92 GrzB KO cells. The GrzB KO did not influence the intracellular perforin level. light purple = NK92 GrzB KO cells, dark purple = NK92 wt cells (right). **B** Co-culture of NK92 GrzB KO cells with HeLa CD48^{+} PM^{mGFP}ER^{mC} GrzB reporter cells (E:T ratio of 1:1) for 5 h during live cell imaging. Quantification of PM as well as ER reporter cleavage is presented as reporter cleavage (%) over time. Only outcome 1 (no reporter cleavage) was observed in killed PM^{mGFP}ER^{mC} GrzB reporter cells (left). Representative images of a PM^{mGFP}ER^{mC} GrzB reporter cell killed by an NK92 GrzB KO cell show the reporter distribution at the first measurement time point (intact reporter state, -213 min), at 0 min (TOD) and +12 min after TOD. PM reporter = green, ER reporter = red. Brightfield images show GrzB reporter cells as well as NK92 cells which are marked by blue arrows (right). Pooled data include 4 independent experiments (N = 2 – 4 cells per experiment N = 12 cells in total). Data are shown as Mean ± SD. Images were acquired using the Axio Observer 7, 40 x magnification.

4.1.4 GrzB activity at ER is confirmed by a non-cleavable ER reporter which sets threshold for specific cleavage at 20 %

When target cells shrink, the internal background fluorescence may increase without any of the FLRs being cleaved. Therefore, we investigated whether the observed minor activity of GrzB at the ER in figure 11**B** (outcome 3) is specifically induced by GrzB or is the result of a measurement artifact caused e.g. by cellular volume compression. We approached this issue by exchanging the VGPD linker sequence of the ER reporter with a non-cleavable linker sequence consisting of an alanine stretch (figure 13**A**). The substrate specificity of GrzB strictly requires an aspartic acid on P1 upstream of the cleavage site, while the choice of amino acids in positions P4 – P2 are less strict but indicate certain preferences (Thornberry et al., 1997, Harris et al., 1998). By replacing all four amino acids of the positions P4-P1 with alanine, the sequence cannot be cleaved by GrzB. Therefore, we hypothesize that a non-cleavable ER reporter will not show GrzB-induced ER reporter cleavage and may help to establish a threshold to distinguish between background noise and cleavage.

HeLa CD48+ cells were transfected successfully with the $PM^{mC}ER^{mGFP,\ non\text{-}cl.}$ GrzB reporter construct (figure 13**A**, fluorescence images). Importantly, the fluorophores in this construct are switched (PM – mCherry; ER – mGFP). In the co-culture of $PM^{mC}ER^{mGFP,\ non\text{-}cl.}$ GrzB reporter cells with primary preactivated NK cells, dead target cells reported two outcomes: In the first outcome (17 cells, figure 13**B** top), no GrzB activity was detected (6.5 % PM and 2.98 % ER reporter cleavage). In contrast, the second outcome indicates a strong GrzB activity at the PM (79.3 %) starting 12 min before reporter cell death (26 cells, figure 13**B** bottom) but no ER activity (7.3 %). However, the third outcome which was observed before (compare figure 11**B** bottom row) with a dominant GrzB activity at the PM and minor activity at the ER did not occur anymore. This suggests that the detected activity at the ER was specifically induced by GrzB. During analysis of individual cells, PM reporter cleavage of up to 19.2 % was observed at TOD (13.8 % ER, no GrzB activity group), without a visible PM or ER reporter redistribution in the respective fluorescence images (data not shown). The highest measured value for the ER reporter was 18.5 % at TOD (corresponding PM reporter: 13 %, no GrzB activity group). Again, no clear redistribution was visually observed (data not shown). Therefore, we decided to set a threshold of 20 % for specific reporter cleavage for both FLRs. Accordingly, results below 20 % are considered as background noise due to rounding or shrinkage of cells. This threshold

was used to categorize all previous and subsequent results into the described outcomes.

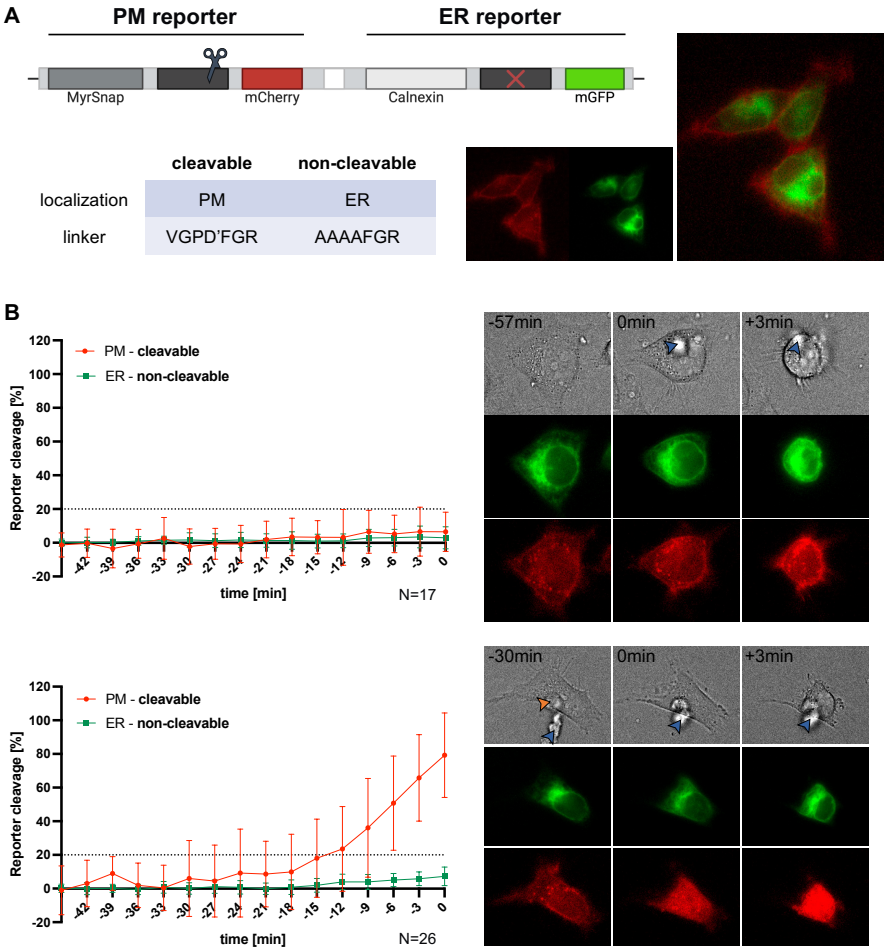

Figure 13: Non-cleavable ER reporter confirms activity of GrzB at the ER and sets threshold for specific cleavage at 20 %. A Design of the PM^{mC} vs. $ER^{mGFP,\ non\text{-}cl.}$ GrzB reporter construct. 'X' symbol within the dark box = non-cleavable linker sequence (AAAAFGR). The table summarizes which reporter part owns a cleavable and which owns a non-cleavable linker sequence. Representative image of HeLa $CD48^{+}$ $PM^{mC}ER^{mGFP,\ non\text{-}cl.}$ GrzB reporter cells. PM reporter = red, ER reporter = green (40 x magnification, Axio Observer 7). **B** Co-culture of pre-activated NK cells (isolated from whole blood and cultured for 3 – 4 weeks) with HeLa $CD48^{+}$ $PM^{mC}ER^{mGFP,\ non\text{-}cl.}$ GrzB reporter cells (E:T ratio of 1:1) for 3 h during live cell imaging. Quantification of PM as well as ER reporter cleavage (reporter cleavage (%) over time; left panel) showing no reporter cleavage (outcome 1; top row) and PM reporter cleavage but no ER reporter cleavage (outcome 3; bottom row). Representative snapshots of $PM^{mC}ER^{mGFP,\ non\text{-}cl.}$ GrzB reporter cells killed by pre-activated NK cells showing reporter distribution of the intact reporter state and at 0 min. Brightfield images show GrzB reporter cells and pre-activated cells (blue arrows); orange arrow indicates cell debris/other non-NK cell particle. Pooled data include 5 independent experiments (n = 3 donors; N = 2 – 14 cells per experiment, N = 43 cells in total). Data are shown as Mean ± SD. Images were acquired using the Axio Observer 7, 40 x magnification.

4.2 Dependence of the GrzB entry mechanism on the NK cell type

NK cell cytotoxicity and expression of GrzB and perforin can be increased by activating NK cells e.g. with IL-2 (Bhat and Watzl, 2007). In addition to the NK cell line NK92 (figure 11**B**), we frequently use pre-activated primary NK cells (cultured for at least 3 weeks in the presence of IL-2) and resting primary NK cells (freshly isolated and rested overnight in low dose IL-15 – which does not affect GrzB expression (Bönnemann, 2023)). Hence, after validating the functionality of our GrzB reporter system, we wanted to answer the question of whether the GrzB entry mechanism is influenced by the activation state of the NK cells.

4.2.1 Expression levels of perforin and GrzB differ between NK92, primary pre-activated and primary resting NK cells

First, we assessed whether NK92 cells, pre-activated and resting primary human NK cells show differences regarding the expression levels of GrzB and perforin, which were analyzed by intracellular flow cytometry staining (figure 14). The quantification reveals a higher expression of GrzB in NK92 cells than in primary human NK cells, which in turn show no significant differences in GrzB levels between pre-activated and resting states. Conversely, primary resting NK cells contain higher levels of perforin compared to pre-activated NK cells and NK92, with no significant differences between the latter two, although NK92 cells tend to express more perforin than pre-activated NK cells. Interestingly, two distinguishable populations can be observed in resting NK cells (representative histograms) in the perforin staining. For GrzB, however, this distinction was less clear. Tracing back of the smaller population with lower fluorescence intensity leads to CD56 bright NK cells, while the larger population with higher fluorescence intensity originates from CD56 dim NK cells (data not shown).

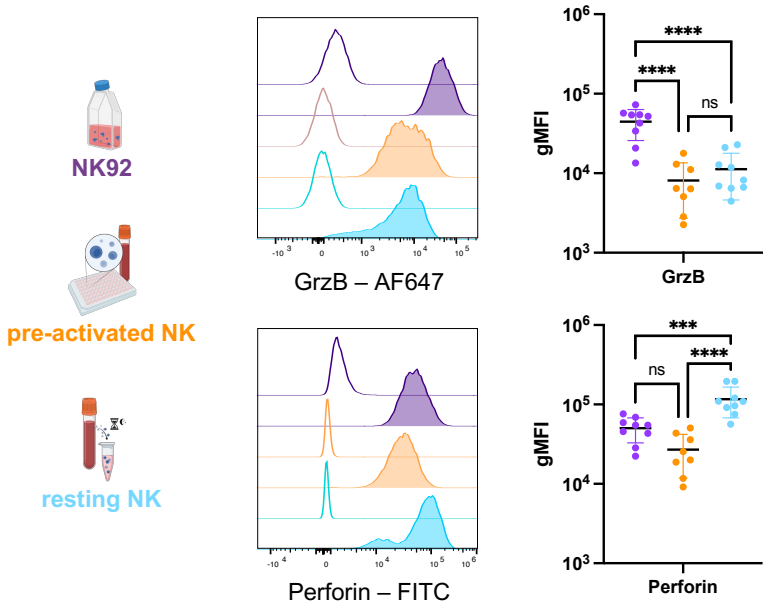

Figure 14: The expression levels of perforin and GrzB differ between NK cell types. NK cells were isolated from whole blood, and either were cultured for 3 – 4 weeks or were rested overnight with low dose of IL-15 (0.5 ng/ml). Flow cytometry analysis of intracellular levels of GrzB (top row) and perforin (bottom row) in NK92 cells (purple), pre-activated NK cells (orange) and resting NK cells (blue). NK92 cells, pre-activated NK cells and resting NK cells were analyzed on the same day. Representative normalized (normalized to mode) histograms with corresponding unstained control (left panel). gMFI of GrzB and perforin levels (geoMean stained – geoMean unstained; right panel). Data are shown as Mean ± SD. Data include 9 independent experiments (pre-activated NK cells: n = 8 donors; resting NK cells: n = 8 donors; 1 donor was measured twice after repeated isolation on different time points). Statistical analysis was performed by ordinary one-way ANOVA with Tukey's multiple comparisons test with statistical significance indicated by asterisks: * $P \leq 0.05$, ** $P \leq 0.01$, *** $P \leq 0.001$, **** $P \leq 0.0001$.

4.2.2 GrzB is predominately active at the PM independent of the NK cell type

We wondered whether these differences in the GrzB and perforin levels eventually lead to an increased uptake of GrzB via endocytosis or may even cause a switch in the favored entry mechanism, such that the endocytic uptake dominates over the PM pore entry. Therefore, we investigated which outcomes can be induced in $PM^{mGFP}ER^{mC}$ GrzB reporter cells by pre-activated NK cells (figure 15). Consistent with the NK92 cell data (figure 11**B**), pre-activated NK cells induce 3 cleavage outcomes. Some reporter cells died without detectable GrzB activity (outcome 1, 24 cells; figure 15, top; PM: 7.2 %, ER: 5.6 % at TOD). All other analyzed cells displayed GrzB activity. Starting 9 – 12 min before death, most cells only show a strong GrzB activity at the PM (outcome 2, 85 cells; figure 15, middle). At TOD, the PM reporter cleavage was up to 81.0 %, whereas no ER reporter cleavage (10.1 %) was detected. Killing events assigned to the third outcome (13 cells; figure 15, bottom) demonstrate a strong GrzB activity at the PM (103.1 % at TOD) and a lower activity at the ER (33.9 % at TOD). Like for NK92 cells (figure 11**B**, bottom), we also observed a higher PM reporter

cleavage in this group, although the onset of cleavage was earlier (12 – 15 min before TOD).

To conclude, the pre-activated primary NK cells induce the main GrzB activity at the PM, hence favoring the PM pore model for GrzB entry.

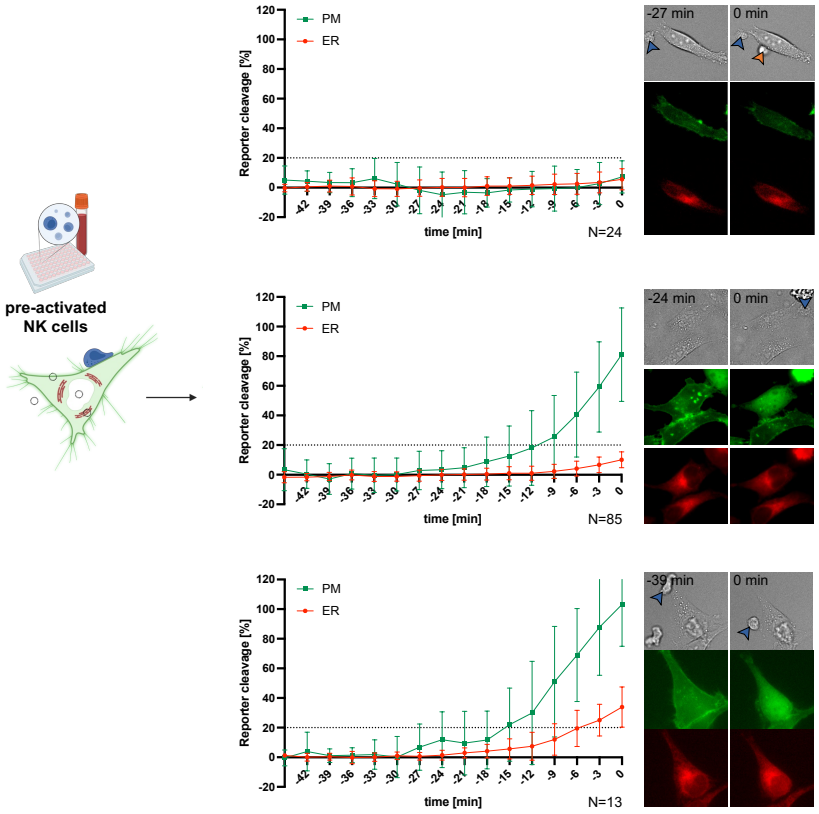

Figure 15: Killing of HeLa CD48^{+} PM^{mGFP}ER^{mC} GrzB reporter cells by pre-activated NK cells shows GrzB activity predominantly at the PM. Pre-activated NK cells (isolated from buffy coats (BC) or whole blood and cultured for 3 – 4 weeks) were co-cultured with HeLa CD48^{+} PM^{mGFP}ER^{mC} GrzB reporter cells (E:T ratio of 1:1) for 3 h during live cell imaging. Three different reporter cleavage outcomes were observed: no reporter cleavage (outcome 1; top row), only PM reporter cleavage (outcome 2; middle row) or cleavage of both FLRs with dominant PM reporter cleavage (outcome 3; bottom row). Quantification of reporter cleavage (left panel). Representative snapshots of a PM^{mGFP}ER^{mC} reporter cell killed by a pre-activated NK cell show the reporter distribution of the intact reporter state and at 0 min (TOD). PM reporter = green, ER reporter = red. Brightfield images show GrzB reporter cells and pre-activated NK cells (blue arrows); orange arrows = cell debris/other non-NK cell particles (right panel). Pooled data include 10 independent experiments with N = 122 cells in total (6 experiments from BC derived NK cells, n = 3 donors, N = 61 cells with N = 7 – 14 cells per experiment; 4 experiments from whole blood derived NK cells, n = 4 donors, N = 61 cells with N = 14 – 16 cells per experiment). Data are shown as Mean ± SD. Images were acquired using the Axio Observer 7, 40 x magnification.

Next, we analyzed whether the preferred GrzB entry is different when using resting primary NK cells, which show the highest perforin levels compared to the other NK cells. The differences in GrzB and perforin levels observed between CD56dim and CD56bright resting primary NK cells (figure 14) were neglected here, since we added unsorted resting primary NK cells to PM^{mGFP}ER^{mC} GrzB reporter cells (figure 16). Like NK92 and pre-activated primary NK cells, resting primary NK cells induced the 3

cleavage outcomes in reporter cells. Most resting NK cells killed their targets without detectable GrzB activity at PM (7.2 % at TOD) or ER (3.95 % at TOD) (22 cells, outcome 1, figure 16, top). In outcome 2 (14 cells, figure 16, middle) the predominant GrzB activity was displayed at the PM (62.2 % at TOD) while none was found at the ER (12.5 % at TOD). Onset of PM reporter cleavage was 12 – 15 min before death. Only a few events (4 cells) of GrzB activity at PM (108.5 % at TOD, onset 9 – 12 min before TOD) and ER (37.4 % at TOD) were detected (outcome 3, figure 16, bottom). Again, GrzB activity predominates at the PM and thus favoring the PM pore entry model.

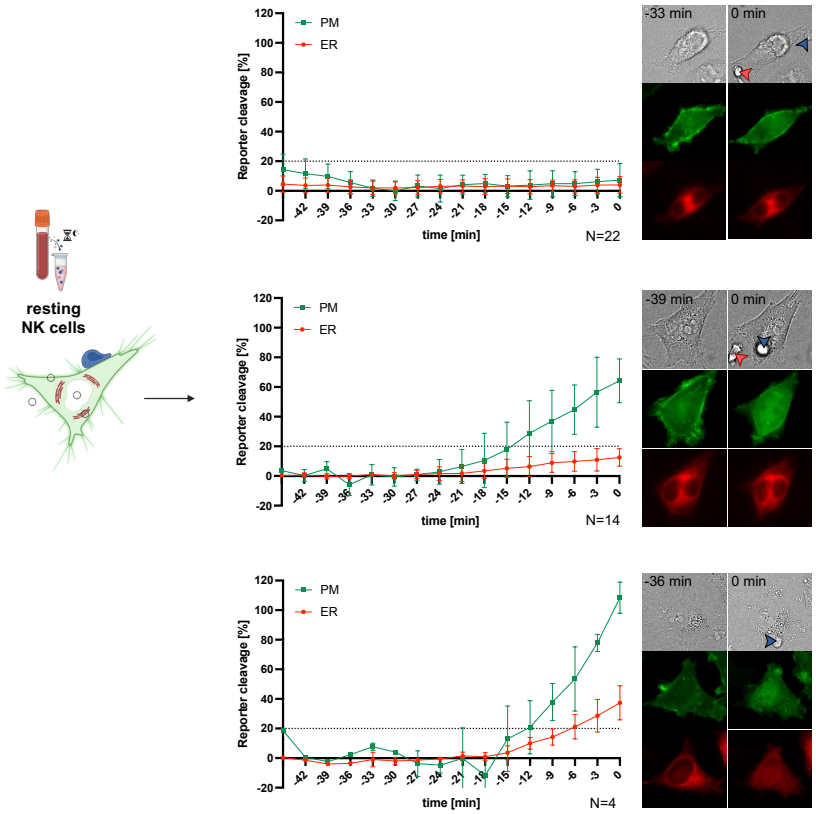

Figure 16: Killing of HeLa CD48⁺ PM^{mGFP}ER^{mC} GrzB reporter cells by resting NK cells show GrzB activity predominantly at the PM. Freshly isolated NK cells (isolated from whole blood) were rested overnight with low dose IL-15 (0.5 ng/ml) and then co-cultured with HeLa CD48⁺ PM^{mGFP}ER^{mC} GrzB reporter cells (E:T ratio of 1:1) for 3 h during live cell imaging. Three different reporter cleavage outcomes were observed: no reporter cleavage (outcome 1; top row), only PM reporter cleavage (outcome 2; middle row) or cleavage of both FLRs with dominant PM reporter cleavage (outcome 3; bottom row). Quantification of reporter cleavage (left panel). Representative snapshots of a PM^{mGFP}ER^{mC} reporter cell killed by an resting NK cell show the reporter distribution of the intact reporter state and at 0 min (TOD). PM reporter = green, ER reporter = red. Brightfield images show GrzB reporter cells and resting NK cells (blue arrows); red arrows = resting NK cells in proximity of the killed GrzB reporter cell but do not contribute to the kill (right panel). Pooled data include 4 independent experiments (n = 4 donors, N = 40 cells with N = 8 – 12 cells per experiment). Data are shown as Mean ± SD. Images were acquired using the Axio Observer 7, 40 x magnification.

The side-by-side comparison of all analyzed cells (figure 17) shows mostly differences between the proportions of kills without (light gray) and with (medium and dark gray)

detected GrzB activity. Focusing on the proportions of cells with measured GrzB activity, the dominant presence of GrzB activity at the PM becomes evident (NK92: 53.33 %, pre-activated NK cells: 69.67 %, resting NK cells: 35 %), hence strengthening the role of PM pores for GrzB entry. Furthermore, it is underlined that the proportions in which ER activity – i.e. endocytic uptake - was observed in addition to the dominant PM activity are in the minority (NK92: 4.44 %, pre-activated NK cells: 10.66 %, resting NK cells: 10 %), regardless of the three NK cell types tested. Consequently, we suggest that the NK cell activation state is not decisive for the entry mechanism of GrzB into target cells.

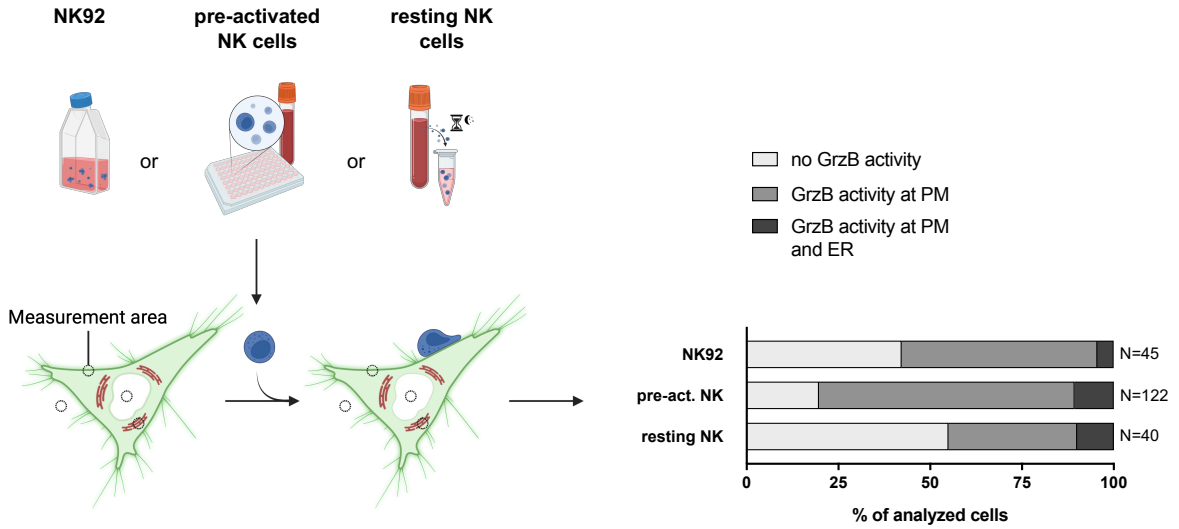

Figure 17: When GrzB is used for killing, GrzB activity predominates at the PM regardless of the NK cell type. Summary of reporter cleavage data from figures 11 (NK92 cells), 15 (pre-activated NK cells) and 16 (resting NK cells) presented as parts of whole stacked bar graphs with each bar representing the results for one of the NK cell types. The segments represent the three observed reporter cleavage outcomes as parts of all analyzed cells (%): light gray = no reporter cleavage (outcome 1, no GrzB activity), medium gray = only PM reporter cleavage (outcome 2, GrzB activity at PM), dark gray = cleavage of both FLRs with dominant PM reporter cleavage (outcome 3, GrzB activity at PM and ER).

4.3 mGFP-labelled ER reporter is superior in detecting GrzB activity at the ER

Using the $PM^{mGFP}ER^{mC}$ GrzB reporter, only few events with ER reporter cleavage were observed and so far, we never saw a case of dominant ER reporter cleavage. To account for fluorophore effects and to avoid underestimation of ER reporter cleavage, the fluorescent proteins of the PM vs. ER GrzB reporter were switched (figure 18**A**). In this case, the PM reporter was bound to an mCherry, while the ER reporter was labeled with mGFP. HeLa $CD48^+$ $PM^{mC}ER^{mGFP}$ GrzB reporter cells in co-culture with pre-activated primary NK cells gave 3 different cleavage outcomes (figure 18**B** and **C**) consistent with our previous data. The smallest proportion of cells (12 cells; 23.5 % of all analyzed cells) died with intact PM and ER reporter localization (PM: 4.7 %; ER: 6.4 % at TOD; no GrzB activity, outcome 1). Again, all other analyzed cells indicated cleavage: In 35.3 % of all events (18 cells), we only observed a PM reporter cleavage, which was detected 9 min before TOD and reached up to 63.9 %. The ER reporter did not redistribute with 13.5 % at TOD (GrzB activity at PM, outcome 2). Surprisingly, for the first time, the additional ER reporter cleavage (38.7 % at TOD) was detected in the majority of all events (41.2 %, 21 cells). Despite the increased percentage, PM reporter cleavage still clearly dominated (90.4 % at TOD) over the ER cleavage (GrzB activity at PM and ER, outcome 3). Consistent with our previous results, the onset of PM activity started around 12 – 15 min before TOD, while the ER activity was measured 3 – 6 min before TOD (6 min delay). The same 3 outcomes were also observed using NK92 cells (figure S7), although 60 % of all analyzed cells died without detectable GrzB activity (figure 18**C**). Moreover, of the remaining 40 % of deaths, GrzB was solely active at the PM in 26 %, while again in only 14 % the activity predominated at the PM with an additional lower activity at the ER. The $PM^{mC}ER^{mGFP}$ GrzB reporter results differ significantly from results of the $PM^{mGFP}ER^{mC}$ GrzB reporter for NK92 and pre-activated NK cells (already shown in figure 17 and partially shown again in figure 18**C** for comparison). The general distribution of reporter cells dying without (light gray) or with detected GrzB activity (medium and dark gray) showed a similar pattern. However, focusing on the proportion of deaths with GrzB activity, $PM^{mC}ER^{mGFP}$ GrzB reporter cells identify more killing events with additional minor activity at the ER. This was evident for NK92 cells and pre-activated primary NK cells. Nevertheless, the GrzB activity at the PM remained dominant.

Consequently, also the PM^{mC}ER^{mGFP} GrzB reporter points towards a main entry of GrzB via PM pores, although this new reporter indicates more events with activity at the ER, i.e. a potentially stronger role of uptake via endocytosis, than previously seen.

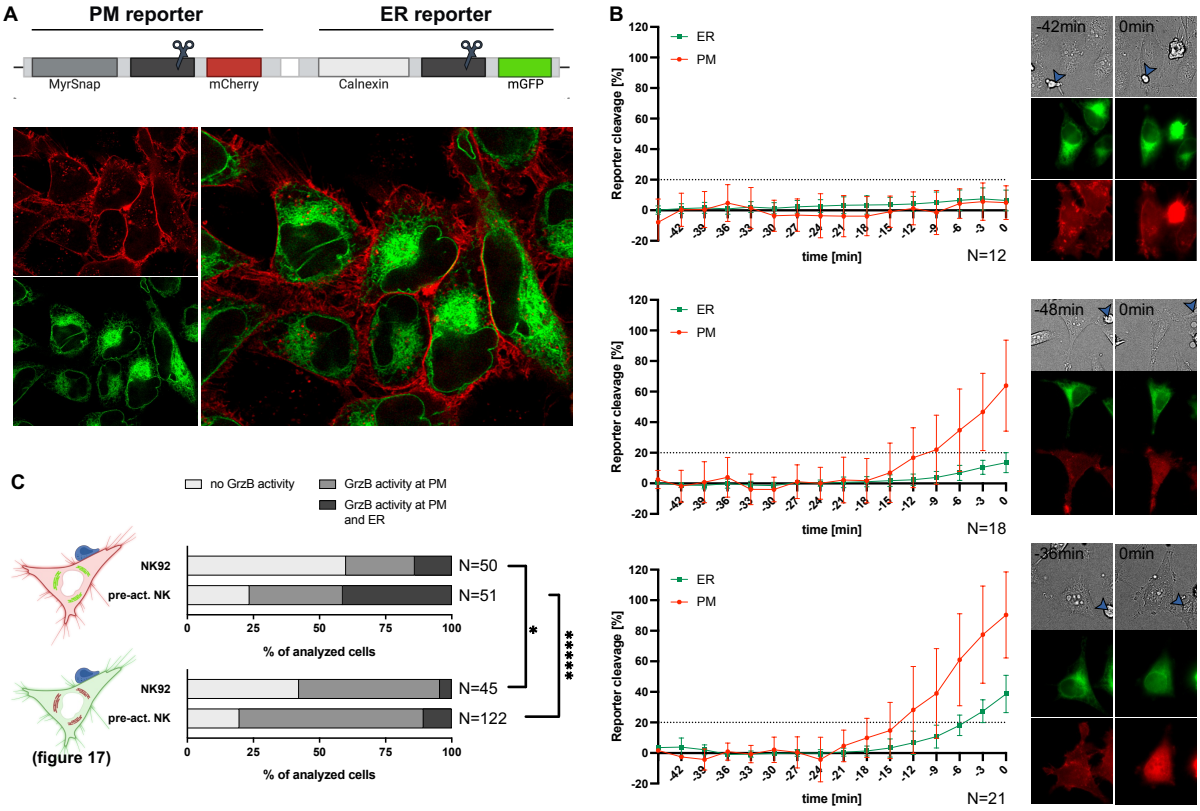

Figure 18: A mGFP labelled ER reporter is more efficient in detecting GrzB activity at the ER, but GrzB activity still predominates at the PM. A Design of the PM^{mC} vs. ER^{mGFP} GrzB reporter construct (top) and representative images of HeLa CD48^{+} PM^{mC}ER^{mGFP} GrzB reporter cells. PM reporter = red, ER reporter = green (63 x magnification, MICA WideFocal live cell microscope; bottom). **B** Pre-activated NK cells (isolated from whole blood and cultured for 3 – 4 weeks) were co-cultured with HeLa CD48^{+} PM^{mC}ER^{mGFP} GrzB reporter cells (E:T ratio of 1:1) for 3 h during live cell imaging. Three different reporter cleavage outcomes were observed: no reporter cleavage (outcome 1; top row), only PM reporter cleavage (outcome 2; middle row) or cleavage of both FLRs with dominant PM reporter cleavage (outcome 3; bottom row). Quantification of reporter cleavage (left panel). Representative snapshots show the reporter distribution of the intact reporter state and at 0 min (TOD). Brightfield images show GrzB reporter cells and pre-activated NK cells (blue arrows). Data include 4 independent experiments with N = 51 cells in total (n = 3 donors, N = 9 – 24 cells per experiment) and are shown as Mean ± SD. Images were acquired using the Axio Observer 7, 40 x magnification. **C** Upper panel: Parts of whole stacked bar graphs (% of all analyzed cells) of results from (**B**) and of results from experiments with NK92 (figure S7). Lower panel: Parts of whole stacked bar graphs (% of all analyzed cells) of PM^{mGFP}ER^{mC} GrzB reporter cleavage results with NK92 cells and pre-activated NK cells already shown in figure 17. The segments represent reporter cleavage outcomes: light gray = no reporter cleavage (outcome 1, no GrzB activity), medium gray = only PM reporter cleavage (outcome 2, GrzB activity at PM), dark gray = cleavage of both FLRs with dominant PM reporter cleavage (outcome 3, GrzB activity at PM and ER). Statistical comparison was performed by Chi-Squared test with statistical significance indicated by asterisks: * $P \leq 0.05$ ($P_{Chi\text{-}square} = 0.016$); ***** $P \leq 0.00001$ ($P_{Chi\text{-}square} = 4.923e\text{-}06$).

4.4 Limited diffusion of GrzB from PM into the cell

GrzB activity at the ER was detected approximately 6 – 9 min after activity at PM and 3 – 6 min before cell death (figures 11, 15, 16, 18). Assuming that GrzB diffuses deeper into the cell after entering through PM pores, GrzB would reach the vicinity of the ER reporter. As a consequence, the ER reporter would be cleaved and indicate a GrzB activity, although entry via endocytic uptake has by no means occurred. Under these circumstances, GrzB would also be able to cleave other organelle-specific FLRs, possibly indicating diffusion rather than endocytic uptake. Therefore, we generated a new GrzB reporter construct. The PM localization domain was replaced with a shortened version of MitoNEET, which resides in the outer membrane of mitochondria (Wiley et al., 2007). In the past, this localization domain reliably directed a Caspase-8 specific FLR to mitochondria (Beaudouin et al., 2013). Here, the ER reporter is connected to mGFP, whereas the mitochondrial (short: Mito) reporter is labeled with mCherry (figure 19**A**). We transfected HeLa CD48^{+} cells with the ER^{mGFP}Mito^{mC} GrzB reporter construct (figure 19**B**). After expression, the ER and Mito reporter are distributed structurally distinct. Hence, the co-translational separation was successful. The ER reporter was localized similarly as before. For validation of the Mito reporter localization, the cells were stained with a mitochondria specific dye (BioTracker^{TM} 405 Mitochondria). The staining visually displays a mitochondrial-like distribution, which strongly resembles the distribution of the Mito reporter (figure 19**B**) suggesting the correct localization of the Mito reporter. Next, we co-cultured ER^{mGFP}Mito^{mC} GrzB reporter cells with pre-activated primary NK cells, with three different cleavage outcomes being observed (figure 19**C**). Both, ER and Mito reporter remained intact in the vast majority of analyzed cells (57 cells, outcome 1, figure 19**C**, top), thus indicating no GrzB activity at these organelles at TOD (6.7% Mito reporter and 6.3% ER reporter cleavage). Presumably, these cells were killed either with a GrzB activity at the PM or completely without GrzB involvement. However, we also measured ER reporter cleavage (32.1 % at TOD), while Mito reporter cleavage remained below threshold (14.6 % at TOD) (3 cells, outcome 2, figure 19**C**, middle). In this case, the sole activity at the ER would argue for an endocytic uptake of GrzB. The activity at the ER is detected 6 min before death (mean above threshold), which is consistent with previous results. Lastly, in only one cell (outcome 3, figure 19**C**, bottom), we detected a slight redistribution of the ER reporter (25.2 % cleavage) and additionally of the Mito reporter (22.1 % cleavage) immediately before death. This might indicate a GrzB activity at both organelles which could suggest diffusion. Additionally, we also observed these results

with resting primary NK cells (figure S8) and NK92 cells (figure S9). The comparison of the frequency of all analyzed cells between different NK cell types (figure 19**D**) revealed a similar pattern. Besides the largest proportion of $ER^{mGFP}Mito^{mC}$ GrzB reporter cells killed without GrzB activity at the ER and mitochondria (light gray; NK92 cells and pre-activated NK cells: 93.44 %; resting NK cells: 95.65 %), the proportion of cells showing GrzB activity is low (gray and black). However, even within this small proportion, the percentage of GrzB activity at the ER alone (NK92 cells and pre-activated NK cells: 4.92 %; resting NK cells: 4.35 %) tends to outweigh that at both organelles (NK92 cells and pre-activated NK cells: 1.64 %; resting NK cells: 0 %). These results argue against a general diffusion of GrzB into the cell after PM pore entry. Whether these cleavage events were also specifically triggered by GrzB was verified in the absence of GrzB using NK92 GrzB KO cells (figure 19**E**). As described before (chapter 4.1.3), cells were included in the analysis which were killed by 1 or more NK92 GrzB KO cells. Only outcome 1 – both FLRs remained intact – was observable in killed reporter cells (12 cells). Hence no GrzB activity at either organelle was detected (3.3 % ER reporter and 2.99 % Mito reporter cleavage at TOD) providing proof for the GrzB reporters' specificity. Additionally, we found reporter cells to exhibit a prolonged time from first NK cell contact until TOD of 192.3 min, suggestive for death receptor- or granzyme A-mediated killing as mentioned before.

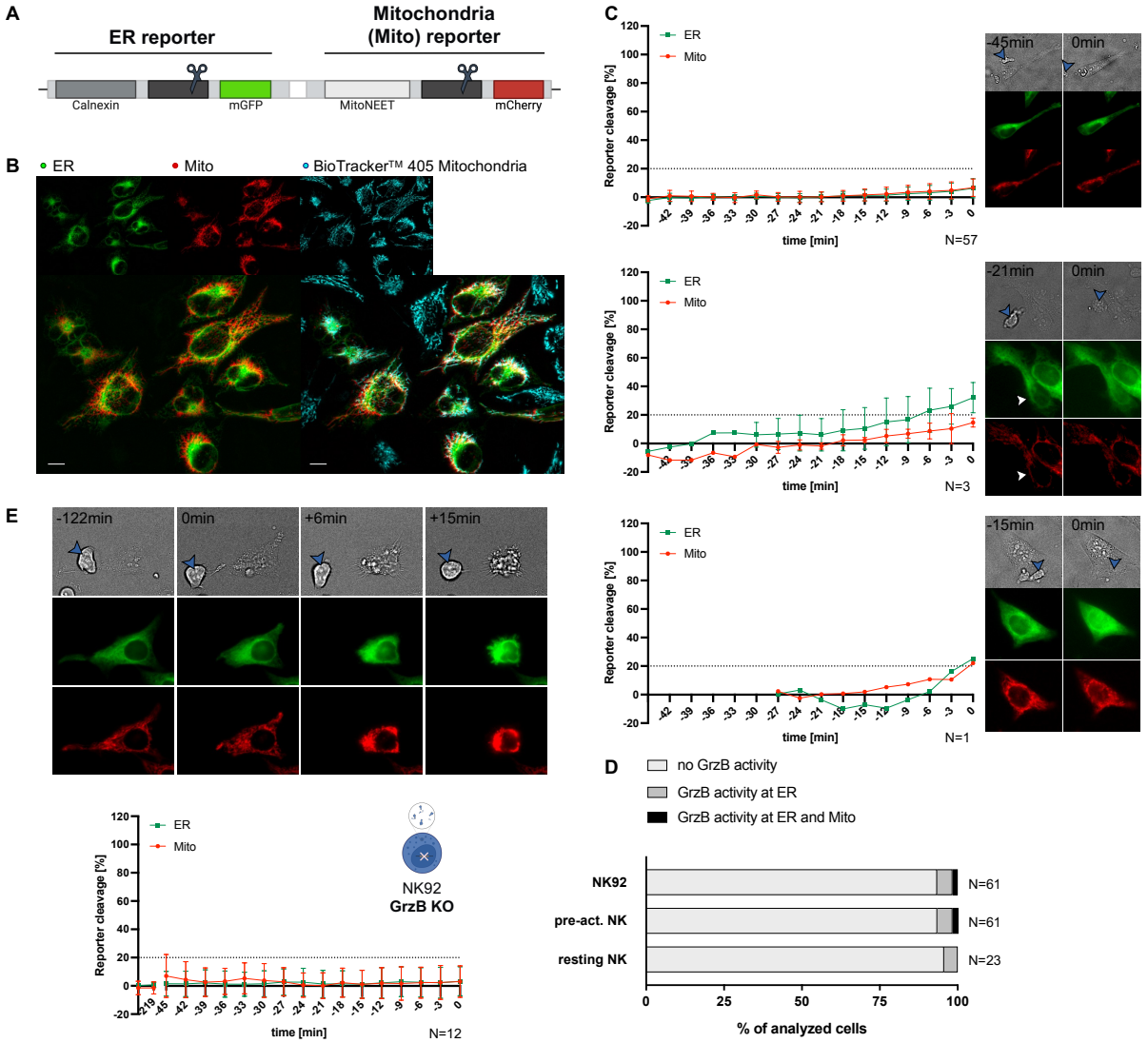

Figure 19: Limited diffusion of GrzB from the PM into the cell. A Design of the ER^{mGFP} vs. Mitochondria (Mito)^{mC} GrzB reporter construct. Mito reporter localization domain: MitoNEET. **B** Representative images of HeLa CD48^{+} ER^{mGFP}Mito^{mC} GrzB reporter cells (ER reporter = green, Mito reporter = red) and qualitative confirmation of Mito reporter localization. GrzB reporter cells were stained with BioTracker^{TM} 405 Mitochondria dye. Images were acquired using the EVOS fl auto microscope (60 x magnification). Scale bar = 10 µm. **C** Pre-activated NK cells (isolated from buffy coats (BC) and cultured for 3 – 4 weeks) were co-cultured with HeLa CD48^{+} ER^{mGFP}Mito^{mC} GrzB reporter cells (E:T ratio of 1:1) for 3 h during live cell imaging. Three different reporter cleavage outcomes were observed: no reporter cleavage (outcome 1; top row), only ER reporter cleavage (outcome 2; middle row) or cleavage of both FLRs (outcome 3; bottom row). Quantification of reporter cleavage (left panel). Representative snapshots show the reporter distribution of the intact reporter state and at 0 min (TOD; right panel). Data include 7 independent experiments with N = 61 cells in total (n = 4 donors, N = 5 – 17 cells per experiment). **D** Parts of whole stacked bar graphs (% of all analyzed cells) with bars representing the results from (**C**) and results from experiments with resting NK cells (figure **S8**) and NK92 cells (figure **S9**). The segments represent reporter cleavage outcomes: light gray = no reporter cleavage (outcome 1; no GrzB activity), gray = only ER reporter cleavage (outcome 2; GrzB activity at ER), black = cleavage of both FLRs (outcome 3; GrzB activity at ER and Mito),. **E** Co-culture of NK92 GrzB KO cells with HeLa CD48^{+} ER^{mGFP}Mito^{mC} GrzB reporter cells (E:T ratio of 1:1) for 5 h. Representative snapshots show the reporter distribution at the intact reporter state (-122 min), at 0 min (TOD) and 6 min as well as 15 min after TOD (top). Quantification of ER and Mito reporter cleavage (reporter cleavage (%) over time) only shows outcome 1 (no reporter cleavage) in killed ER^{mGFP}Mito^{mC} GrzB reporter cells. Data include 4 independent experiments with N = 12 cells in total (N = 2 – 5 cells per experiment) (bottom). Data are shown as Mean ± SD. Images were acquired using the Axio Observer 7, 40 x magnification. ER reporter = green, Mito reporter = red. White arrows point at reporter cell of interest. Brightfield images show GrzB reporter cells and pre-activated NK cells (blue arrows).

4.5 Limited endocytic uptake as detected by early endosomal reporter

The limited diffusion of GrzB to the ER supports the assumption that the activity at the ER is due to endocytic uptake of GrzB (figure 19). After perforin pore-induced membrane repair, damaged membrane parts are taken up together with perforin and GrzB into enlarged vesicles, which are positive for early endosome antigen 1 (EEA1) (Thiery et al., 2011) – a marker and tethering protein of early endosomes (Lawe et al., 2000). Given the possibility that higher amounts of GrzB may be released early in the recycling process, we were concerned about the ER reporter being located far downstream where only few vesicles reach the vicinity of the ER. Hence the ER reporter might underestimate the role of endocytosis for the entry mechanism of GrzB and might not be suitable for its detection. Consequently, we developed a new FLR for GrzB activity, by replacing the ER localization domain with EEA1 to direct the FLR to early endosomes (EE) (figure 20**A**). Unlike the other reporter cells, however, keeping the FLR expression stable in HeLa CD48$^+$ cells and with both FLRs being correctly localized over a longer period was challenging. To overcome this, we decided to transiently transfect HeLa CD48$^+$ before each experiment. HeLa CD48$^+$ cells expressing the PM^{mC}EE^{mGFP} GrzB reporter showed large differences in expression levels of both FLRs and localization of the EE reporter: Both punctual localization of the EE reporter and diffuse localization within the cytosol have been observed, with both frequently occurring in combination (figure 20**A**, fluorescence images), which complicated the reporter analysis after co-culture with pre-activated NK cells. Nevertheless, as with previous results, we only observed the already known outcomes 1 – 3 (figure 20**B** and **C**). The largest proportion of all analyzed cells (54.65 %, 47 cells) showed intact PM and EE reporter localization (no GrzB activity; outcome 1) with 4.9 % PM reporter and 5.5 % EE reporter cleavage at TOD. All other events indicated a GrzB activity, which again was always predominantly found at the PM. Among these events, 40.7 % (35 cells) showed PM activity (88.6 % at TOD; starting 12 – 15 min before TOD) without any contributing activity at EE (7.4 % at TOD) (GrzB activity at PM, outcome 2). However, in the smallest proportion of all analyzed events (4.65 %, 4 cells), we observed an additional redistribution of the EE reporter (EE: 32.1 % at TOD) starting between 3 – 6 min before TOD. As before, the PM reporter cleavage started 12 min before TOD and was up to 122.4 % at TOD (GrzB activity at PM and EE, outcome 3).

To conclude, the proportion of events with GrzB activity at EE remained in the minority and were always accompanied by a dominant GrzB activity at the PM. This strengthens the PM pore model as the preferred entry mechanism of GrzB and pushes the endocytic uptake model in a supportive role. However, we have not yet observed any switch in the preferred entry mechanism here either.

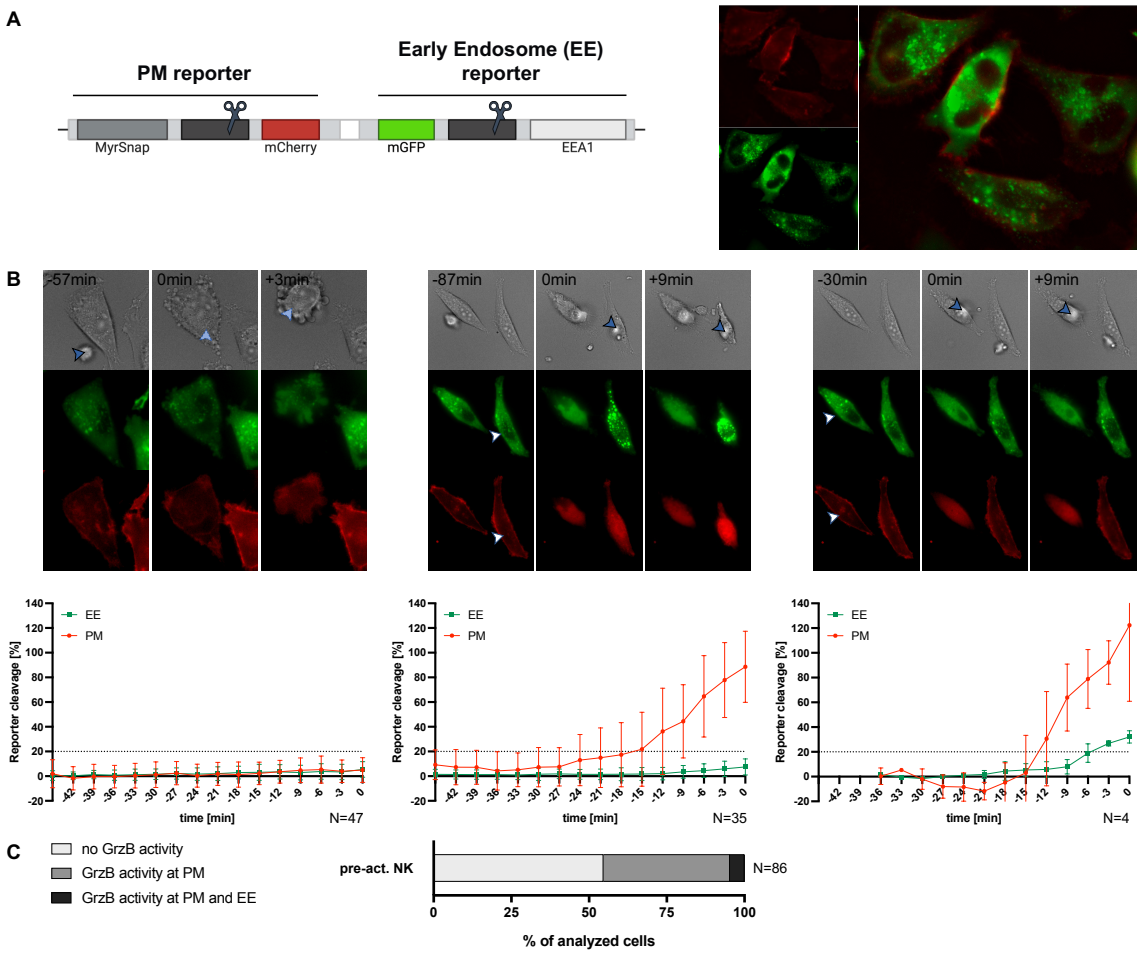

Figure 20: PM^{mC}EE^{mGFP} GrzB reporter reveals limited endocytic uptake of GrzB. A Design of the PM^{mC} vs. early endosome (EE) ^{mGFP} GrzB reporter construct. EE reporter localization domain: EEA1 (left). Representative images of HeLa CD48^{+} PM^{mC}EE^{mGFP} GrzB reporter cells (PM reporter = red, EE reporter = green) acquired with the MICA WideFocal, 40 x magnification (right). **B** Pre-activated NK cells (isolated from whole blood and cultured for 3 – 4 weeks) were co-cultured with HeLa CD48^{+} PM^{mC}EE^{mGFP} GrzB reporter cells (E:T ratio of 1:1) for 3 – 5 h during live cell imaging. Representative snapshots show the reporter distribution of the intact reporter state, at 0 min (TOD) and 9 min after TOD (top). Quantification of ER and Mito reporter cleavage (reporter cleavage (%) over time) shows 3 different reporter cleavage outcomes: no reporter cleavage (outcome 1; left panel), only PM reporter cleavage (outcome 2; middle panel) or cleavage of both FLRs (outcome 3; right panel). Data include 4 independent experiments with N = 86 cells in total (N = 14 – 31 cells per experiment). Data are shown as Mean ± SD. Images were acquired using the Axio Observer 7, 40 x magnification. PM reporter = red, EE reporter = green. White arrows point at reporter cell of interest. Brightfield images show GrzB reporter cells and pre-activated NK cells (blue arrows; light blue = NK cell underneath target cell). Experiments were performed using the Axio Observer 7 and the MICA WideFocal in widefield as well as confocal mode. **C** Parts of whole stacked bar graph (% of all analyzed cells) with bar representing the results from (**B**). The segments represent reporter cleavage outcomes: light gray = no reporter cleavage (outcome 1; no GrzB activity), gray = only PM reporter cleavage (outcome 2; GrzB activity at PM), black = cleavage of both FLRs (outcome 3; GrzB activity at PM and EE).

4.6 Dependence of the GrzB entry mechanism on the perforin concentration

So far, our results strengthen the role of the PM pore model, yet they do not necessarily exclude endocytosis as a potential supporting or even, under certain conditions, an alternative uptake mechanism. Perforin might dose-dependently influence the preferred GrzB access to target cells, with PM pores being favored at a high perforin abundance (Browne et al., 1999). Can the endocytic model be of decisive importance for GrzB entry, e.g. when perforin availability is restricted?

4.6.1 Isolated lytic granules of NK cells lack lytic capabilities

To mimic different constellations of available perforin and GrzB concentrations, e.g. by reducing the perforin while maintaining the GrzB concentration, we attempted to isolate lytic granules of NK cells which lack perforin or GrzB. In a preliminary work, perforin or GrzB KOs were generated in the NK cell line NKL and lytic granules were isolated successfully, although the latter showed no functionality (Bruning, 2020). This approach was further pursued and adapted here aiming to isolate functional lytic granules. Since optimization of the isolation was not yet fully finalized, one isolation with wt NKL and one with pre-activated primary NK cells are presented here.

Due to the simple handling of NKL, we first started isolating lytic granules from wt NKL. The lytic granule containing crude lysosomal fraction (CLF) of 1.095 x 10^9 wt NKL cells was separated by ultracentrifugation resulting in six fractions (figure 21**A**). Western blot analysis of perforin, GrzB and lysosomal marker CD107a, which is also stored in lytic granules (Peters et al., 1991) indicate the enrichment of lytic granules compared to a whole lysate (WL) control (figure 21**B**). While immature und mature forms of perforin were present to varying amounts in fractions 1 – 5, CD107a as well as GrzB were only detected in fractions 2, 3 and 4, but most abundant in fraction 3. Surprisingly, we did not detect GrzB in WL control. Due to co-presence of all three proteins, we suspected lytic granules in fractions 2 – 4. Nevertheless, we tested all fractions regarding their lytic abilities against target cells by differentiating between early apoptotic and late apoptotic/necrotic cells (Rudd-Schmidt et al., 2019b). Early apoptotic cells can be identified using Annexin V, which binds to phosphatidylserine flopping to the extracellular space (van Engeland et al., 1998). Once membrane integrity is lost in late apoptotic/necrotic cells, 7-AAD enters cells and intercalates into the DNA, resulting in double positive cells (Rudd-Schmidt et al., 2019b). Since HeLa cells could adhere to the walls of the reaction tubes during the incubation period, which may result in

differences between samples, we switched to the suspension cell line K562 CD48$^+$ for this flow cytometry based killing assay.

K562 CD48$^+$ were treated with different dilutions of all 6 sonicated fractions, HB buffer (solvent) or medium (figures 21**C** and S12) in the presence of 5 mM $CaCl_2$. Medium or HB buffer (solvent control) treated K562 revealed similar amounts of early apoptotic (Annexin V – FITC$^+$) and late apoptotic/necrotic (Annexin V – FITC$^+$ and 7-AAD$^+$) cells, suggesting no effect of the solvent on cell viability. As a positive control for cell death detection, we subjected K562 to heat shock, with most cells being late apoptotic/necrotic (94.6%) and the remainder early apoptotic (4.85%). However, the distinction between viable and dying/dead cells became less clear when K562 cells were treated with lytic granules at a dilution of 1:2. Interestingly, except fraction 1, which indicates an increasing amount of early apoptotic K562, the Annexin V staining was partially diminished (fraction 6) or completely lost (fractions 2 – 5). Reducing the amount of lytic granules to a dilution of 1:32 restored the staining for fractions 5 and 6, but not for fractions 3 and 4 (for dilutions of 1:4, 1:8 and 1:16 refer to figure S12). Unfortunately, we were not able to perform all dilutions for all fractions (especially fraction 2), as we only obtained limited fraction volumes. Surprisingly, 40.9 % of K562 exposed to fraction 5 were 7-AAD-positive, i.e. late apoptotic/necrotic. When increasing the dilution of fraction 5 (1:32), most K562 were Annexin V-positive (69.1 %), indicating early apoptosis of these cells. This would suggest a lytic activity of fraction 5. Of the three proteins analyzed by Western blot (figure 21**B**), only mature perforin was detectable in fraction 5 (even after prolonged exposure, data not shown). However, we suspected lytic granules in fractions 2 – 4, which showed no indication of dead cells in the killing assay. Therefore, we assumed that these fractions were incapable to induce lysis.

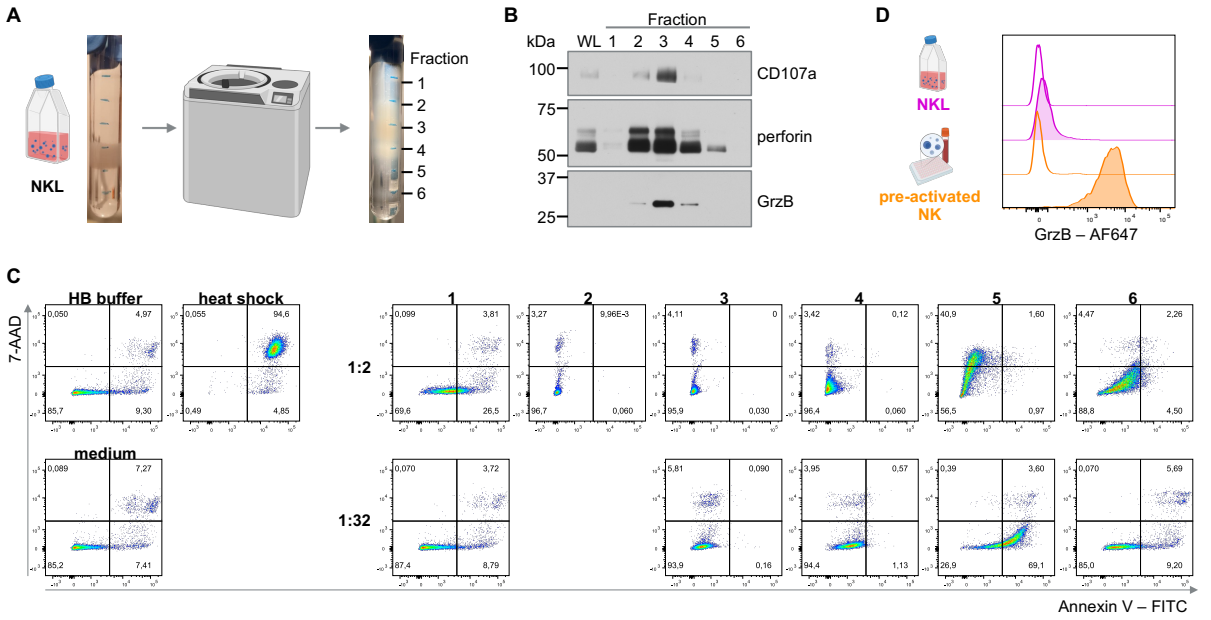

Figure 21: NKL derived lytic granules were isolated successfully, yet analysis of functionality led to inconclusive results. A Crude lysosomal fraction (CLF) of 1.095 x 10^9 NKL cells on OptiPrep™ step gradient before (left) and after (right) 4 h ultracentrifugation. 6 fractions were collected from the top of the gradient (marked by lines). **B** Western blot analysis of CD107a, perforin and GrzB of fractions 1 – 6 (1 % of isolation output) and whole lysate (WL, lysate from 0.01 % of the initial NKL input, of which 1 % was loaded onto the gel). **C** K562 CD48$^+$ were treated with HB buffer (solvent control) or lytic granules from fractions 1 – 6 (dilution 1:2 and 1:32) in the presence of 5mM $CaCl_2$ for 2 h. Dot plots of late apoptotic/necrotic (7-AAD$^+$) and early apoptotic (Annexin V$^+$) flow cytometry staining. Controls: medium, heat shock (5 min, 70 °C) and solvent control (left). Fractions 1 – 6 (right) with 1:2 dilution of lytic granules (top row) and 1:32 dilution (bottom row). **D** Flow cytometry staining of GrzB in NKL cells (pink) and pre-activated NK cells (orange; isolated from whole blood, cultured for 3 weeks). Normalized (normalized to mode) histograms with unstained control.

Additionally, since the NKL cells poorly expressed GrzB (figure 21**D**), we repeated the isolation with pre-activated primary NK cells. Expression of perforin and GrzB was confirmed in advance of the isolation (figure 22**A**). Following a 5-week expansion, the CLF of 1.285 x 10^9 pre-activated NK cells was prepared and, for better separation, loaded on two gradients (figure 22**B**) with each yielding 6 fractions. Again, the killing assay results show the complete loss of Annexin V staining, which occurred with increasing concentrations of lytic granules of all fractions except fraction 6 (figure 22**C** and S13), although the onset of loss differs between fractions. Again, only K562 treated with the fifth fraction showed an increase in 7-AAD-positive staining, suggesting the lysis of some cells at a dilution of 1:8 and above.

However, due to the still unknown interfering factor that compromises the Annexin V staining, the interpretation of the functionality remains difficult. With no indication of whether isolation, storage or functionality assessment posed potential problems affecting the lytic granules, the isolation from large numbers of primary NK cells simply turned out to be costly and, especially, time-consuming. Consequently, mimicking

scenarios with varying perforin concentrations using isolated lytic granules could not be performed.

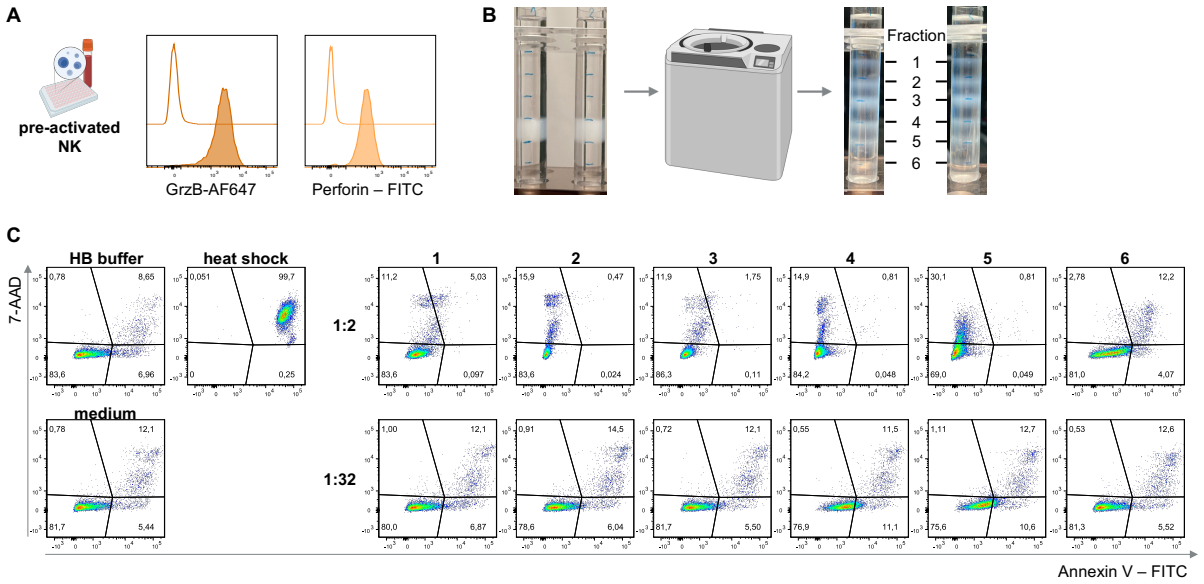

Figure 22: Pre-activated NK cell derived lytic granules demonstrate inconclusive results regarding functionality. Pre-activated NK cells were isolated from BC and expanded for 5 weeks. **A** Flow cytometry analysis of intracellular levels of GrzB (left) and perforin (right). Representative normalized (normalized to mode) histograms with corresponding unstained control. **B** Crude lysosomal fraction (CLF) of 1.285 x 10^9 pre-activated NK cells on OptiPrep™ step gradient (divided into 2 gradients) before (left) and after (right) 4 h ultracentrifugation. 6 fractions were collected from the top of each gradient (marked by lines) and pooled appropriately. **C** K562 CD48$^+$ were treated with HB buffer (solvent control) or lytic granules from fractions 1 – 6 (dilution 1:2 and 1:32) in the presence of 5mM $CaCl_2$ for 2 h. Dot plots of late apoptotic/necrotic (7-AAD$^+$) and early apoptotic (Annexin V$^+$) flow cytometry staining. Controls: medium, heat shock (5 min, 70 °C) and solvent control (left). Fractions 1 – 6 (right) with 1:2 dilution of lytic granules (top row) and 1:32 dilution (bottom row).

4.6.2 Pre-activated NK cells with reduced perforin levels induce GrzB activity predominantly at the PM

Alternatively, we investigated a different approach, which allows us to analyze the importance of the perforin concentrations for GrzB entry in a more physiologically relevant setting. During storage of endogenous perforin, NK cells are protected against autolysis by the acidic pH of lytic granules (Praper et al., 2010), among other factors (outlined in chapter 1.2.2). Neutralizing lytic granules, e.g. by inhibiting the vacuolar type H$^+$ – ATPase with concanamycin A (CMA), resulted in defective maturation and degradation of perforin (Kataoka et al., 1994, House et al., 2017). In a previous work, pre-activated primary NK cells exposed to CMA for 180 min completely degraded the mature form of perforin, which was stable at least for additional 240 min after washout (Anft et al., 2020). As we intended to achieve a titration of perforin degradation, we pre-treated pre-activated primary NK cells for 30 min, 60 min and 180 min. Indeed, CMA induced a decline in the intracellular perforin levels with a significant reduction after 60

min and 180 min compared to the DMSO control (figure 23**A**). The rising pH value inside lytic granules did not affect the GrzB content of NK cells, suggesting different regulatory mechanisms to protect against perforin and GrzB during storage within NK cells. Simultaneously, the CMA or DMSO pre-treated NK cells were co-cultured with $PM^{mC}ER^{mGFP}$ GrzB reporter cells, which were used here based on easier handling than the $PM^{mC}EE^{mGFP}$ GrzB reporter cells and increased detection of ER activity (figure 18). Interestingly, compared to the DMSO control, CMA pre-treated NK cells demonstrated a reduced cytotoxicity against $PM^{mC}ER^{mGFP}$ GrzB reporter cells (figure 23**B**). The amount of reporter cell deaths (including all observed reporter cell deaths) decreased with only an insignificant trend for 30 min and 60 min CMA, while a significant reduction was observed for 180 min CMA treated NK cells. Focusing on reporter cells which could be analyzed (figure 23**C**) – that is, reporter cells killed by a single NK cell – the reduced cytotoxicity with increasing CMA treatment duration is also observed here (DMSO: 46 cells, 30 min CMA: 23 cells, 60 min CMA: 10 cells; 180 min CMA: 1 cell). NK cells treated with DMSO or 30 min CMA induced the 3 usual outcomes in killed reporter cells (figure 23**C** and S14, table S4). While the frequency of deaths without GrzB activity appear to be similar (DMSO: 41.3 %, 30 min CMA: 43.5 %), a trend may emerge for deaths with GrzB activity: overall, the GrzB activity still predominates at the PM, where the frequency of sole PM activity (outcome 2) seemed to increase for 30 min CMA (39.1 %) compared to DMSO (32.6 %). Accordingly, the combined GrzB activity at PM and ER (outcome 3) showed a reduced occurrence with 30 min CMA treatment (17.4 %) compared to DMSO (26.1 %). This trend seemed to continue with 60 min CMA treated NK cells, which killed 50% without GrzB activity (at PM or ER) and 50% with GrzB activity only at PM, while deaths with additional activity at the ER (outcome 3) did not occur anymore. Moreover, the one cell that was killed by a 180 min CMA treated NK cell died without GrzB activity. Once again, no killing event with a dominant GrzB activity at the ER was observed.

We conclude that reducing the amount of perforin does not alter the entry mechanism of GrzB from PM pore entry towards endocytosis. However, we again could confirm the importance of perforin for the NK cell cytotoxicity and the general entrance of GrzB into target cells.

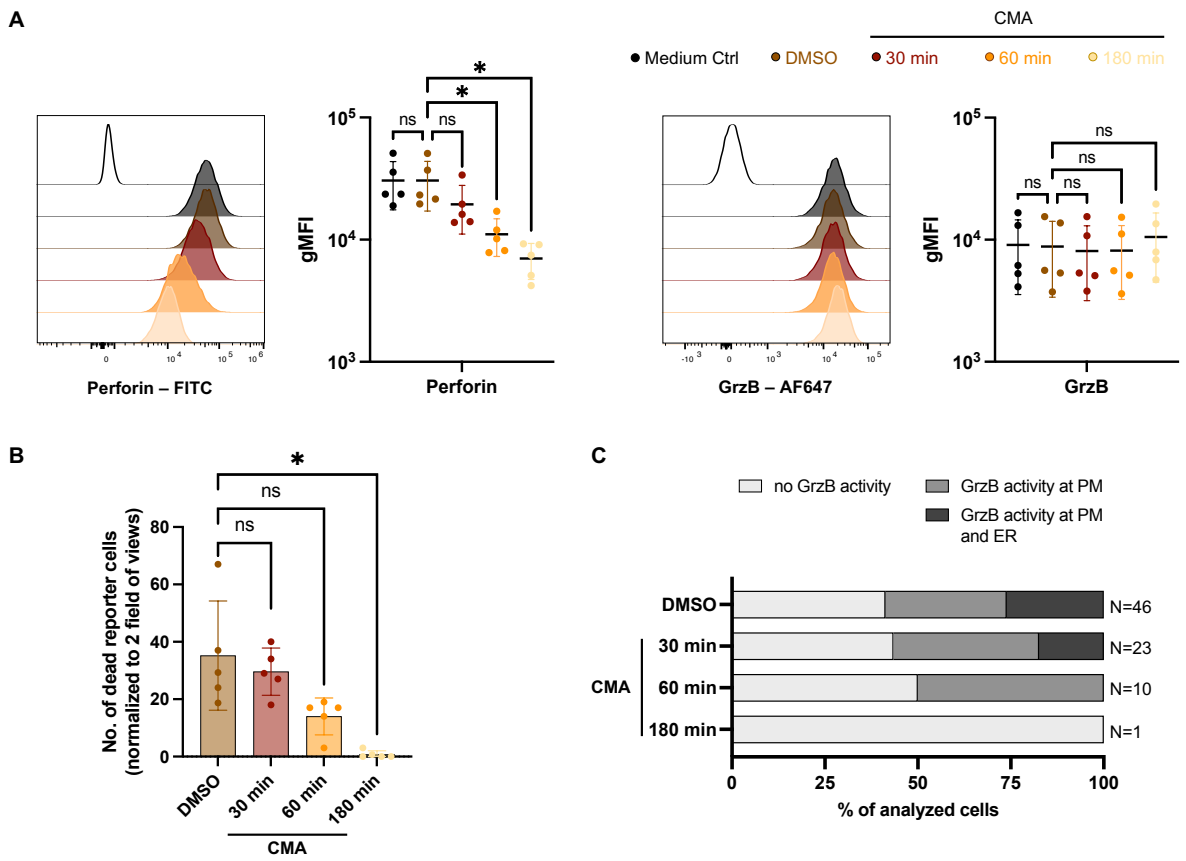

Figure 23: Pre-activated NK cells with less perforin still induced GrzB activity predominantly at the PM. Pre-activated NK cells (isolated from whole blood and cultured for 3 – 4 weeks) were treated with DMSO (0.02 %; solvent control; 180 min) or CMA (50 nM) for 30 min, 60 min and 180 min. **A** Flow cytometry analysis of intracellular levels of perforin (left) and GrzB (right) after treatment. Representative normalized (normalized to mode) histograms with corresponding unstained control and gMFI of GrzB and perforin levels (geoMean stained – geoMean unstained). **B** CMA and DMSO treated pre-activated NK cells were co-cultured with HeLa CD48^{+} PM^{mC}ER^{mGFP} GrzB reporter cells (E:T ratio of 1:1) for 3 h during live cell imaging. Number of dead reporter cells (counted after 3 h, normalized to two field of views) per treatment. Dots = number of all killed GrzB reporter cells per experiment including cells, that could not be analyzed regarding reporter cleavage. **C** Parts of whole stacked bar graphs (% of analyzed cells) with bars representing the reporter cleavage after CMA and DMSO treatments. The segments represent reporter cleavage outcomes: light gray = no reporter cleavage (outcome 1; no GrzB activity), medium gray = only PM reporter cleavage (outcome 2; GrzB activity at PM), dark gray = cleavage of both FLRs (outcome 3; GrzB activity at PM and ER). Data are shown as Mean ± SD. Data include 5 independent experiments. Statistical analysis was performed by RM one-way ANOVA with Dunnett's multiple comparisons test (each treatment was compared to DMSO control). Statistical significance is indicated by asterisks: * $P \leq 0.05$.

4.7 Dependence of the GrzB entry mechanism on the target cell

Thus far, neither the NK cell activation state nor a reduction in perforin concentration influenced the preference for PM pores or endocytosis with GrzB delivery via PM pores being consistently favored. Nevertheless, perforation of the target cell PM triggers a membrane repair mechanism as a protective measure, which could lead to the endocytic uptake of GrzB and perforin (Thiery et al., 2010, Thiery et al., 2011). However, HeLa cells have been shown to repair the PM pores within 80 seconds (Lopez et al., 2013b). Hence, differences in target cells' membrane dynamics may influence the entry mechanism of GrzB substantially. Since we mainly used HeLa cells as targets, we analyzed the GrzB delivery mechanism in a suspension and another adherent cell line.

4.7.1 K562 cells mainly died without detected GrzB activity

The chronic myelogenous leukemia K562 cell line, which grows in suspension, is frequently used as an NK cell target. Therefore, K562 cells were stably transduced with the $PM^{mC}ER^{mGFP}$ GrzB reporter construct (figure 24**A**). Despite the relatively large nucleus and roundness of K562 cells, the PM and ER reporters were clearly distinguishable by confocal microscopy. We investigated whether GrzB enters the suspension cell line K562 differently than adherent HeLa cells. In the co-culture of K562 $PM^{mC}ER^{mGFP}$ GrzB reporter cells with pre-activated NK cells, we only observed 2 outcomes (figure 24**B** and **C**). 98.98 % of all analyzed cells died without GrzB activity (PM reporter: 0.1 %; ER reporter: – 0.94 % at TOD, outcome 1). However, in the remaining 1.02 % of all events GrzB activity occurred at the PM (45.3 % at TOD) and ER (41.98 % at TOD) almost simultaneously (outcome 2). Moreover, most reporter K562 started to swell, many shortly after NK cell contact (data not shown, but can be seen in 0 min images of outcomes 1 and 2), which may suggest a perforin-induced osmotic lysis of K562 cells.

We observed a clear difference between K562 and HeLa cells, not in terms of GrzB entry mechanism, but rather in the overall sensitivity towards NK cell cytotoxicity.

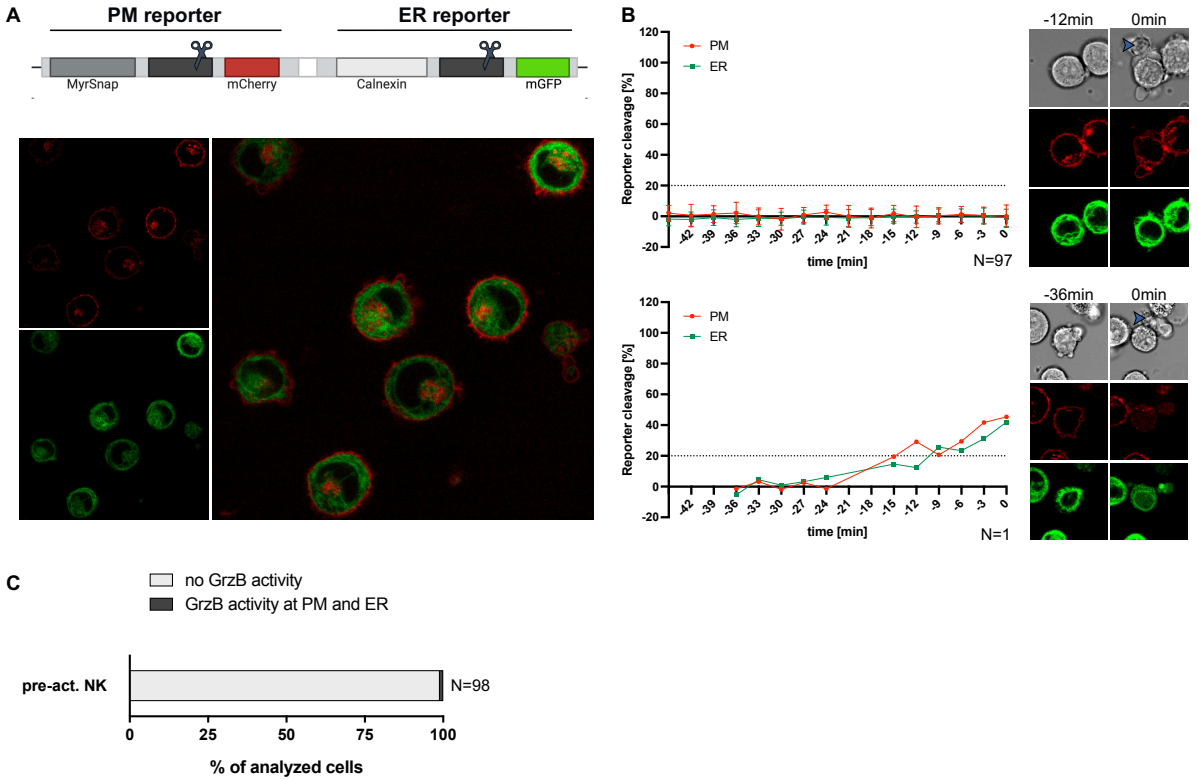

Figure 24: K562 PM^{mC}ER^{mGFP} GrzB reporter cells were almost exclusively killed without detectable GrzB activity. A Design of the PM^{mC} vs. ER^{mGFP} GrzB reporter construct (top) and representative images of K562 PM^{mC}ER^{mGFP} GrzB reporter cells. PM reporter = red, ER reporter = green (MICA WideFocal, 40 x magnification, confocal mode; bottom). **B** Pre-activated NK cells (isolated from whole blood) were cultured for 3 – 4 weeks and then co-cultured with K562 PM^{mC}ER^{mGFP} GrzB reporter cells (E:T ratio of 1:1) for 3 h during live cell imaging. Only two reporter cleavage outcomes were observed: no reporter cleavage (outcome 1; top row) or cleavage of both FLRs with dominant PM reporter cleavage (outcome 3; bottom row). Quantification of reporter cleavage (left panel). Representative snapshots show the reporter distribution of the intact reporter state and at 0 min (TOD). Brightfield images show K562 GrzB reporter cells and pre-activated NK cells (blue arrows). Data include 3 independent experiments with N = 98 cells in total (n = 3 donors, N = 31 – 35 cells per experiment) and are shown as Mean ± SD. Images were acquired using the MICA WideFocal, 40 x magnification, confocal modus. **C** Parts of whole stacked bar graphs (% of all analyzed cells) with bar representing the results from (**B**). The segments represent reporter cleavage outcomes: light gray = no reporter cleavage (outcome 1; no GrzB activity), dark gray = cleavage of both FLRs (outcome 3; GrzB activity at PM and ER).

4.7.2 Rare events of dominant GrzB activity at the ER were recorded in MDA-MB #468 cell deaths

Originating from breast cancer, MDA-MB #468 is an adherent cell line. We stably transduced MDA-MB #468 cells with the $PM^{mC}ER^{mGFP}$ GrzB reporter construct (figure 25**A**). For the first time, we detected four outcomes during the co-culture (figure 25**B** and **C**). 52.94 % of pre-activated NK cell mediated deaths indicate no GrzB activity, which accounts for the largest proportion of all deaths (outcome 1, 54 cells; PM: 13.1 %, ER: 4.7 % at TOD). In addition, in 20.59 % of all deaths GrzB was only active at the PM (outcome 2) with a reporter cleavage up to 50.4 % at TOD, rapidly starting 3 – 6 min before death. The ER reporter cleavage remained below threshold (9.9 % at TOD). Moreover, we observed almost equal numbers of deaths (23.53 %) with a dominant GrzB activity at the PM (69.8 %) and additional activity at the ER (43.0 %; outcome 3). Again, the PM cleavage was initiated 3 – 6 min before TOD, while the ER reporter was cleaved almost at the same time, with an approximately 3 min delay. The final and fourth outcome was only a rare event (2.94 % of all analyzed deaths). 3 – 6 min before death, GrzB showed dominant activity at the ER (62.1 % ER reporter cleavage at TOD) while low or no activity was observed at the PM (7.2% at TOD), suggesting a preferred delivery of GrzB via endocytosis in these cells.

We conclude, that GrzB was mainly delivered into MDA-MB #468 cells via PM pores, as shown by its dominant activity at the PM. Again, this further emphasizes the importance of the PM pore model. However, we also observed rare cases in which GrzB was solely active at the ER, hence transferred preferably via endocytosis. In addition to a supporting role, the endocytic uptake model could offer a potential yet rare alternative pathway for GrzB in certain target cells.

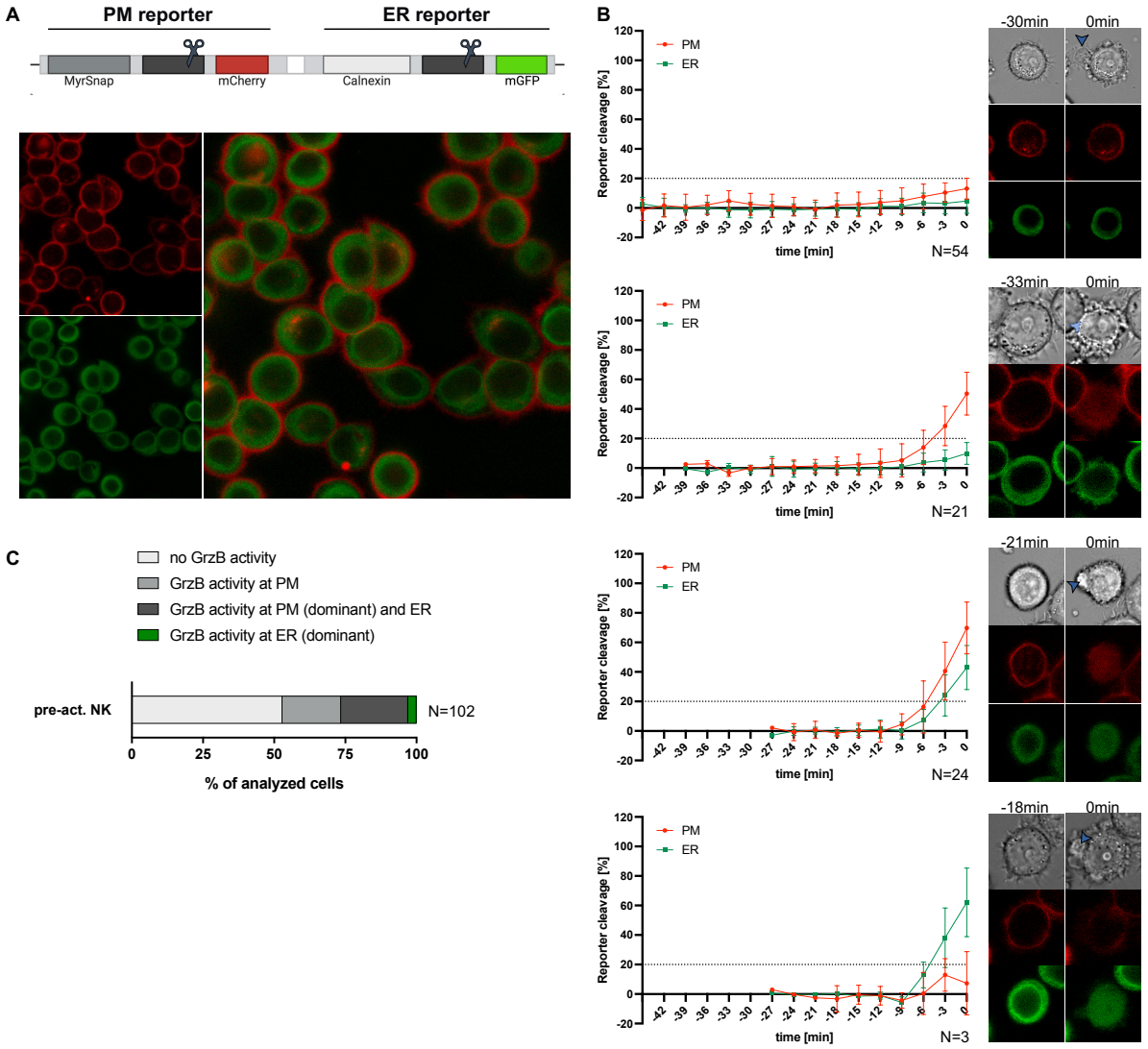

Figure 25: Pre-activated NK cells induce rare events of dominant GrzB activity at the ER in MDA-MB #468 PM^{mC}ER^{mGFP} GrzB reporter cells. A Design of the PM^{mC} vs. ER^{mGFP} GrzB reporter construct (top) and representative images of MDA-MB #468 PM^{mC}ER^{mGFP} GrzB reporter cells. PM reporter = red, ER reporter = green (40 x magnification, MICA WideFocal; bottom). **B** Pre-activated NK cells (isolated from whole blood; cultured for 3 – 4 weeks) were co-cultured with MDA-MB #468 PM^{mC}ER^{mGFP} GrzB reporter cells (E:T ratio of 1:2) for 3 h during live cell imaging. Four different reporter cleavage outcomes were observed (top to bottom row): no reporter cleavage (outcome 1), only PM reporter cleavage (outcome 2), cleavage of both FLRs with dominant PM reporter cleavage (outcome 3) and dominant ER reporter cleavage (outcome 4). Quantification of reporter cleavage (left panel). Representative snapshots show the reporter distribution at the intact reporter state and at 0 min (TOD). Brightfield images show GrzB reporter cells and pre-activated NK cells (blue arrows). Data include 3 independent experiments with N = 102 cells in total (n = 3 donors, N = 32 – 38 cells per experiment) and are shown as Mean ± SD. Images were acquired using the MICA WideFocal, 40 x magnification). **C** Parts of whole stacked bar graph (% of all analyzed cells) with bar representing the results from (**B**). The segments represent reporter cleavage outcomes: Light gray = no reporter cleavage (outcome 1; no GrzB activity), medium gray = only PM reporter cleavage (outcome 2; GrzB activity at PM), dark gray = cleavage of both FLRs (outcome 3; GrzB activity at PM and ER), green = dominant ER reporter cleavage (outcome 4; GrzB activity dominant at ER)

4.7.3 Treatment with (S)-4'-nitro-Blebbistatin enhanced NK cell cytotoxicity and tended to increase killing events with GrzB activity at the ER

Recent studies have demonstrated the efficiency of perforin to be substantially influenced by the target cells' membrane tension with softer membranes providing less vulnerability to perforin during T cell (Liu et al., 2021, Zhou et al., 2024) and NK cell cytotoxicity (Yanamandra et al., 2024). To manipulate membrane tension, the noncompetitive Myosin II ATPase inhibitor Blebbistatin (Kovacs et al., 2004) was utilized before with softening (Liu et al., 2021) or stiffening effects (Yanamandra et al., 2024), presumably depending on target cells' adhesive properties (Chan et al., 2015). However, due to the fluorescent nature of Blebbistatin, which might interfere with our mGFP-linked reporter, we used (S)-4'-nitro-Blebbistatin – a derivative with similar inhibitory dynamics but improvements regarding autofluorescence, photostability and -toxicity (Kepiro et al., 2014). First, we analyzed the effect of (S)-4'-nitro-Blebbistatin on NK cell cytotoxicity in a bulk setup using an impedance-based real-time cell analysis system. This system generates a cell index, as a measure of impedance, which increases upon cell attachment and proliferation (increase in electron flow impedance) but decreases when killed cells round and detach (less disturbed electron flow) (Hamidi et al., 2017). To monitor the effect of (S)-4'-nitro-Blebbistatin on MDA-MB #468 cells during the 12 h treatment, the cell index was recorded starting with seeding (figure 26). The cell index strongly increased for DMSO and medium-treated MDA-MB #468 cells, which is due to the attachment of the cells to the collagen-coated slide. However, cells treated with 50 µM (S)-4'-nitro-Blebbistatin already displayed a comparatively lower cell index. Observations by transmitted light microscopy after 12 h revealed an altered morphological phenotype from a small and roundish (DMSO and medium) to more spread-out phenotype ((S)-4'-nitro-Blebbistatin) (data not shown). Since (S)-4'-nitro-Blebbistatin induced inhibition is reversible (Straight et al., 2003), it should remain in the assay. However, this could potentially affect the cytotoxicity of NK cells. Therefore, we added NK cells after 12 h of treatment and either removed (S)-4'-nitro-Blebbistatin and DMSO (washout) or added them again (no washout). For (S)-4'-nitro-Blebbistatin, a clear difference was observed between samples with and without washout, with the latter stagnating at a comparatively lower cell index. After NK cell addition, the cell index dropped. However, this quickly leveled out again, hence arguing against killing. This difference was not observed for DMSO. Furthermore, the cell indices of MDA cells with NK cells (all except 'no washout' Blebbistatin) and without NK cells (MDA only) were similar within the first 12 h after addition of NK cells or medium, respectively.

Passing the 24 h timestamp, MDA cells without NK cells started to proliferate as indicated by the increasing cell index. However, cell index of samples with NK cells also increased, but to a lesser extent. This suggests that some killing events may have occurred, but not enough to strongly impact the overall MDA population. Presumably, this may be explained by the low E:T ratio (0.25:1). Moreover, cells treated with the 'no washout' Blebbistatin control started to proliferate approximately after 36 h.

To conclude, re-adding (S)-4'-nitro-Blebbistatin had a drastic effect on MDA. Since we also wanted to ensure that NK cells would not be affected, we decided to wash out (S)-4'-nitro-Blebbistatin.

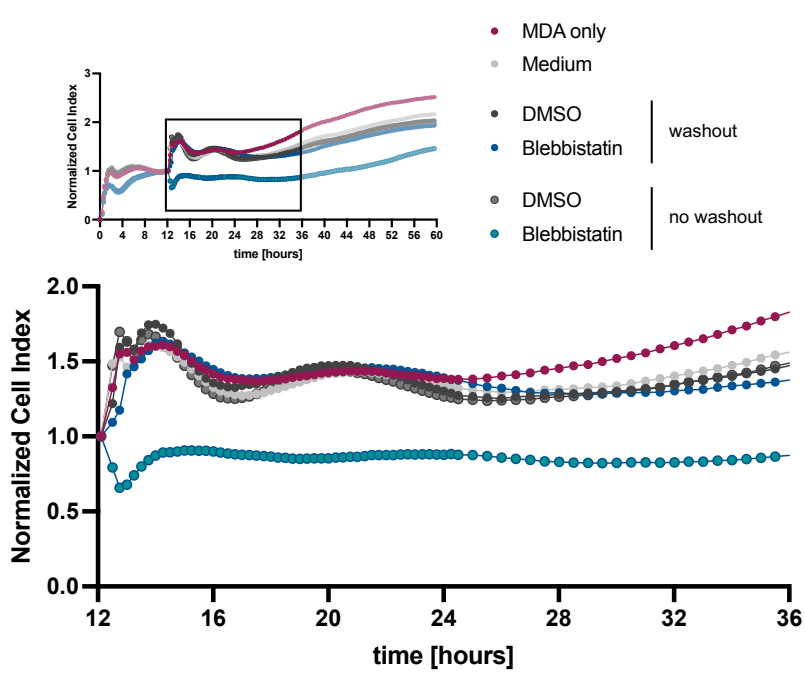

Figure 26: Re-addition of (S)-4'-nitro-Blebbistatin affected MDA-MB #468. Impedance based analysis of DMSO or 50 µM (S)-4'-nitro-Blebbistatin (abbrev. here as Blebbistatin) treated MDA-MB #458 $PM^{mC}ER^{mGFP}$ GrzB reporter cells for 12 h. After 12 h, DMSO or (S)-4'-nitro-Blebbistatin were washed out or readded to the assay, followed by addition of pre-activated NK cells (E:T of 1:4). Normalized cell index is shown over time (normalized to 12 h). Full graph (top), cut-out 12 – 36 h (bottom).

After washout, the cell index of (S)-4'-nitro-Blebbistatin treated cells approached DMSO and medium levels (figure 27**A**). Upon NK cell addition, which's number was increased to an E:T of 1:1, differences in NK cell cytotoxicity were observed (figure 27**B**). During the first 4 h after addition, the cell index rapidly dropped below pre-addition conditions for medium and DMSO treated MDA-MB #468 cells. This drop was more pronounced for (S)-4'-nitro-Blebbistatin treated MDA-MB #468 cells, suggesting higher susceptibility of target cells to NK cell cytotoxicity. Area under curve (AUC) analysis of these first 4 h demonstrates a significant difference compared to DMSO and Medium (figure 27**C**). In the following, MDA-MB #468 without NK cells started to proliferate rapidly, whereas no to little proliferation was detectable for DMSO and medium as well as for (S)-4'-nitro-Blebbistatin treated MDA-MB #468 cells. Next, we switched from bulk setting to our single-cell system and investigated whether GrzB

enters target cells differently. During live cell imaging, we observed 4 outcomes each for medium, DMSO and (S)-4'-nitro-Blebbistatin treated MDA-MB #468 $PM^{mC}ER^{mGFP}$ GrzB reporter cells (figure 27**D**). The proportion of deaths without GrzB activity was similar between medium (67.8 %) and (S)-4'-nitro-Blebbistatin (68.2 %) while DMSO may show a tendency to induce fewer deaths without GrzB activity (64.7 %). However, the number of deaths with GrzB being only active at the PM show a trend to decrease from DMSO (18.8 %) to medium (14.4 %) to (S)-4'-nitro-Blebbistatin (6.8 %). The opposite is evident for deaths with additional GrzB activity at the ER (DMSO: 15.3 %, medium: 16.7 %, (S)-4'-nitro-Blebbistatin: 19.3 %). The fourth outcome – dominant GrzB activity at the ER – was observed rarely in DMSO (1.2 %) and medium (1.1 %) but tended to be slightly more common in (S)-4'-nitro-Blebbistatin treated MDA (5.7 %). The pairwise comparison using the Cochran-Mantel-Haenszel Chi-squared test (Agresti, 2002) indicates significant differences between (S)-4'-nitro-Blebbistatin and DMSO, which, however, disappeared after correction for multiple testing. Moreover, no significant difference was found comparing (S)-4'-nitro-Blebbistatin and medium.

Taken together, adding to the cytotoxicity enhancing effect on NK cells, (S)-4'-nitro-Blebbistatin may also tend to increase kills with additional or sole GrzB activity at the ER while reducing sole PM-localized activity. Overall, GrzB activity at the PM still dominates further supporting PM pores as the main entry mechanism of GrzB.

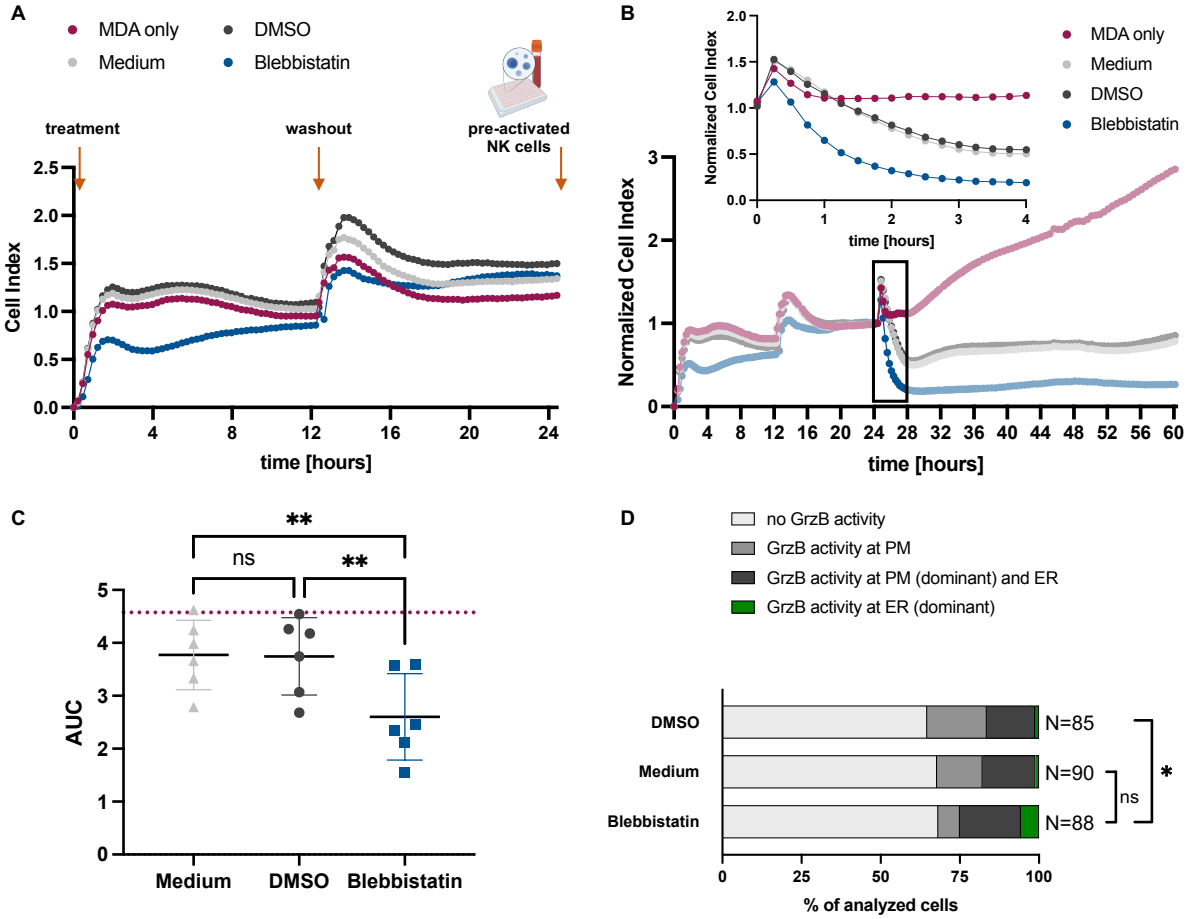

Figure 27: (S)-4'-nitro-Blebbistatin treatment increased NK cell cytotoxicity and showed a tendency towards more kills with GrzB being active at the ER. MDA-MB #468 PM^{mC}ER^{mGFP} GrzB reporter cells were pretreated with DMSO or 50 µM (S)-4'-nitro-Blebbistatin (abbreviated here as Blebbistatin) for 12 h. After 12 h, DMSO or (S)-4'-nitro-Blebbistatin were washed out and pre-activated NK cells were added after additional 12 h (E:T of 1:1). **A – C** Impedance based analysis. **A** Cell Index of the first 24 h showing the treatment and washout effect. **B** Normalized cell index over time (normalized to 24 h; before NK cell addition). Representative full graph (bottom, 0 – 60 min) and respective cut-out of 24 – 28 h (top). **A** and **B** are from the same experiment. **C** Area under curve (AUC) of first 4 h after NK cell addition. Dotted line represents mean AUC of the MDA only control. Data include 3 independent experiments (2 donors per independent experiment; n = 6 donors in total). Statistical analysis was performed by RM one-way ANOVA with Tukey's multiple comparisons test with statistical significance indicated by asterisks: * $P \leq 0.05$, ** $P \leq 0.01$. **D** Parts of whole stacked bar graph (% of all analyzed cells) with bars representing the results from 4 h live cell imaging of pre-activated NK cells and MDA-MB #468 PM^{mC}ER^{mGFP} GrzB reporter cells (figure S15). The segments represent reporter cleavage outcomes: Light gray = no reporter cleavage (outcome 1; no GrzB activity), medium gray = only PM reporter cleavage (outcome 2; GrzB activity at PM), dark gray = cleavage of both FLRs (outcome 3; GrzB activity at PM and EE), green = dominant ER reporter cleavage (outcome 4; GrzB activity dominant at ER). Statistic comparison was performed by Cochran-Mantel-Haenszel Chi-Squared test with ns $P > 0.05$ ($P_{CMH} = 0.164$), * $P \leq 0.05$ ($P_{CMH} = 0.041$).

5. Discussion

NK cells secrete perforin and GrzB, which synergistically induce death of target cells (Backes et al., 2018, Prager and Watzl, 2019, Nüssing et al., 2022). Perforin pores induce lesions in the target cell PM, which, however, are quickly resealed (Keefe et al., 2005, Lopez et al., 2013a, Lopez et al., 2013b). GrzB, on the other hand, cleaves key apoptosis inducing proteins inside target cells (Andrade et al., 1998, Chowdhury and Lieberman, 2008, Prager and Watzl, 2019). However, a clear consensus on how GrzB is delivered into the cytosol is lacking despite extensive research on this matter. Historically, scientists mainly toggled between two hypotheses – PM pore delivery and membrane repair-triggered endocytic uptake – with the former being favored (Nüssing et al., 2022, Spicer et al., 2022). Previously, protease-specific FLRs have contributed valuable insights into effector cell-mediated killing of target cells, especially regarding NK cell cytotoxicity (Liesche et al., 2018, Prager et al., 2019, Siegler et al., 2022, Bönnemann, 2023, Sandoz et al., 2023, Domagala et al., 2025). Here, we investigated the GrzB delivery using FLRs during NK cell cytotoxicity. This study provides further support for the PM pore model as the main GrzB delivery mechanism. However, we also found evidence for the co-existence of endocytic uptake.

Although providing valuable information on GrzB entry mechanisms, it has been cautioned that purified or recombinant proteins could not mimic conditions inside immune synapses (Catalfamo and Henkart, 2003, Kurschus et al., 2008, Thiery et al., 2011, Voskoboinik et al., 2015, Bird et al., 2005). Yet only few studies have implemented effector cells to recapitulate the GrzB entry in a physiologically relevant context (Keefe et al., 2005, Kurschus et al., 2008, Thiery et al., 2010, Thiery et al., 2011, Lopez et al., 2013b). FLRs allow the spatial, temporal and parallel quantification of GrzB activity at two different sites during NK cell cytotoxicity (Beaudouin et al., 2013, Liesche et al., 2018), enabling an estimate on how GrzB is delivered. However, we are aware that our assumptions are based on redistribution of a fluorescent signal, which we understand as a representative for reporter cleavage, hence GrzB activity (Beaudouin et al., 2013, Liesche et al., 2018). Unlike the previously used NES reporters, the organelle-bound reporters are not evenly distributed in the cell and thus may be differently representative for each observed plane (Beaudouin et al., 2013). Especially the measurement of PM areas has been challenging as the signal intensity of the PM-standing FLR fluctuated depending on cell movements. It has been advised to determine the total intensity of the organelle-bound FLRs in advance by confocal microscopy and use the obtained signal intensity value for normalizations (Beaudouin

et al., 2013, supplemental material). As we mostly used conventional widefield fluorescence microscopy, we consider this less problematic given the flat appearance of our adherent target cells. Nevertheless, while being aware of this less ideal situation, we were careful to validate our GrzB FLR system and the specificity of the measured reporter cleavage. Our observation that the VGPD linker sequence is specifically cleaved by GrzB (figure 12) is supported by earlier findings of NES FLRs, which remained intact upon GrzB inhibition, specific DR-pathway activation or in the absence of GrzB (Liesche et al., 2018, Bönnemann, 2023). Moreover, NK92 GrzB KO cells have been shown to compensate for their GrzB loss by utilizing GrzA, which was also unable to cleave the VGPD sequence (Bönnemann, 2023). Due to widefield fluorescence microscopy, we were oftentimes troubled with unspecific noise and contaminating signals in cytosolic and nuclear areas, which complicated measurements. This pushed us to define a threshold value to distinguish specific cleavage from background noise, especially regarding the observed comparably weak ER reporter redistribution. The application of a relatively high threshold (20 %) is also in agreement with the background noise previously observed in a non-cleavable NES FLR setting where widefield fluorescence microscopy has also been used (Bönnemann, 2023). Further evidence for the specific ER reporter cleavage was found in the absence of the GrzB activity at the ER when using a non-cleavable ER reporter (figure 13), consistent with a previous non-cleavable ER reporter examined by confocal microscopy (Beaudouin et al., 2013). While we have ensured that the observed reporter cleavage is specifically attributable to GrzB activity, we were surprised by our finding of a relatively large fluorophore effect when replacing mCherry with mGFP for the ER reporter. Combining the less frequently cleaved ER reporter with the brighter fluorophore enabled us to detect more events of GrzB activity at the ER (figure 18). Unlike Beaudouin et al., 2013, who directly compared different fluorophores within the same cell, our observation relied on comparison between different HeLa GrzB reporter cells. We cannot exclude differences between HeLa cells, as they have gone through different rounds of cell sorting until a sufficiently stable population of GrzB reporter^{+} cells was achieved. However, we still observed the same behavior regarding kinetic and amount of ER reporter cleavage within individual cells for both, ER^{mC} and ER^{GFP} reporters (figures 11, 15, 16, 18 and S7). Despite GrzB and perforin accumulation in EEA1^{+} vesicles (Keefe et al., 2005, Thiery et al., 2010, Thiery et al., 2011), the use of an EE reporter did not prevail over the ER reporter. We can conclude that our FLR system reliably distinguishes PM pore entry and endocytosis mediated delivery. Yet our approach is

limited in addressing the underlying mechanism of how GrzB is endocytosed. The clathrin-dynamin dependent pathway is involved in endocytic uptake of GrzB (Trapani et al., 2003, Veugelers et al., 2004, Thiery et al., 2010). Combining the FLR system with a suitable inhibitor of this pathway could also add a further valuable control for ER reporter cleavage due to endocytic uptake of GrzB. When designing this approach, however, possible effects on NK cells by inhibitors should be considered. Alternatively, knockdown of clathrin or dynamin (Thiery et al., 2010) or overexpressing the dominant-negative dynamin mutant K44A (Trapani et al., 2003, Veugelers et al., 2004) could be useful in that regard.

Unfortunately, we had to exclude a relatively large amount of target cells from analysis at the expense of detecting rare events. Drop-out factors included e.g. cells which were successfully killed but negative for FLR expression or cells whose FLR signal was obscured by NK cells squeezing between target cell and the slide. However, the largest drop-out factor comprised cells which were engaged by more than one NK cell or when the contribution of another NK cell could not be excluded with certainty. Within a single degranulation event, NK cells already secrete an excess of lytic granules onto target cells; more than is sufficient for successful killing (Gwalani and Orange, 2018). We were careful to exclude target cells being potentially exposed to high loads of GrzB and perforin from multiple NK cells. This was especially important regarding the question whether the perforin dose regulates between GrzB delivery mechanisms. While reducing the amount of NK cells per experiment even further could aid in overcoming this issue (Liesche et al., 2018), how many NK cells enter the observed fields of view, and their movements cannot be controlled. Although the reporter cleavage analysis is rather time consuming and despite the above-mentioned limitations, we have analyzed a sufficient amount of cells.

We observed a GrzB activity in most, but not all killing events. Given the broad spectrum of different cytotoxic weapons, NK cells are not limited to use GrzB; they can employ different strategies to eliminate their targets ranging from DR-engagement to other Grz or to perforin lysing cells on its own (Backes et al., 2018, Prager et al., 2019, Prager and Watzl, 2019, Liesche et al., 2018, Bönnemann, 2023). It is therefore not surprising that some HeLa cells display no GrzB activity when dying. However, the identification of the responsible pathway or protein is out of scope of the FLRs used in this study. Hence, it remains to be assumed that these cells were killed by one of the above-mentioned strategies. Interestingly, we observed most differences in frequency

of “no GrzB activity” killing events depending on NK cell type used in this study (figures 17 and 18). This could hint at different regulations of cytotoxic strategies between NK cells. Differences in killing events without involvement of GrzB have been observed before using a FRET based GrzB reporter (Zhu et al., 2016). However, our observed distributions differ in that we observed a higher frequency of “no GrzB activity” deaths induced by NK92 cells than pre-activated NK cells, which was the opposite in the previously mentioned study of Zhu et al., 2016. These differences might be explained by the use of differently cultivated primary NK cells and NK92 cell subtypes.

The influx of cell-impermeable dye propidium iodide (PI) into HeLa cells during effector cell cytotoxicity led to the suggestion that a small GrzB amount could gain access to the cytosol via PM pores before the lesions are resealed (Lopez et al., 2013b). Moreover, cell rounding was initiated within 10 minutes after PI influx for most death events, though longer time spans have been observed (Lopez et al., 2013b). In line with that, we always found the main GrzB activity at the PM and our PM-bound FLR detected GrzB activity at the PM within 12 – 15 min prior to cell rounding. The agreement of our data with the PI-based observations of Lopez et al., 2013a and Lopez et al., 2013b indicate direct evidence that perforin pores allow not only PI but also GrzB to rapidly access the cytosol in a physiologically relevant context, providing further strong support for the PM pore model. This is also evident regardless of the NK cell activation state and expression levels of perforin and GrzB which indicates that the NK cell is only involved as a supplier of cargo but plays no decisive role for the GrzB uptake mechanism. Moreover, the preferential PM pore entry of GrzB could indicate the presence of critical GrzB targets mainly in vicinity of the PM. This conjecture may be supported by our observation of an absent GrzB activity at mitochondria (figure 19), suggesting a limited GrzB diffusion within the cytosol after entering via PM pores. Further, this would also question the biological relevance of many previously proposed GrzB targets for apoptosis induction like ones located within the nucleus. This assumption might be supported by the finding of a caspase-3 activity in short delay to a GrzB activity (Liesche et al., 2018). Hence, we hypothesize that GrzB rather initiates than executes apoptosis by cleaving cytosolic targets such as caspase-3 or BID proximal to the PM. Nevertheless, neither can we completely exclude the possibility that GrzB diffuses within the cell, but the amount of cleaved reporters is insufficient in exceeding the detection limit, nor do we deny that GrzB reaches e.g. the nucleus which could still be possible at advanced stages of apoptosis.

To our knowledge, the coexistence of both entry models within individual cells has not been demonstrated before within a physiologically relevant context. The endocytic uptake involves many steps until GrzB is released (Keefe et al., 2005, Thiery et al., 2010, Thiery et al., 2011), which would be evident in a different kinetic than PM pore delivery. Indeed, we observed a delayed onset of activity at the ER in HeLa cells starting about 6 – 9 min after activity at the PM; slightly faster than previously demonstrated (Thiery et al., 2011). Interestingly, we observed the same kinetics using an EE reporter (figure 20), which could imply a late release – not necessarily temporally, but rather spatially – but still argues for endocytosis. In agreement with Lopez et al. 2013b, our data argue against a critical role of the endocytosis model in the induction of HeLa target cell death, since most HeLa cells died with a sole GrzB activity at the PM, hence delivery of GrzB via PM pores is already sufficient (as stressed above). Rather, on basis of this study, the coexistence of several routes is plausible to ensure and support the delivery of GrzB. This assumption could be strengthened by indications on possible co-existence of several endocytosis pathways in HeLa cells (Bird et al., 2005, Trapani et al., 2003, Raja et al., 2005). It might as well be convincing to assume that the observed coexistence is rather a result of a purely accidental transfer of sufficient GrzB and perforin into the target cell during membrane repair.

Defective or absent perforin results in impaired NK and T cell cytotoxicity which has been demonstrated manifold, e.g. in patients suffering from the perforin affecting disease FHL (Voskoboinik and Trapani, 2013), in mice inheriting a perforin KO (Kägi et al., 1994) and *in vitro* for perforin KO effector cells (Kägi et al., 1994, Althaus et al., 2023) and cells deprived of mature perforin using ammonia or CMA (Domagala et al., 2025, House et al., 2017, Anft et al., 2020). Indeed, we observed a dose-dependent impairment of NK cell cytotoxicity upon CMA-induced perforin depletion also in this study (figure 23). Without perforin at hand, it could be speculated that the DR-mediated pathway was responsible for the few remaining deaths, as it has been shown before for HeLa cells in response to perforin KO NK cells (Prager et al., 2019). Moreover, the amount of available perforin has been proposed to direct the decision for a certain entry mechanism with PM pore model entry occurring at high but endocytosis at lower perforin concentrations (Browne et al., 1999). This has been put into context of early and late degranulation events of effector cells (Browne et al., 1999). During early degranulation events, NK cells are loaded with perforin and GrzB, but the storage gets reduced over time with each degranulation (Prager et al., 2019). This implies the

analysis of rather rare serial killing NK cells. We bypassed this analysis and took a shortcut by depleting mature perforin with CMA, which enabled us a less time-consuming analysis. Contrary to the assumption of a switch from PM pores to endocytosis we observed a trend of fewer events with additional GrzB uptake by endocytosis, while the preferential role of the PM pore model remained unchanged (figure 23). During the repair of membrane damage, perforin and GrzB are co-endocytosed (Keefe et al., 2005, Thiery et al., 2010). Subsequently, GrzB is released into the cytosol by perforin pores breaching endosomal vesicles (Thiery et al., 2011). It is therefore conceivable that by reducing the amount of perforin, less perforin is taken up by the cell, making the release of GrzB into the cytosol more difficult and unlikely. This could be supported by the finding of perforin being required for GrzB delivery into the cell cytosol, as otherwise GrzB would be trapped inside vesicles without inducing apoptosis (Keefe et al., 2005, Shi et al., 2005, Bird et al., 2005). On the contrary, it has been suggested that arc-shaped structures enable GrzB delivery across the PM whereas membrane repair is rather triggered by ring-shaped pores (Metkar et al., 2015, Leung et al., 2017). Accordingly, it could be suggested that by reducing the availability of active perforin, hardly any complete pores but rather arc or incomplete pore structures are assembled in the PM, hence limiting membrane repair induced GrzB uptake. Instead of a switch between different GrzB entry mechanisms allowing either one or the other, we conclude that perforin is decisively involved for the general successful transfer of GrzB into the target cell cytosol, which still occurs predominantly via PM pores even when perforin is limited.

While we observed a diversity of different death morphologies for HeLa cells, killed K562 cells mostly showed characteristics such as swelling and leakage (figure 24), which could be indicative of necrosis (Backes et al., 2018). Perforin on its own has the ability to induce necrotic death (Keefe et al., 2005, Backes et al., 2018), and it has been shown before that K562 mostly died with a necrotic phenotype during NK cell mediated killing (Backes et al., 2018). In alignment, this may suggest an increased sensitivity of K562 towards perforin mediated lysis and may even hint at a reduced effectiveness in terms of membrane repair or other protective measures exploited by target cells to evade perforin-mediated lysis. However, it should be cautioned that this assumption is only based on subjective observations on morphological changes, and this limitation should be addressed by implementing a suitable cell death marker. Further, this would also aid regarding the determination of the TOD, which was more difficult for suspension cells than for adherent cells given their round morphology.

Interestingly, our K562 cells were almost exclusively killed without GrzB activity (figure 24). Consistent with this, another GrzB biosensor also showed no activity in K562 cells but only in response to isolated primary NK cells but strikingly not in response to NK92 cells or NK cells expanded from PBMC (Vrazo et al., 2015). Other studies indicate the involvement of GrzB in K562 cell death (Mahrus and Craik, 2005, Andrade et al., 1998). We do not assume that GrzB was unable to enter K562, as it may well be that GrzB or other Grz are active within K562 cells past our TOD, yet GrzB is not necessarily the primary cause of K562 cell death, at least in our setting.

MDA-MB #468 cells – like HeLa cells – show the preferred GrzB delivery via PM pores, yet they display a markedly shortened time between the onset of GrzB activity and TOD, as well as a shortened delay between activity at PM and ER (figure 25). MDA-MB #468 seem to have a different cytosol-nucleus ratio than HeLa cells, hence it may appear that PM and ER FLRs are spatially in closer proximity in MDA-MB #468. This could suggest a shorter distance which has to be covered during endocytic uptake for GrzB to reach the ER FLR, which in turn could lead to a faster kinetic. However, this scenario could also indicate diffusion after PM entry – unlike in HeLa cells. However, we are lacking evidence for either explanation. Collagen is an extracellular matrix (ECM) component, which can influence e.g. cell adhesion and spreading (Rømer et al., 2021, Cho and Lee, 2023). Interestingly when using collagen-coated slides (ref to figure S15), the kinetics largely, but not entirely, approximate the kinetics observed with HeLa cells. The presence of a rare dominant endocytic uptake and the tendency that this – and endocytic uptake in general – may be increased by changing the membrane tension is striking (figures 25 and 26). It has been indicated that the membrane mechanical properties of a cell could have an influence on membrane repair (Togo et al., 2000, Gauthier et al., 2011). Furthermore, softer membrane properties of tumor cells impair immune cell killing by perforin (Liu et al., 2021, Zhou et al., 2024, Yanamandra et al., 2024, Tuomela et al., 2022, Basu et al., 2016). We used the improved Blebbistatin derivative (S)-4'-nitro-Blebbistatin to manipulate the membrane tension of MDA-MB #468 cells. Despite our observation of an increased susceptibility to NK cell mediated killing (figure 27), which is consistent with previous findings (Yanamandra et al., 2024), we cannot determine the stability of (S)-4'-nitro-Blebbistatin-mediated inhibition after washout. Furthermore, we came across inconsistencies in the literature regarding the membrane tension-modifying effect of Blebbistatin, which may be attributed to differences in cell attachment properties (Chan et al., 2015). Therefore, our results with (S)-4'-nitro-Blebbistatin should be taken with

caution. Nevertheless, MDA-MB #468 cells grow adherently and one may assume that their membrane is softened in response to treatment, according to reports on other adherent cell lines (Chan et al., 2015, Swaminathan et al., 2011, Liu et al., 2021). In addition, perforin has been found less likely to assemble pores in soft membranes (Liu et al., 2021, Tuomela et al., 2022, Yanamandra et al., 2024, Zhou et al., 2024). Taking it to the extreme, one could now suggest that perforin still forms few, small pores into the PM, which might be rapidly repaired and could result in an increased uptake of GrzB and perforin via endocytosis rather than PM pore entry. Yet, the higher sensitivity to NK cell mediated cytotoxicity after (S)-4'-nitro-Blebbistatin treatment would be in favor of a stiffened membrane as observed for Blebbistatin-treated K562 (Yanamandra et al., 2024). Furthermore, our MDA-MB #468 cells were cultured on collagen in this setup, which might have affected the membrane tension. For example, for hydrogels it has been outlined that its mechanical properties directly influence the membrane tension of a cell (Basu et al., 2016, Tuomela et al., 2022). However, without any indication on how (S)-4'-nitro-Blebbistatin affected the membrane tension of MDA-MB #468 cells in our setting, our assumptions remain speculative. Furthermore, our results only illustrate a possibility which, in our opinion, is of little relevance for GrzB entry given the low frequency of occurrence, at least in our 2D context. This may become more important in a 3D *in vitro* setting or in tissues when cells are surrounded by ECM of different stiffnesses.

In conclusion, this study adds to current understanding of a preferred GrzB delivery via PM pores. This is unchanged by conditions like NK cell activation state and perforin concentration. Nevertheless, we could show the coexistence of endocytic uptake as possible supportive mechanism, which may contribute differently depending on the target cell and presumably its membrane tension properties. Differences between target cells should be considered in the future when analyzing mechanisms of effector cell cytotoxicity. While our observation of a dominant entry into the PM pore holds true for GrzB, it would be intriguing to analyze whether the remaining 4 human Grz follow a similar pathway, especially considering the larger GrzA homodimer (Trapani, 2001), which could be relatively easily addressed by modifying the existing GrzA specific FLRs (Liesche et al., 2018, Bönnemann, 2023).

6. References

ADRAIN, C., MURPHY, B. M. & MARTIN, S. J. 2005. Molecular ordering of the caspase activation cascade initiated by the cytotoxic T lymphocyte/natural killer (CTL/NK) protease granzyme B. *J Biol Chem,* 280**,** 4663-4673.

AGRESTI, A. 2002. *Categorical Data Analysis,* Hoboken, NJ, Wiley.

ALAM, R. 1998. A brief review of the immune system. *Prim Care,* 25**,** 727-738.

ALTER, G., MALENFANT, J. M. & ALTFELD, M. 2004. CD107a as a functional marker for the identification of natural killer cell activity. *J Immunol Methods,* 294**,** 15-22.

ALTHAUS, J., NILIUS-ELILIWI, V., MAGHNOUJ, A., DORING, S., SCHROERS, R., HUDECEK, M., HAHN, S. A. & MIKA, T. 2023. Cytotoxicity of CD19-CAR-NK92 cells is primarily mediated via perforin/granzyme pathway. *Cancer Immunol Immunother,* 72**,** 2573-2583.

ANDRADE, F., ROY, S., NICHOLSON, D., THORNBERRY, N., ROSEN, A. & CASCIOLA-ROSEN, L. 1998. Granzyme B directly and efficiently cleaves several downstream caspase substrates: implications for CTL-induced apoptosis. *Immunity,* 8**,** 451-460.

ANDRIN, C., PINKOSKI, M. J., BURNS, K., ATKINSON, E. A., KRAHENBUHL, O., HUDIG, D., FRASER, S. A., WINKLER, U., TSCHOPP, J., OPAS, M., BLEACKLEY, R. C. & MICHALAK, M. 1998. Interaction between a Ca2+-binding protein calreticulin and perforin, a component of the cytotoxic T-cell granules. *Biochemistry,* 37**,** 10386-10394.

ANFT, M., NETTER, P., URLAUB, D., PRAGER, I., SCHAFFNER, S. & WATZL, C. 2020. NK cell detachment from target cells is regulated by successful cytotoxicity and influences cytokine production. *Cell Mol Immunol,* 17**,** 347-355.

BACKES, C. S., FRIEDMANN, K. S., MANG, S., KNÖRCK, A., HOTH, M. & KUMMEROW, C. 2018. Natural killer cells induce distinct modes of cancer cell death: Discrimination, quantification, and modulation of apoptosis, necrosis, and mixed forms. *J Biol Chem,* 293**,** 16348-16363.

BALAJI, K. N., SCHASCHKE, N., MACHLEIDT, W., CATALFAMO, M. & HENKART, P. A. 2002. Surface cathepsin B protects cytotoxic lymphocytes from self-destruction after degranulation. *J Exp Med,* 196**,** 493-503.

BARAN, K., CICCONE, A., PETERS, C., YAGITA, H., BIRD, P. I., VILLADANGOS, J. A. & TRAPANI, J. A. 2006. Cytotoxic T lymphocytes from cathepsin B-deficient mice survive normally in vitro and in vivo after encountering and killing target cells. *J Biol Chem,* 281**,** 30485-30491.

BASU, R., WHITLOCK, B. M., HUSSON, J., LE FLOC'H, A., JIN, W., OYLER-YANIV, A., DOTIWALA, F., GIANNONE, G., HIVROZ, C., BIAIS, N., LIEBERMAN, J., KAM, L. C. & HUSE, M. 2016. Cytotoxic T Cells Use Mechanical Force to Potentiate Target Cell Killing. *Cell,* 165**,** 100-110.

BEAUDOUIN, J., LIESCHE, C., ASCHENBRENNER, S., HORNER, M. & EILS, R. 2013. Caspase-8 cleaves its substrates from the plasma membrane upon CD95-induced apoptosis. *Cell Death Differ,* 20**,** 599-610.

BEDNAR, C., KUBEL, S., CORDSMEIER, A., SCHOLZ, B., MENSCHIKOWSKI, H. & ENSSER, A. 2023. A Genetically Encoded Dark-to-Bright Biosensor for Visualisation of Granzyme-Mediated Cytotoxicity. *Int J Mol Sci,* 24**,** 1-15.

BERGERON, J. J., BRENNER, M. B., THOMAS, D. Y. & WILLIAMS, D. B. 1994. Calnexin: a membrane-bound chaperone of the endoplasmic reticulum. *Trends Biochem Sci,* 19**,** 124-128.

BEZIAT, V., DUFFY, D., QUOC, S. N., LE GARFF-TAVERNIER, M., DECOCQ, J., COMBADIERE, B., DEBRE, P. & VIEILLARD, V. 2011. CD56brightCD16+ NK cells: a functional intermediate stage of NK cell differentiation. *J Immunol,* 186**,** 6753-6761.

BHAT, R. & WATZL, C. 2007. Serial killing of tumor cells by human natural killer cells - Enhancement by therapeutic antibodies. *PLoS One,* 2**,** 1-7.

BIRD, C. H., SUN, J., UNG, K., KARAMBALIS, D., WHISSTOCK, J. C., TRAPANI, J. A. & BIRD, P. I. 2005. Cationic sites on granzyme B contribute to cytotoxicity by promoting its uptake into target cells. *Mol Cell Biol,* 25**,** 7854-7867.

BIRD, C. H., SUTTON, V. R., SUN, J., HIRST, C. E., NOVAK, A., KUMAR, S., TRAPANI, J. A. & BIRD, P. I. 1998. Selective Regulation of Apoptosis: the Cytotoxic Lymphocyte Serpin Proteinase Inhibtior 9 Protects against Granzyme B-Mediated Apoptosis without Perturbing the Fas Cell Death Pathway. *Mol Cell Biol,* 18**,** 6387-6398.

BÖNNEMANN, V. 2023. *The Role of Granzymes in Natural Killer Cell Cytotoxicity.* Doctor of Natural Sciences, Technische Universität Dortmund.

BROWNE, K. A., BLINK, E., SUTTON, V. R., FROELICH, C. J., JANS, D. A. & TRAPANI, J. A. 1999. Cytosolic Delivery of Granzyme B by Bacterial Toxins: Evidence that Endosomal Disruption, in Addition to Transmembrane Pore Formation, Is an Important Function of Perforin. *Mol Cell Biol,* 19**,** 8604-8615.

BRUNING, N. 2020. *Investigation on how granzyme B enters target cells via fluorescence localization reporter.* Master of Science, Technische Universität Dortmund.

BRUNING, N., BÖNNEMANN, V. & WATZL, C. 2023. Analyzing the activity of the proteases granzyme B and caspase-8 inside living cells using fluorescence localization reporters. *Methods Cell Biol,* 178**,** 13-24.

BRYCESON, Y. T., LJUNGGREN, H. G. & LONG, E. O. 2009. Minimal requirement for induction of natural cytotoxicity and intersection of activation signals by inhibitory receptors. *Blood,* 114**,** 2657-2666.

BRYCESON, Y. T., MARCH, M. E., BARBER, D. F., LJUNGGREN, H. G. & LONG, E. O. 2005. Cytolytic granule polarization and degranulation controlled by different receptors in resting NK cells. *J Exp Med,* 202**,** 1001-1012.

BURKHARDT, J. K., HESTER, S. & ARGON, Y. 1989. Two proteins targeted to the same lytic granule compartment undergo very different posttranslational processing. *Proc Natl Acad Sci U S A,* 86**,** 7128-7132.

BURKHARDT, J. K., HESTER, S., LAPHAM, C. K. & ARGON, Y. 1990. The Lytic Granules of Natural Killer Cells Are Dual-Function Organelles Combining Secretory and Pre-lysosomal Compartments. *J Cell Biol,* 111**,** 2327-2340.

CATALFAMO, M. & HENKART, P. A. 2003. Perforin and the granule exocytosis cytotoxicity pathway. *Curr Opin Immunol,* 15**,** 522-527.

CHAN, C. J., EKPENYONG, A. E., GOLFIER, S., LI, W., CHALUT, K. J., OTTO, O., ELGETI, J., GUCK, J. & LAUTENSCHLAGER, F. 2015. Myosin II Activity Softens Cells in Suspension. *Biophys J,* 108**,** 1856-1869.

CHO, A. Y. & LEE, H. J. 2023. Investigating the Impact of Mechanical Properties and Cell-Collagen Interaction on NIH3T3 Function: A Comparative Study on Different Substrates and Culture Environments. *Gels,* 9**,** 1-16.

CHOI, P. J. & MITCHISON, T. J. 2013. Imaging burst kinetics and spatial coordination during serial killing by single natural killer cells. *Proc Natl Acad Sci U S A,* 110**,** 6488-6493.

CHOWDHURY, D. & LIEBERMAN, J. 2008. Death by a thousand cuts: granzyme pathways of programmed cell death. *Annu Rev Immunol,* 26**,** 389-420.

CLAUS, M., WINGERT, S. & WATZL, C. 2016. Modulation of natural killer cell functions by interactions between 2B4 and CD48 in cis and in trans. *Open Biol,* 6**,** 1-11.

COHNEN, A., CHIANG, S. C., STOJANOVIC, A., SCHMIDT, H., CLAUS, M., SAFTIG, P., JANSSEN, O., CERWENKA, A., BRYCESON, Y. T. & WATZL, C. 2013. Surface CD107a/LAMP-1 protects natural killer cells from degranulation-associated damage. *Blood,* 122**,** 1411-1418.

COLUCCI, F., CALIGIURI, M. A. & DI SANTO, J. P. 2003. What does it take to make a natural killer? *Nat Rev Immunol,* 3**,** 413-425.

D'ANGELO, M. E., BIRD, P. I., PETERS, C., REINHECKEL, T., TRAPANI, J. A. & SUTTON, V. R. 2010. Cathepsin H is an additional convertase of pro-granzyme B. *J Biol Chem,* 285**,** 20514-20519.

DANIELS, R. W., ROSSANO, A. J., MACLEOD, G. T. & GANETZKY, B. 2014. Expression of multiple transgenes from a single construct using viral 2A peptides in Drosophila. *PLoS One,* 9**,** 1-10.

DOMAGALA, J., GRZYWA, T. M., BARANOWSKA, I., JUSTYNIARSKA, M., TANNIR, R., GRACZYK-JARZYNKA, A., KUSOWSKA, A., LECKA, M., POREBA, M., FIDYT, K., MARHELAVA, K., PILCH, Z., PICARD, L. K., WEGIERSKI, T., JASTRZEBSKI, K., KRAWCZYK, M., KLOPOTOWSKA, M., GRANICA, M., URLAUB, D., HAJDUK, S., NEESER, A., MOROS, S., KOZLOWSKI, P., BOBROWICZ, M., MIACZYNSKA, M., MA, L., WATZL, C. & WINIARSKA, M. 2025. Ammonia Suppresses the Antitumor Activity of Natural Killer Cells and T Cells by Decreasing Mature Perforin. *Cancer Res*.

DRESSEL, R., RAJA, S. M., HONING, S., SEIDLER, T., FROELICH, C. J., VON FIGURA, K. & GUNTHER, E. 2004. Granzyme-mediated cytotoxicity does not involve the mannose 6-phosphate receptors on target cells. *J Biol Chem,* 279**,** 20200-20210.

EARNSHAW, W. C., MARTINS, L. M. & KAUFMANN, S. H. 1999. Mammalian caspases: structure, activation, substrates, and functions during apoptosis. *Annu Rev Biochem,* 68**,** 383-424.

ELMORE, S. 2007. Apoptosis: A Review of Programmed Cell Death. *Toxicol Pathol,* 35**,** 495-516.

FAURIAT, C., LONG, E. O., LJUNGGREN, H. G. & BRYCESON, Y. T. 2010. Regulation of human NK-cell cytokine and chemokine production by target cell recognition. *Blood,* 115**,** 2167-2176.

FISCHER, U., JANICKE, R. U. & SCHULZE-OSTHOFF, K. 2003. Many cuts to ruin: a comprehensive update of caspase substrates. *Cell Death Differ,* 10**,** 76-100.

FRASER, S. A., KARIMI, R., MICHALAK, M. & HUDIG, D. 2000. Perforin lytic activity is controlled by calreticulin. *J Immunol,* 164**,** 4150-4155.

FRASER, S. A., MICHALAK, M., WELCH, W. H. & HUDIG, D. 1998. Calreticulin, a component of the endoplasmic reticulum and of cytotoxic lymphocyte granules, regulates perforin-mediated lysis in the hemolytic model system. *Biochem Cell Biol,* 76**,** 881-887.

FROELICH, C. J., ORTH, K., TURBOV, J., SETH, P., GOTTLIEB, R., BABIOR, B., SHAH, G. M., BLEACKLEY, R. C., DIXIT, V. M. & HANNA, W. 1996. New paradigm for lymphocyte granule-mediated cytotoxicity. Target cells bind and internalize granzyme B, but an endosomolytic agent is necessary for cytosolic delivery and subsequent apoptosis. *J Biol Chem,* 271**,** 29073-29079.

GALVIN, J. P., SPAENY-DEKKING, L. H., WANG, B., SETH, P., HACK, C. E. & FROELICH, C. J. 1999. Apoptosis induced by granzyme B-glycosaminoglycan complexes: implications for granule-mediated apoptosis in vivo. *J Immunol,* 162**,** 5345-5350.

GAUTHIER, N. C., FARDIN, M. A., ROCA-CUSACHS, P. & SHEETZ, M. P. 2011. Temporary increase in plasma membrane tension coordinates the activation of exocytosis and contraction during cell spreading. *Proc Natl Acad Sci U S A,* 108**,** 14467-14472.

GRIFFITHS, G. M. & ISAAZ, S. 1993. Granzymes A and B Are Targeted to the Lytic Granules of Lymphocytes by the Mannose-6-Phosphate Receptor. *The Journal of Cell Biology,* 120**,** 885-896.

GROSCURTH, P., QIAO, B. Y., PODACK, E. R. & HENGARTNER, H. 1987. Cellular localization of perforin 1 in murine cloned cytotoxic T lymphocytes. *J Immunol,* 138**,** 2749-2752.

GRUJIC, M., BRAGA, T., LUKINIUS, A., ELORANTA, M. L., KNIGHT, S. D., PEJLER, G. & ABRINK, M. 2005. Serglycin-deficient cytotoxic T lymphocytes display

defective secretory granule maturation and granzyme B storage. *J Biol Chem,* 280**,** 33411-33418.

GWALANI, L. A. & ORANGE, J. S. 2018. Single Degranulations in NK Cells Can Mediate Target Cell Killing. *J Immunol,* 200**,** 3231-3243.

HAMIDI, H., LILJA, J. & IVASKA, J. 2017. Using xCELLigence RTCA Instrument to Measure Cell Adhesion. *Bio Protoc,* 7**,** 1-16.

HARRIS, J. L., PETERSON, E. P., HUDIG, D., THORNBERRY, N. A. & CRAIK, C. S. 1998. Definition and redesign of the extended substrate specificity of granzyme B. *J Biol Chem,* 273**,** 27364-27373.

HEIM, R., CUBITT, A. B. & TSIEN, R. Y. 1995. Improved green fluorescence. *Nature,* 373**,** 663-664.

HIRST, C. E., BUZZA, M. S., BIRD, C. H., WARREN, H. S., CAMERON, P. U., ZHANG, M., ASHTON-RICKARDT, P. G. & BIRD, P. I. 2003. The intracellular granzyme B inhibitor, proteinase inhibitor 9, is up-regulated during accessory cell maturation and effector cell degranulation, and its overexpression enhances CTL potency. *J Immunol,* 170**,** 805-815.

HODEL, A. W., RUDD-SCHMIDT, J. A., NOORI, T., LUPTON, C. J., CHEUK, V. C. T., TRAPANI, J. A., HOOGENBOOM, B. W. & VOSKOBOINIK, I. 2025. Acidic pH can attenuate immune killing through inactivation of perforin. *EMBO Rep,* 26**,** 929-947.

HOUSE, I. G., HOUSE, C. M., BRENNAN, A. J., GILAN, O., DAWSON, M. A., WHISSTOCK, J. C., LAW, R. H., TRAPANI, J. A. & VOSKOBOINIK, I. 2017. Regulation of perforin activation and pre-synaptic toxicity through C-terminal glycosylation. *EMBO Rep,* 18**,** 1775-1785.

IDA, H., NAKASHIMA, T., KEDERSHA, N. L., YAMASAKI, S., HUANG, M., IZUMI, Y., MIYASHITA, T., ORIGUCHI, T., KAWAKAMI, A., MIGITA, K., BIRD, P. I., ANDERSON, P. & EGUCHI, K. 2003. Granzyme B leakage-induced cell death: a new type of activation-induced natural killer cell death. *Eur J Immunol,* 33**,** 3284-3292.

IVANOVA, M. E., LUKOYANOVA, N., MALHOTRA, S., TOPF, M., TRAPANI, J. A., VOSKOBOINIK, I. & SAIBIL, H. R. 2022. The pore conformation of lymphocyte perforin. *Sci Adv,* 8**,** 1-10.

JAMES, A. M., HSU, H. T., DONGRE, P., UZEL, G., MACE, E. M., BANERJEE, P. P. & ORANGE, J. S. 2013. Rapid activation receptor- or IL-2-induced lytic granule convergence in human natural killer cells requires Src, but not downstream signaling. *Blood,* 121**,** 2627-2637.

JENNE, D. E. & TSCHOPP, J. 1988. Granzymes, a family of serine proteases released from granules of cytolytic T lymphocytes upon T cell receptor stimulation. *Immunol Rev,* 103**,** 53-71.

JOST, S. & ALTFELD, M. 2013. Control of human viral infections by natural killer cells. *Annu Rev Immunol,* 31**,** 163-194.

KÄGI, D., LEDERMANN, B., BÜRKI, K., SEILER, P., ODERMATT, B., OLSEN, K. J., PODACK, E. R., ZINKGERNAGEL, R. M. & HENGARTNER, H. 1994. Cytotoxicity mediated by T cells and natural killer cells is greatly impaired in perforin-deficient mice. *Nature,* 369**,** 31-37.

KÄRRE, K., LJUNGGREN, H. G., PIONTEK, G. & KIESSLING, R. 1986. Selective rejection of H-2-deficient lymphoma variants suggests alternative immune defence strategy. *Nature,* 319**,** 675-678.

KATAOKA, T., TAKAKU, K., MAGAE, J., SHINOHARA, N., TAKAYAMA, H., KONDO, S. & NAGAI, K. 1994. Acidification is essential for maintaining the structure and function of lytic granules of CTL. Effect of concanamycin A, an inhibitor of vacuolar type H(+)-ATPase, on CTL-mediated cytotoxicity. *J Immunol,* 153**,** 3938-3947.

KATAOKA, T., TOGASHI, K., TAKAYAMA, H., TAKAKU, K. & NAGAI, K. 1997. Inactivation and proteolytic degradation of perforin within lytic granules upon neutralization of acidic pH. *Immunology,* 91**,** 493-500.

KEEFE, D., SHI, L., FESKE, S., MASSOL, R., NAVARRO, F., KIRCHHAUSEN, T. & LIEBERMAN, J. 2005. Perforin triggers a plasma membrane-repair response that facilitates CTL induction of apoptosis. *Immunity,* 23**,** 249-262.

KEPIRO, M., VARKUTI, B. H., VEGNER, L., VOROS, G., HEGYI, G., VARGA, M. & MALNASI-CSIZMADIA, A. 2014. para-Nitroblebbistatin, the non-cytotoxic and photostable myosin II inhibitor. *Angew Chem Int Ed Engl,* 53**,** 8211-8215.

KEPPLER, A., KINDERMANN, M., GENDREIZIG, S., PICK, H., VOGEL, H. & JOHNSSON, K. 2004. Labeling of fusion proteins of O6-alkylguanine-DNA alkyltransferase with small molecules in vivo and in vitro. *Methods,* 32**,** 437-444.

KIESSLING, R., KLEIN, E. & WIGZELL, H. 1975. "Natural" killer cells in the mouse. I. Cytotoxic cells with specificity for mouse Moloney leukemia cells. Specificity and distribution according to genotype. *Eur J Immunol,* 5**,** 112-117.

KONJAR, S., SUTTON, V. R., HOVES, S., REPNIK, U., YAGITA, H., REINHECKEL, T., PETERS, C., TURK, V., TURK, B., TRAPANI, J. A. & KOPITAR-JERALA, N. 2010. Human and mouse perforin are processed in part through cleavage by the lysosomal cysteine proteinase cathepsin L. *Immunology,* 131**,** 257-267.

KOVACS, M., TOTH, J., HETENYI, C., MALNASI-CSIZMADIA, A. & SELLERS, J. R. 2004. Mechanism of blebbistatin inhibition of myosin II. *J Biol Chem,* 279**,** 35557-35563.

KRZEWSKI, K., GIL-KRZEWSKA, A., NGUYEN, V., PERUZZI, G. & COLIGAN, J. E. 2013. LAMP1/CD107a is required for efficient perforin delivery to lytic granules and NK-cell cytotoxicity. *Blood,* 121**,** 4672-4683.

KUPFER, A., SINGER, S. J. & DENNERT, G. 1986. On the mechanism of unidirectional killing in mixtures of two cytotoxic T lymphocytes. Unidirectional polarization of cytoplasmic organelles and the membrane-associated cytoskeleton in the effector cell. *J Exp Med,* 163**,** 489-498.

KURSCHUS, F. C., BRUNO, R., FELLOWS, E., FALK, C. S. & JENNE, D. E. 2005. Membrane receptors are not required to deliver granzyme B during killer cell attack. *Blood,* 105**,** 2049-2058.

KURSCHUS, F. C., FELLOWS, E., STEGMANN, E. & JENNE, D. E. 2008. Granzyme B delivery via perforin is restricted by size, but not by heparan sulfate-dependent endocytosis. *Proc Natl Acad Sci,* 105**,** 13799-13804.

LAW, R. H., LUKOYANOVA, N., VOSKOBOINIK, I., CARADOC-DAVIES, T. T., BARAN, K., DUNSTONE, M. A., D'ANGELO, M. E., ORLOVA, E. V., COULIBALY, F., VERSCHOOR, S., BROWNE, K. A., CICCONE, A., KUIPER, M. J., BIRD, P. I., TRAPANI, J. A., SAIBIL, H. R. & WHISSTOCK, J. C. 2010. The structural basis for membrane binding and pore formation by lymphocyte perforin. *Nature,* 468**,** 447-451.

LAWE, D. C., PATKI, V., HELLER-HARRISON, R., LAMBRIGHT, D. & CORVERA, S. 2000. The FYVE domain of early endosome antigen 1 is required for both phosphatidylinositol 3-phosphate and Rab5 binding. Critical role of this dual interaction for endosomal localization. *J Biol Chem,* 275**,** 3699-3705.

LEUNG, C., HODEL, A. W., BRENNAN, A. J., LUKOYANOVA, N., TRAN, S., HOUSE, C. M., KONDOS, S. C., WHISSTOCK, J. C., DUNSTONE, M. A., TRAPANI, J. A., VOSKOBOINIK, I., SAIBIL, H. R. & HOOGENBOOM, B. W. 2017. Real-time visualization of perforin nanopore assembly. *Nat Nanotechnol,* 12**,** 467-475.

LI, J., FIGUEIRA, S. K., VRAZO, A. C., BINKOWSKI, B. F., BUTLER, B. L., TABATA, Y., FILIPOVICH, A., JORDAN, M. B. & RISMA, K. A. 2014. Real-time detection of CTL function reveals distinct patterns of caspase activation mediated by Fas versus granzyme B. *J Immunol,* 193**,** 519-528.

LI, Y. & ORANGE, J. S. 2021. Degranulation enhances presynaptic membrane packing, which protects NK cells from perforin-mediated autolysis. *PLoS Biol,* 19**,** 1-29.

LIESCHE, C., SAUER, P., PRAGER, I., URLAUB, D., CLAUS, M., EILS, R., BEAUDOUIN, J. & WATZL, C. 2018. Single-Fluorescent Protein Reporters Allow Parallel Quantification of Natural Killer Cell-Mediated Granzyme and Caspase Activities in Single Target Cells. *Front Immunol,* 9**,** 1-12.

LIU, Y., ZHANG, T., ZHANG, H., LI, J., ZHOU, N., FISKESUND, R., CHEN, J., LV, J., MA, J., ZHANG, H., TANG, K., CHENG, F., ZHOU, Y., ZHANG, X., WANG, N. & HUANG, B. 2021. Cell Softness Prevents Cytolytic T-cell Killing of Tumor-Repopulating Cells. *Cancer Res,* 81**,** 476-488.

LJUNGGREN, H. G. & KÄRRE, K. 1990. In search of the 'missing self': MHC molecules and NK cell recognition. *Immunol Today,* 11**,** 237-244.

LOPEZ, J. A., JENKINS, M. R., RUDD-SCHMIDT, J. A., BRENNAN, A. J., DANNE, J. C., MANNERING, S. I., TRAPANI, J. A. & VOSKOBOINIK, I. 2013a. Rapid and unidirectional perforin pore delivery at the cytotoxic immune synapse. *J Immunol,* 191**,** 2328-2334.

LOPEZ, J. A., SUSANTO, O., JENKINS, M. R., LUKOYANOVA, N., SUTTON, V. R., LAW, R. H., JOHNSTON, A., BIRD, C. H., BIRD, P. I., WHISSTOCK, J. C.,

TRAPANI, J. A., SAIBIL, H. R. & VOSKOBOINIK, I. 2013b. Perforin forms transient pores on the target cell plasma membrane to facilitate rapid access of granzymes during killer cell attack. *Blood,* 121**,** 2659-2668.

MACE, E. M., DONGRE, P., HSU, H. T., SINHA, P., JAMES, A. M., MANN, S. S., FORBES, L. R., WATKIN, L. B. & ORANGE, J. S. 2014. Cell biological steps and checkpoints in accessing NK cell cytotoxicity. *Immunol Cell Biol,* 92**,** 245-255.

MACE, E. M., MONKLEY, S. J., CRITCHLEY, D. R. & TAKEI, F. 2009. A dual role for talin in NK cell cytotoxicity: activation of LFA-1-mediated cell adhesion and polarization of NK cells. *J Immunol,* 182**,** 948-956.

MACE, E. M., ZHANG, J., SIMINOVITCH, K. A. & TAKEI, F. 2010. Elucidation of the integrin LFA-1-mediated signaling pathway of actin polarization in natural killer cells. *Blood,* 116**,** 1272-1279.

MAHRUS, S. & CRAIK, C. S. 2005. Selective chemical functional probes of granzymes A and B reveal granzyme B is a major effector of natural killer cell-mediated lysis of target cells. *Chem Biol,* 12**,** 567-77.

MASSON, D., PETERS, P. J., GEUZE, H. J., BORST, J. & TSCHOPP, J. 1990. Interaction of chondroitin sulfate with perforin and granzymes of cytolytic T-cells is dependent on pH. *Biochemistry,* 29**,** 11229-11235.

MELSEN, J. E., LUGTHART, G., LANKESTER, A. C. & SCHILHAM, M. W. 2016. Human Circulating and Tissue-Resident CD56(bright) Natural Killer Cell Populations. *Front Immunol,* 7**,** 1-10.

MENTLIK, A. N., SANBORN, K. B., HOLZBAUR, E. L. & ORANGE, J. S. 2010. Rapid lytic granule convergence to the MTOC in natural killer cells is dependent on dynein but not cytolytic commitment. *Mol Biol Cell,* 21**,** 2241-2256.

METKAR, S. S., MARCHIORETTO, M., ANTONINI, V., LUNELLI, L., WANG, B., GILBERT, R. J., ANDERLUH, G., ROTH, R., POOGA, M., PARDO, J., HEUSER, J. E., SERRA, M. D. & FROELICH, C. J. 2015. Perforin oligomers form arcs in cellular membranes: a locus for intracellular delivery of granzymes. *Cell Death Differ,* 22**,** 74-85.

METKAR, S. S., WANG, B., AGUILAR-SANTELISES, M., RAJAR, S. M., UHLIN-HANSEN, L., PODACK, E., TRAPANI, J. A. & FROELICH, C. J. 2002. Cytotoxic Cell Granule-Mediated Apoptosis: Perforin Delivers Granzyme B-Serglycin Complexes into Target Cells without Plasma Membrane Pore Formation. *Immunity,* 16**,** 417-428.

MOTYKA, B., KORBUTT, G. S., PINKOSKI, M. J., HEIBEIN, J. A., CAPUTO, A., HOBMAN, M., BARRY, M., SHOSTAK, I., SAWCHUK, T., HOLMES, C. F. B., GAULDIE, J. & BLEACKLEY, R. C. 2000. Mannose 6-Phosphate/Insulin-like Growth Factor II Receptor is a Death Receptor for Granzyme B during Cytotoxic T Cell-Induced Apoptosis. *Cell,* 103**,** 491-500.

NETTER, P., ANFT, M. & WATZL, C. 2017. Termination of the Activating NK Cell Immunological Synapse Is an Active and Regulated Process. *J Immunol,* 199**,** 2528-2535.

NOIVA, R. & LENNARZ, W. J. 1992. Protein disulfide isomerase. A multifunctional protein resident in the lumen of the endoplasmic reticulum. *J Biol Chem,* 267**,** 3553-3556.

NÜSSING, S., SUTTON, V. R., TRAPANI, J. A. & PARISH, I. A. 2022. Beyond target cell death - Granzyme serine proteases in health and disease. *Mol Aspects Med,* 88**,** 1-11.

ORANGE, J. S. 2008. Formation and function of the lytic NK-cell immunological synapse. *Nat Rev Immunol,* 8**,** 713-725.

PACKARD, B. Z., TELFORD, W. G., KOMORIYA, A. & HENKART, P. A. 2007. Granzyme B activity in target cells detects attack by cytotoxic lymphocytes. *J Immunol,* 179**,** 3812-3820.

PETER, M. E. & KRAMMER, P. H. 2003. The CD95(APO-1/Fas) DISC and beyond. *Cell Death Differ,* 10**,** 26-35.

PETERS, P. J., BORST, J., OORSCHOT, V., FUKUDA, M., KRÄHENBÜHL, O., TSCHOPP, J. & SLOT, J. W. 1991. Cytotoxic T Lymphocyte Granules Are Secretory Lysosomes, Containing Both Perforin And Granzymes. *J Exp Med,* 173**,** 1099-1109.

PINKOSKI, M. J., HOBMAN, M., HEIBEIN, J. A., TOMASELLI, K., LI, F., SETH, P., FROELICH, C. J. & BLEACKLEY, R. C. 1998. Entry and Trafficking of Granzyme B in Target Cells During Granzyme B-Perforin–Mediated Apoptosis. *Blood,* 92**,** 1044-1054.

PRAGER, I., LIESCHE, C., VAN OOIJEN, H., URLAUB, D., VERRON, Q., SANDSTROM, N., FASBENDER, F., CLAUS, M., EILS, R., BEAUDOUIN, J., ONFELT, B. & WATZL, C. 2019. NK cells switch from granzyme B to death receptor-mediated cytotoxicity during serial killing. *J Exp Med,* 216**,** 2113-2127.

PRAGER, I. & WATZL, C. 2019. Mechanisms of natural killer cell-mediated cellular cytotoxicity. *J Leukoc Biol,* 105**,** 1319-1329.

PRAPER, T., BESENICAR, M. P., ISTINIC, H., PODLESEK, Z., METKAR, S. S., FROELICH, C. J. & ANDERLUH, G. 2010. Human perforin permeabilizing activity, but not binding to lipid membranes, is affected by pH. *Mol Immunol,* 47**,** 2492-2504.

PRAPER, T., SONNEN, A., VIERO, G., KLADNIK, A., FROELICH, C. J., ANDERLUH, G., DALLA SERRA, M. & GILBERT, R. J. 2011. Human perforin employs different avenues to damage membranes. *J Biol Chem,* 286**,** 2946-2955.

RAJA, S. M., METKAR, S. S., HONING, S., WANG, B., RUSSIN, W. A., PIPALIA, N. H., MENAA, C., BELTING, M., CAO, X., DRESSEL, R. & FROELICH, C. J. 2005. A novel mechanism for protein delivery: granzyme B undergoes electrostatic exchange from serglycin to target cells. *J Biol Chem,* 280**,** 20752-20761.

RAJA, S. M., WANG, B., DANTULURI, M., DESAI, U. R., DEMELER, B., SPIEGEL, K., METKAR, S. S. & FROELICH, C. J. 2002. Cytotoxic cell granule-mediated apoptosis. Characterization of the macromolecular complex of granzyme B with serglycin. *J Biol Chem,* 277**,** 49523-49530.

RAK, G. D., MACE, E. M., BANERJEE, P. P., SVITKINA, T. & ORANGE, J. S. 2011. Natural killer cell lytic granule secretion occurs through a pervasive actin network at the immune synapse. *PLoS Biol,* 9**,** 1-15.

RAULET, D. H. & VANCE, R. E. 2006. Self-tolerance of natural killer cells. *Nat Rev Immunol,* 6**,** 520-531.

REBOUL, C. F., WHISSTOCK, J. C. & DUNSTONE, M. A. 2016. Giant MACPF/CDC pore forming toxins: A class of their own. *Biochim Biophys Acta,* 1858**,** 475-486.

RØMER, A. M. A., THORSETH, M. L. & MADSEN, D. H. 2021. Immune Modulatory Properties of Collagen in Cancer. *Front Immunol,* 12**,** 791453.

RUDD-SCHMIDT, J. A., HODEL, A. W., NOORI, T., LOPEZ, J. A., CHO, H. J., VERSCHOOR, S., CICCONE, A., TRAPANI, J. A., HOOGENBOOM, B. W. & VOSKOBOINIK, I. 2019a. Lipid order and charge protect killer T cells from accidental death. *Nat Commun,* 10**,** 1-13.

RUDD-SCHMIDT, J. A., TRAPANI, J. A. & VOSKOBOINIK, I. 2019b. Distinguishing perforin-mediated lysis and granzyme-dependent apoptosis. *Methods Enzymol,* 629**,** 291-306.

SANBORN, K. B., RAK, G. D., MARU, S. Y., DEMERS, K., DIFEO, A., MARTIGNETTI, J. A., BETTS, M. R., FAVIER, R., BANERJEE, P. P. & ORANGE, J. S. 2009. Myosin IIA associates with NK cell lytic granules to enable their interaction with F-actin and function at the immunological synapse. *J Immunol,* 182**,** 6969-6984.

SANDOZ, P. A., KUHNIGK, K., SZABO, E. K., THUNBERG, S., ERIKSON, E., SANDSTROM, N., VERRON, Q., BRECH, A., WATZL, C., WAGNER, A. K., ALICI, E., MALMBERG, K. J., UHLIN, M. & ONFELT, B. 2023. Modulation of lytic molecules restrain serial killing in gammadelta T lymphocytes. *Nat Commun,* 14**,** 1-16.

SHANER, N. C., CAMPBELL, R. E., STEINBACH, P. A., GIEPMANS, B. N., PALMER, A. E. & TSIEN, R. Y. 2004. Improved monomeric red, orange and yellow fluorescent proteins derived from Discosoma sp. red fluorescent protein. *Nat Biotechnol,* 22**,** 1567-1572.

SHI, L., KEEFE, D., DURAND, E., FENG, H., ZHANG, D. & LIEBERMAN, J. 2005. Granzyme B Bind to Target Cells Mostly by Charge and Must Be Added at the Same Time as Perforin to Trigger Apoptosis. *J Immunol,* 174**,** 5456-5461.

SHI, L., MAI, S., ISRAELS, S., BROWNE, K., TRAPANI, J. A. & GREENBERG, A. H. 1997. Granzyme B (GraB) autonomously crosses the cell membrane and perforin initiates apoptosis and GraB nuclear localization. *J Exp Med,* 185**,** 855-866.

SIEGLER, J. J., CORREIA, M. P., HOFMAN, T., PRAGER, I., BIRGIN, E., RAHBARI, N. N., WATZL, C., STOJANOVIC, A. & CERWENKA, A. 2022. Human ILC3 Exert TRAIL-Mediated Cytotoxicity Towards Cancer Cells. *Front Immunol,* 13**,** 1-12.

SPICER, J. A., HUTTUNEN, K. M., JOSE, J., DIMITROV, I., AKHLAGHI, H., SUTTON, V. R., VOSKOBOINIK, I. & TRAPANI, J. 2022. Small Molecule Inhibitors of

Lymphocyte Perforin as Focused Immunosuppressants for Infection and Autoimmunity. *J Med Chem,* 65**,** 14305-14325.

STEWART, S. E., KONDOS, S. C., MATTHEWS, A. Y., D'ANGELO, M. E., DUNSTONE, M. A., WHISSTOCK, J. C., TRAPANI, J. A. & BIRD, P. I. 2014. The perforin pore facilitates the delivery of cationic cargos. *J Biol Chem,* 289**,** 9172-9181.

STRAIGHT, A. F., CHEUNG, A., LIMOUZE, J., CHEN, I., WESTWOOD, N. J., SELLERS, J. R. & MITCHISON, T. J. 2003. Dissecting temporal and spatial control of cytokinesis with a myosin II Inhibitor. *Science,* 299**,** 1743-1747.

SUN, J., BIRD, C. H., SUTTON, V., MCDONALD, L., COUGHLIN, P. B., DE JONG, T. A., TRAPANI, J. A. & BIRD, P. I. 1996. A cytosolic granzyme B inhibitor related to the viral apoptotic regulator cytokine response modifier A is present in cytotoxic lymphocytes. *J Biol Chem,* 271**,** 27802-27809.

SUTTON, V. R., BRENNAN, A. J., ELLIS, S., DANNE, J., THIA, K., JENKINS, M. R., VOSKOBOINIK, I., PEJLER, G., JOHNSTONE, R. W., ANDREWS, D. M. & TRAPANI, J. A. 2016. Serglycin determines secretory granule repertoire and regulates natural killer cell and cytotoxic T lymphocyte cytotoxicity. *FEBS J,* 283**,** 947-961.

SUTTON, V. R., DAVIS, J. E., CANCILLA, M., JOHNSTONE, R. W., RUEFLI, A. A., SEDELIES, K., BROWNE, K. A. & TRAPANI, J. A. 2000. Initiation of apoptosis by granzyme B requires direct cleavage of bid, but not direct granzyme B-mediated caspase activation. *J Exp Med,* 192**,** 1403-1414.

SWAMINATHAN, V., MYTHREYE, K., O'BRIEN, E. T., BERCHUCK, A., BLOBE, G. C. & SUPERFINE, R. 2011. Mechanical stiffness grades metastatic potential in patient tumor cells and in cancer cell lines. *Cancer Res,* 71**,** 5075-5080.

THIERY, J., KEEFE, D., BOULANT, S., BOUCROT, E., WALCH, M., MARTINVALET, D., GOPING, I. S., BLEACKLEY, R. C., KIRCHHAUSEN, T. & LIEBERMAN, J. 2011. Perforin pores in the endosomal membrane trigger the release of endocytosed granzyme B into the cytosol of target cells. *Nat Immunol,* 12**,** 770-777.

THIERY, J., KEEFE, D., SAFFARIAN, S., MARTINVALET, D., WALCH, M., BOUCROT, E., KIRCHHAUSEN, T. & LIEBERMAN, J. 2010. Perforin activates clathrin- and dynamin-dependent endocytosis, which is required for plasma membrane repair and delivery of granzyme B for granzyme-mediated apoptosis. *Blood,* 115**,** 1582-1593.

THORNBERRY, N. A., RANO, T. A., PETERSON, E. P., RASPER, D. M., TIMKEY, T., GARCIA-CALVO, M., HOUTZAGER, V. M., NORDSTROM, P. A., ROY, S., VAILLANCOURT, J. P., CHAPMAN, K. T. & NICHOLSON, D. W. 1997. A combinatorial approach defines specificities of members of the caspase family and granzyme B. Functional relationships established for key mediators of apoptosis. *J Biol Chem,* 272**,** 17907-17911.

TOGO, T., KRASIEVA, T. B. & STEINHARDT, R. A. 2000. A decrease in membrane tension precedes successful cell-membrane repair. *Mol Biol Cell,* 11**,** 4339-4346.

TRAPANI, J. A. 2001. Granzymes: a family of lymphocyte granule serine proteases. *Genome Biol,* 2**,** 1-7.

TRAPANI, J. A., JANS, D. A. & SUTTON, V. R. 1998. Lymphocyte granule-mediated cell death. *Springer Semin Immunopathol,* 19**,** 323-343.

TRAPANI, J. A. & SMYTH, M. J. 2002. Functional significance of the perforin/granzyme cell death pathways. *Nat Rev Immunol,* 2**,** 735-747.

TRAPANI, J. A., SUTTON, V. R., THIA, K. Y. T., LI, Y. Q., FROELICH, C. J., JANS, D. A., SANDRIN, M. S. & BROWNE, K. A. 2003. A clathrin/dynamin- and mannose-6-phosphate receptor-independent pathway for granzyme B-induced cell death. *J Cell Biol,* 160**,** 223-233.

TUOMELA, K., AMBROSE, A. R. & DAVIS, D. M. 2022. Escaping Death: How Cancer Cells and Infected Cells Resist Cell-Mediated Cytotoxicity. *Front Immunol,* 13**,** 1-17.

UELLNER, R., ZVELEBIL, M. J., HOPKINS, J., JONES, J., MACDOUGALL, L. K., MORGAN, B. P., PODACK, E., WATERFIELD, M. D. & GRIFFITHS, G. M. 1997. Perforin is activated by a proteolytic cleavage during biosynthesis which reveals a phospholipid-binding C2 domain. *EMBO J,* 16**,** 7287-7296.

VAN ENGELAND, M., NIELAND, L. J., RAMAEKERS, F. C., SCHUTTE, B. & REUTELINGSPERGER, C. P. 1998. Annexin V-affinity assay: a review on an apoptosis detection system based on phosphatidylserine exposure. *Cytometry,* 31**,** 1-9.

VEUGELERS, K., MOTYKA, B., FRANTZ, C., SHOSTAK, I., SAWCHUK, T. & BLEACKLEY, R. C. 2004. The granzyme B-serglycin complex from cytotoxic granules requires dynamin for endocytosis. *Blood,* 103**,** 3845-3853.

VIVIER, E., TOMASELLO, E., BARATIN, M., WALZER, T. & UGOLINI, S. 2008. Functions of natural killer cells. *Nat Immunol,* 9**,** 503-510.

VOSKOBOINIK, I., SMYTH, M. J. & TRAPANI, J. A. 2006. Perforin-mediated target-cell death and immune homeostasis. *Nat Rev Immunol,* 6**,** 940-952.

VOSKOBOINIK, I., THIA, M. C., FLETCHER, J., CICCONE, A., BROWNE, K., SMYTH, M. J. & TRAPANI, J. A. 2005. Calcium-dependent plasma membrane binding and cell lysis by perforin are mediated through its C2 domain: A critical role for aspartate residues 429, 435, 483, and 485 but not 491. *J Biol Chem,* 280**,** 8426-8434.

VOSKOBOINIK, I. & TRAPANI, J. A. 2013. Perforinopathy: a spectrum of human immune disease caused by defective perforin delivery or function. *Front Immunol,* 4**,** 1-7.

VOSKOBOINIK, I., WHISSTOCK, J. C. & TRAPANI, J. A. 2015. Perforin and granzymes: function, dysfunction and human pathology. *Nat Rev Immunol,* 15**,** 388-400.

VRAZO, A. C., HONTZ, A. E., FIGUEIRA, S. K., BUTLER, B. L., FERRELL, J. M., BINKOWSKI, B. F., LI, J. & RISMA, K. A. 2015. Live cell evaluation of granzyme

delivery and death receptor signaling in tumor cells targeted by human natural killer cells. *Blood,* 126**,** 1-10.

WALZER, T., DALOD, M., ROBBINS, S. H., ZITVOGEL, L. & VIVIER, E. 2005. Natural-killer cells and dendritic cells: "l'union fait la force". *Blood,* 106**,** 2252-2258.

WATERHOUSE, N. J., SEDELIES, K. A., BROWNE, K. A., WOWK, M. E., NEWBOLD, A., SUTTON, V. R., CLARKE, C. J., OLIARO, J., LINDEMANN, R. K., BIRD, P. I., JOHNSTONE, R. W. & TRAPANI, J. A. 2005. A central role for Bid in granzyme B-induced apoptosis. *J Biol Chem,* 280**,** 4476-4482.

WATZL, C. 2003. The NKG2D receptor and its ligands-recognition beyond the "missing self"? *Microbes Infect,* 5**,** 31-37.

WATZL, C. 2014. How to trigger a killer: modulation of natural killer cell reactivity on many levels. *Adv Immunol,* 124**,** 137-170.

WATZL, C. & LONG, E. O. 2010. Signal transduction during activation and inhibition of natural killer cells. *Curr Protoc Immunol,* Chapter 11**,** 1-17.

WESTERMANN, J. & PABST, R. 1992. Distribution of lymphocyte subsets and natural killer cells in the human body. *Clin Investig,* 70**,** 539-544.

WILEY, S. E., MURPHY, A. N., ROSS, S. A., VAN DER GEER, P. & DIXON, J. E. 2007. MitoNEET is an iron-containing outer mitochondrial membrane protein that regulates oxidative capacity. *Proc Natl Acad Sci U S A,* 104**,** 5318-5323.

YANAMANDRA, A. K., ZHANG, J., MONTALVO, G., ZHOU, X., BIEDENWEG, D., ZHAO, R., SHARMA, S., HOTH, M., LAUTENSCHLAGER, F., OTTO, O., DEL CAMPO, A. & QU, B. 2024. PIEZO1-mediated mechanosensing governs NK-cell killing efficiency and infiltration in three-dimensional matrices. *Eur J Immunol,* 54**,** 1-11.

ZACHARIAS, D. A., VIOLIN, J. D., NEWTON, A. C. & TSIEN, R. Y. 2002. Partitioning of lipid-modified monomeric GFPs into membrane microdomains of live cells. *Science,* 296**,** 913-916.

ZHOU, Y., WANG, D., ZHOU, L., ZHOU, N., WANG, Z., CHEN, J., PANG, R., FU, H., HUANG, Q., DONG, F., CHENG, H., ZHANG, H., TANG, K., MA, J., LV, J., CHENG, T., FISKESUND, R., ZHANG, X. & HUANG, B. 2024. Cell softness renders cytotoxic T lymphocytes and T leukemic cells resistant to perforin-mediated killing. *Nat Commun,* 15**,** 1-16.

ZHU, Y., HUANG, B. & SHI, J. 2016. Fas ligand and lytic granule differentially control cytotoxic dynamics of natural killer cell against cancer target. *Oncotarget,* 7**,** 47163-47172.

7. Abbreviations

2-ME	2-Mercaptoethanol
7-AAD	7-amino-actinomycin D
ADCC	antibody-dependent cellular cytotoxicity
AF	Alexa Fluor
AUC	area under curve
AVBB	Annexin V binding buffer
BC	buffy coat
BID	BH3 interacting-domain death agonist
BSA	bovine serum albumin
BV	Brilliant Violet
Casp	caspase
CLF	crude lysosomal fraction
CLSM	confocal laser scanning microscopy
CMA	concanamycin A
CMH	Cochran-Mantel-Haenszel
CTL	cytotoxic T lymphocyte
DAPI	4,6-diamidino-2-phenylindole
DISC	death inducing signaling complex
DMSO	dimethyl sulfoxide
DNA-PKcs	DNA-dependent protein kinase catalytic subunit
DR	death receptor
E:T	Effector:Target (effector to target cell ratio)
ECM	extracellular matrix
EE	early endosome
EEA1	early endosome antigen 1
EGF	epidermal growth factor
EGFP	enhanced GFP
ER	endoplasmic reticulum
F-actin	filamentous actin
FA	formaldehyde
FACS	fluorescence activated cell sorting
FADD	Fas-associated death domain
FCS	fetal calf serum
FITC	fluorescein isothiocyanate
FHL	familial hemophagocytic lymphohistiocytosis
FLR	fluorescent localization reporter
FRET	Förster resonance energy transfer
G418	geneticin
GFP	green fluorescent protein
GM130	130 kDa cis-Golgi matrix protein 1
GM-CSF	granulocyte-macrophage colony-stimulating factor
gMFI	geometric mean fluorescence intensity
Grz	granzyme
GrzB	granzyme B
HRP	horseradish peroxidase
IFN	interferon
IL	interleukin
ILC3	type 3 innate lymphoid cells
IS	immune synapse
kDa	kilodalton
KO	knockout

LAMP1	lysosome-associated membrane protein 1 (CD107a)
LFA-1	lymphocyte function-associated antigen 1
LSM	lymphocyte separation medium
M6P	mannose-6-Phosphate
MACPF/CDC	membrane attack complex perforin-like/cholesterol-dependent cytolysins
mC	mCherry (modified variant of red fluorescent protein)
mGFP	monomeric GFP
MHC	major histocompatibility complex
Mito	mitochondria
MPR/ CI MPR	mannose-6-Phosphate receptor/ cation-independent MPR
MTOC	microtubule organizing center
NES	nuclear export sequence
NEAA	non-essential amino acid
NK (cell)	natural killer (cell)
non-cl.	non-cleavable
NuMa	nuclear mitotic apparatus protein 1
P-S	penicillin-streptomycin
PARP-1	poly(ADP-ribose) polymerase 1
PBMCs	peripheral blood mononuclear cells
PDI	protein disulfide-isomerase
PFA	paraformaldehyde
PI	propidium iodide
PM	plasma membrane
PMSF	phenylmethylsulfonyl fluoride
PVDF	polyvinylidene fluoride
Rab27a	Ras-related protein Rab27a
RFI	relative fluorescence intensity
RM	repeated measures
ROI	region of interest
RSB	reducing sample buffer
rt	room temperature
RTCA	real-time cell analysis
SD	standard deviation
SDS	sodium dodecyl sulfate
SNARE	soluble N-ethylmaleimide sensitive attachment protein receptor
T2A	thosea asigna virus 2A
TOD	time of death
TNF	tumor necrosis
WB	western blot
WL	whole lysate
wt	wild type

Definitions

GrzB reporter	tandem FLR for GrzB activity
Single reporter part	FLR (general description) or PM/ER/Mito/EE reporter

8. Supplement

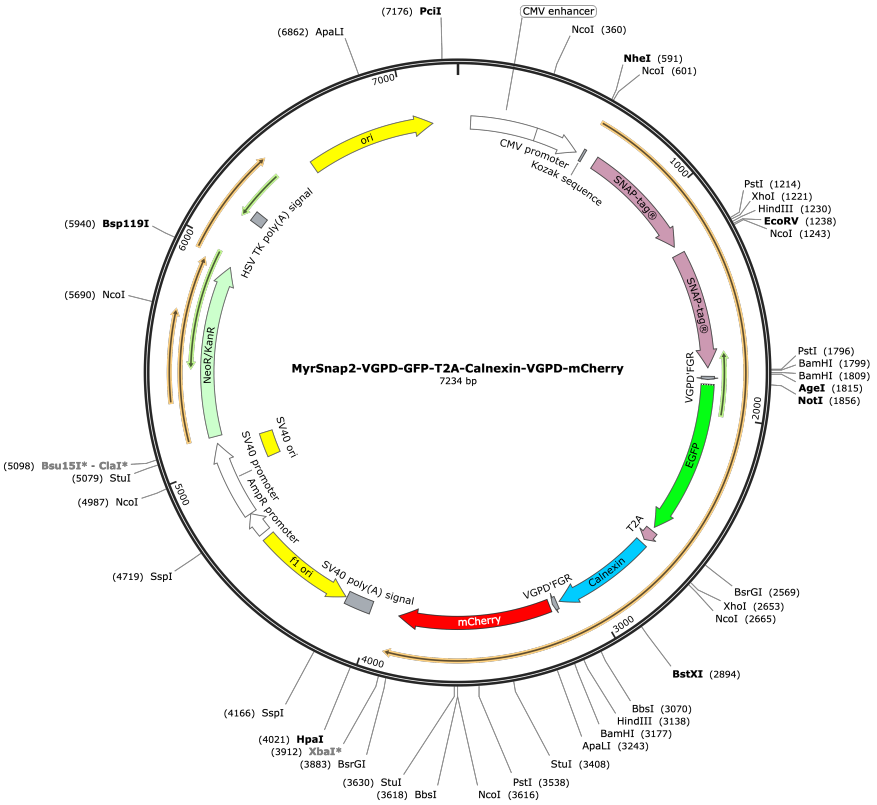

Figure S1: Vector map of the MyrSnap2-VGPD'FGR-mGFP-T2A-Calnexin-VGPD'FGR-mCherry construct (pEGFP backbone). This construct was transfected into HeLa CD48$^+$ cells to generate HeLa CD48$^+$ PM^{mGFP}ER^{mC} GrzB$^+$ reporter cells. For information on individual sequences of the GrzB reporter refer to chapter 3.1.5.

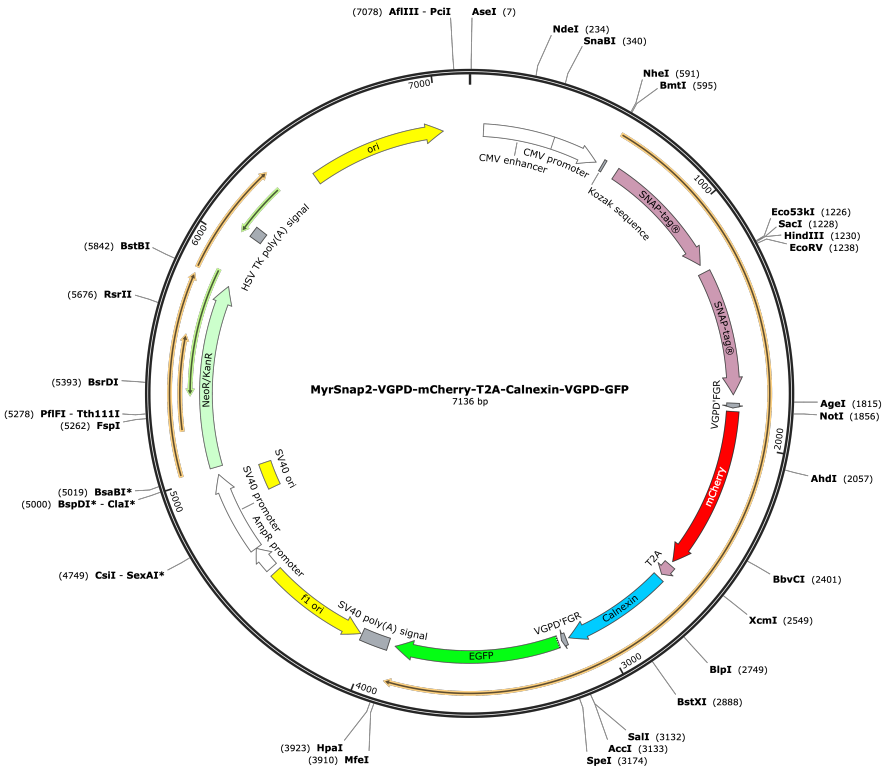

Figure S2: Vector map of the MyrSnap2-VGPD'FGR-mCherry-T2A-Calnexin-VGPD'FGR-mGFP construct (pEGFP backbone). This construct was transfected into HeLa CD48$^+$ cells to generate HeLa CD48$^+$ PM^{mC}ER^{mGFP} GrzB$^+$ reporter cells. For information on individual sequences of the GrzB reporter refer to chapter 3.1.5.

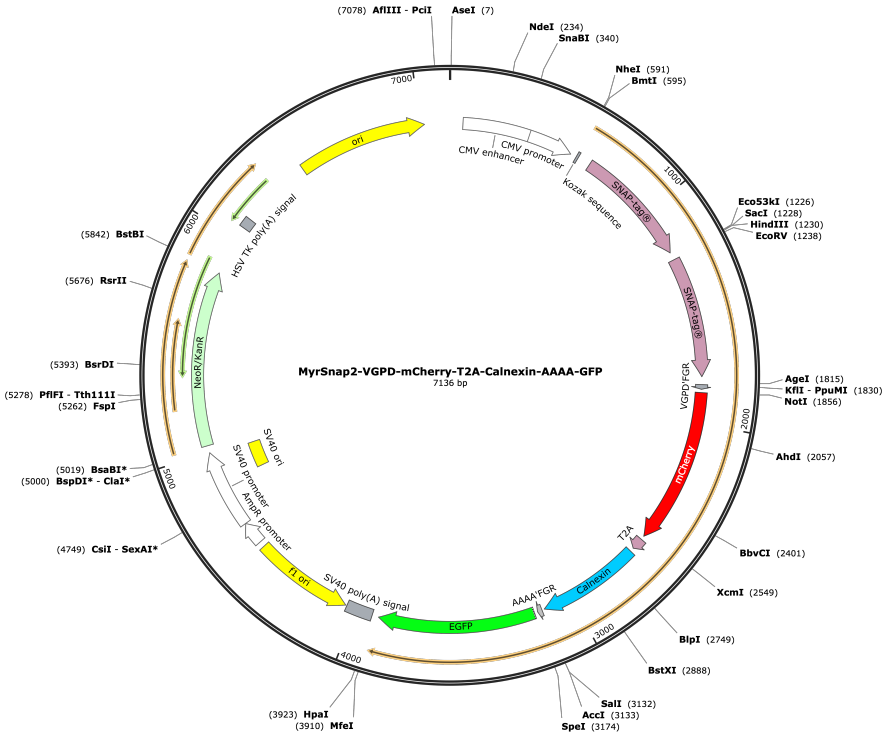

Figure S3: Vector map of the MyrSnap2-VGPD'FGR-mCherry-T2A-Calnexin-AAAA'FGR-mGFP construct (pEGFP backbone). This construct was transfected into HeLa CD48^{+} cells to generate HeLa CD48^{+} PM^{mC}ER$^{mGFP,\ non\text{-}cl.}$ GrzB^{+} reporter cells. For information on individual sequences of the GrzB reporter refer to chapter 3.1.5.

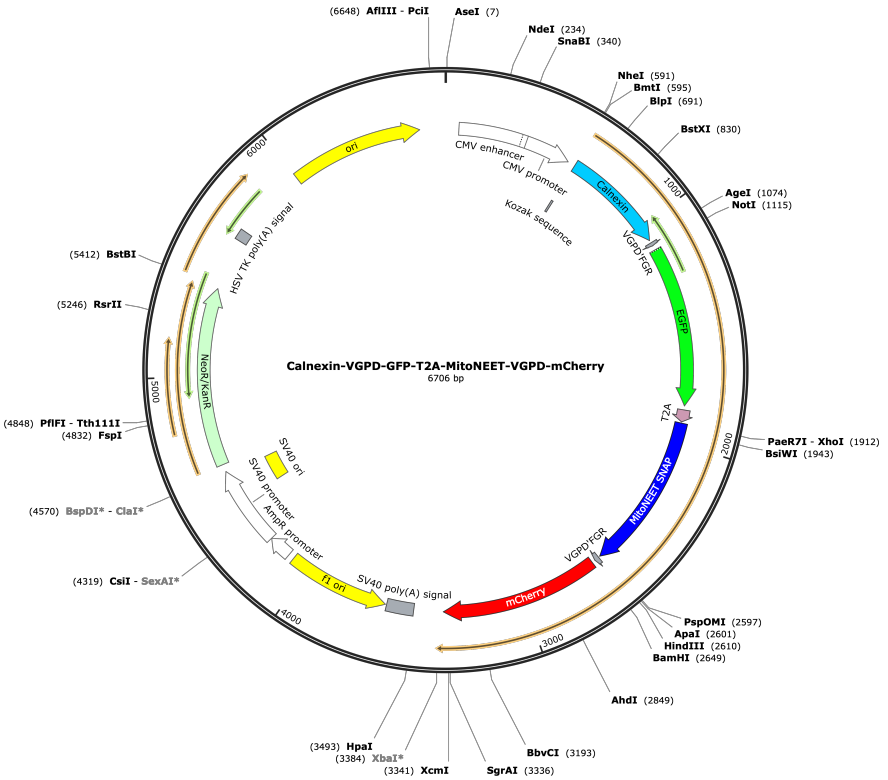

Figure S4: Vector map of the Calnexin-VGPD'FGR-mGFP-T2A-MitoNEET-VGPD'FGR-mCherry construct (pEGFP backbone). This construct was transfected into HeLa CD48^{+} cells to generate HeLa CD48^{+} ER^{mGFP}Mito^{mC} GrzB^{+} reporter cells. For information on individual sequences of the GrzB reporter refer to chapter 3.1.5.

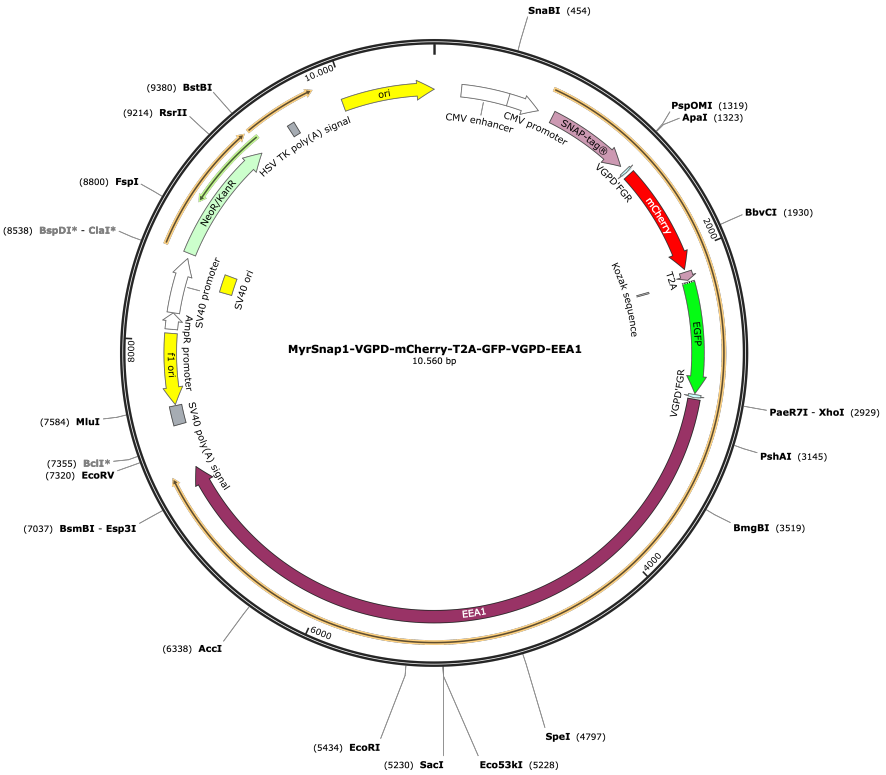

Figure S5: Vector map of the MyrSnap1-VGPD'FGR-mCherry-T2A-mGFP-VGPD'FGR-EEA1 construct (pEGFP backbone). This construct was transfected into HeLa CD48^{+} cells to generate HeLa CD48^{+} PM^{mC}EE^{mGFP} GrzB^{+} reporter cells. For information on individual sequences of the GrzB reporter refer to chapter 3.1.5.

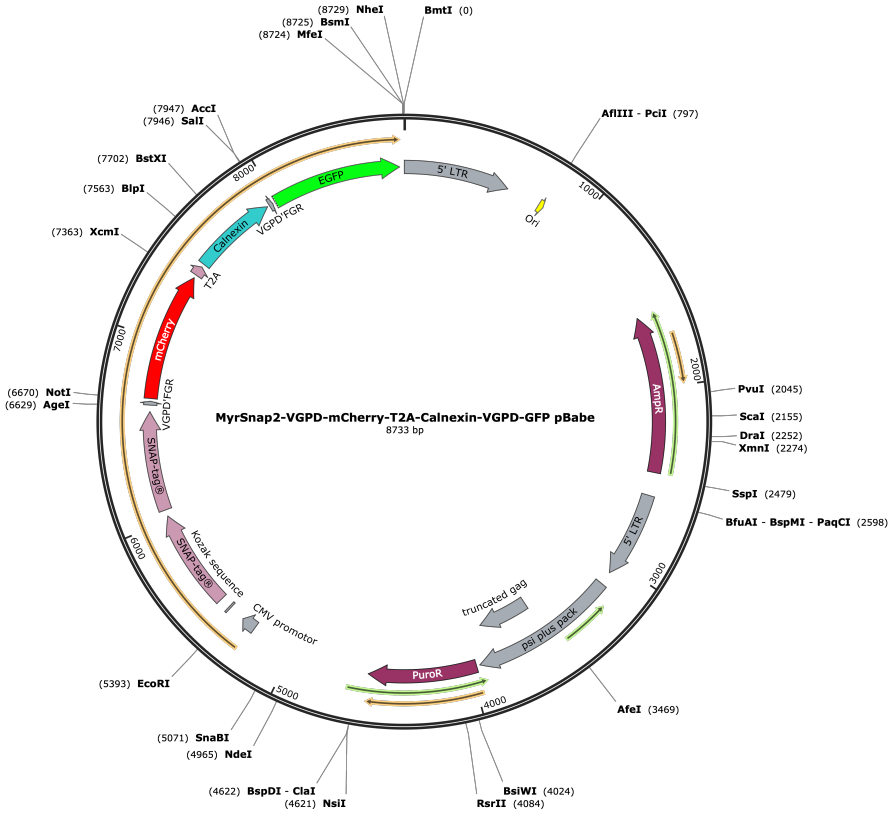

Figure S6: Vector map of the MyrSnap2-VGPD'FGR-mCherry-T2A-Calnexin-VGPD'FGR-mGFP construct (pBabe backbone). This construct was transfected into Phoenix-AMPHO to generate construct containing retroviruses. K562 and MDA-MB #468 cells where transduced with those viruses to generate K562 PM^{mC}ER^{mGFP} GrzB^{+} reporter and MDA-MB #468 PM^{mC}ER^{mGFP} GrzB^{+} reporter cells. For information on individual sequences of the GrzB reporter refer to chapter 3.1.5.

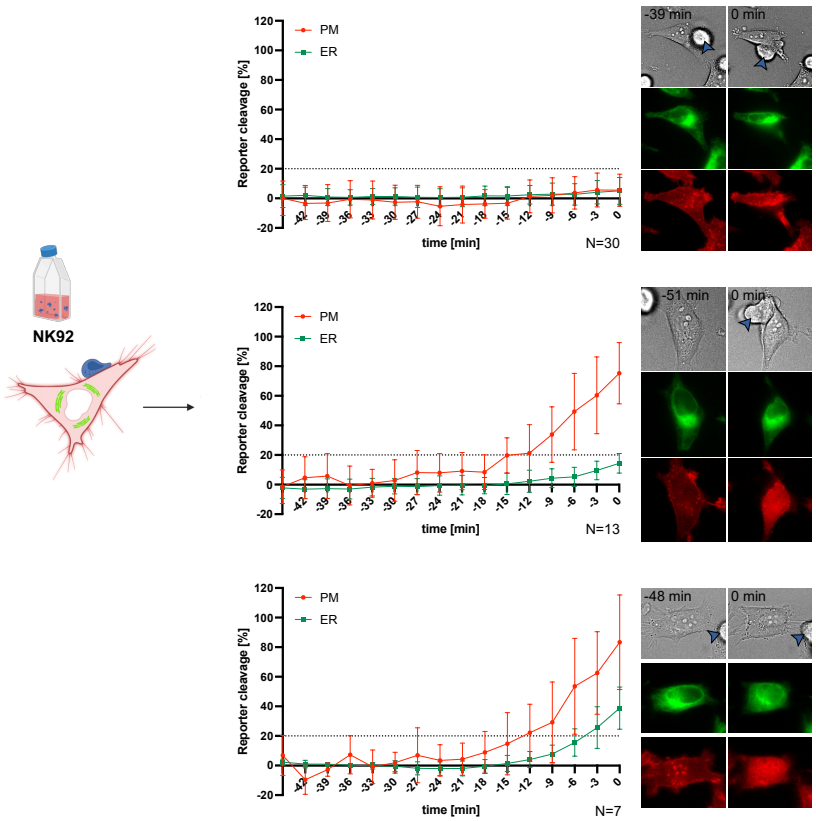

Figure S7: The ER^{mGFP} reporter is better in detecting GrzB activity at the ER, but GrzB activity still predominates at the PM. NK92 cells were co-cultured with HeLa CD48^{+} PM^{mC}ER^{mGFP} GrzB reporter cells (E:T ratio of 1:1) for 5 h during live cell imaging. Three different reporter cleavage outcomes were observed: no reporter cleavage (outcome 1; top row), only PM reporter cleavage (outcome 2; middle row) or cleavage of both FLRs with dominant PM reporter cleavage (outcome 3; bottom row). Quantification of reporter cleavage (left panel). Representative snapshots show the reporter distribution of the intact reporter state and at 0 min (TOD). PM reporter = red, ER reporter = green Brightfield images show GrzB reporter cells and pre-activated NK cells (blue arrows). Data include 7 independent experiments with N = 50 cells in total (N = 3 – 14 cells per experiment) and are shown as Mean ± SD. Images were acquired using the Axio Observer 7, 40 x magnification.

Table S1: PM and ER reporter cleavage (mean at TOD, 0 min) from results of figure S7.

	PM reporter cleavage (mean at TOD)	ER reporter cleavage (mean at TOD)
Outcome 1 (no reporter cleavage)	5.5 %	5.1 %
Outcome 2 (only PM reporter cleavage)	75.3 %	14.4 %
Outcome 3 (cleavage of both FLRs)	83.4 %	38.8 %

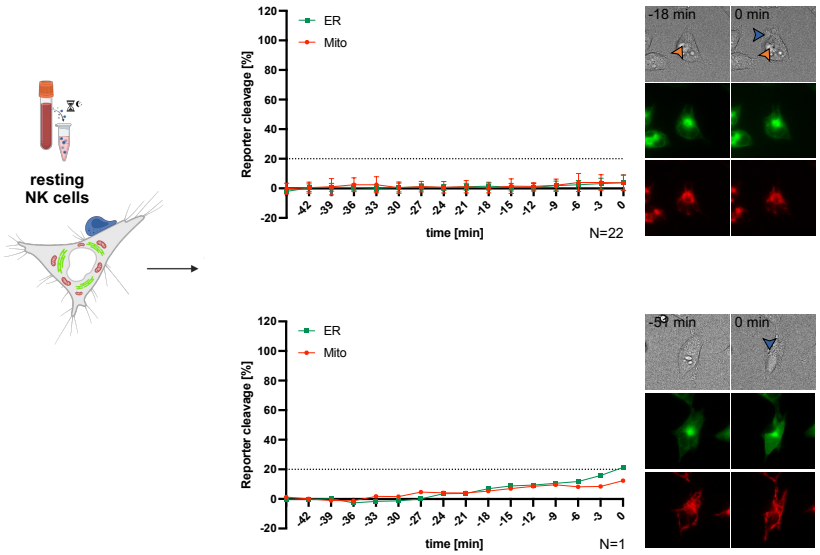

Figure S8: Limited diffusion of resting NK cell derived GrzB from the PM into the cell. Freshly isolated NK cells (isolated from whole blood) were rested overnight with low dose IL-15 (0.5 ng/ml) and then co-cultured with HeLa CD48^{+} ER^{mGFP}Mito^{mC} GrzB reporter cells (E:T ratio of 1:1) for 3 h during live cell imaging. Two reporter cleavage outcomes were observed: no reporter cleavage (outcome 1; top row) or only cleavage of the ER reporter (outcome 2; bottom row). Quantification of reporter cleavage (left panel). Representative snapshots show the reporter distribution at the intact reporter state and at 0 min (TOD). ER reporter = green, Mito reporter = red. Brightfield images show GrzB reporter cells and resting NK cells (blue arrows); orange arrows = cell debris/other non-NK cell particles (right panel). Data include 4 independent experiments (n = 4 donors, N = 23 cells with N = 3 – 11 cells per experiment) and are shown as Mean ± SD. Images were acquired using the Axio Observer 7, 40 x magnification.

Table S2: ER and Mito reporter cleavage (mean at TOD, 0 min) from results of figure S8.

	ER reporter cleavage (mean at TOD)	Mito reporter cleavage (mean at TOD)
Outcome 1 (no reporter cleavage)	3.8 %	3.7 %
Outcome 2 (only ER reporter cleavage)	21.4 %	12.4 %

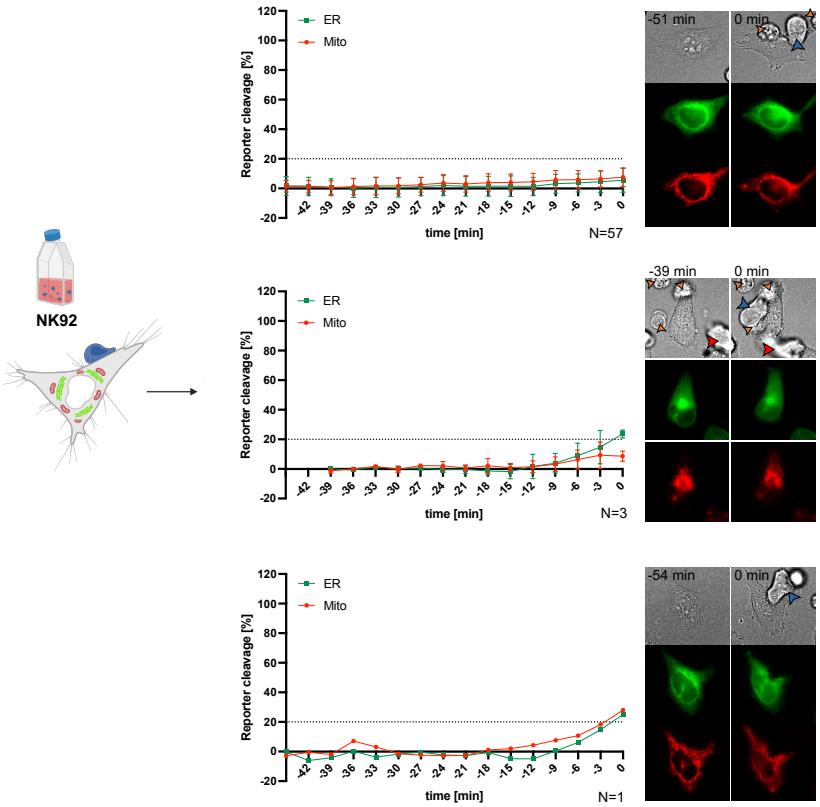

Figure S9: Limited diffusion of NK92 cell derived GrzB from the PM into the cell. NK92 cells were co-cultured with HeLa CD48^{+} ER^{mGFP}Mito^{mC} GrzB reporter cells (E:T ratio of 1:1) for 5 h during live cell imaging. Three different reporter cleavage outcomes were observed: no reporter cleavage (outcome 1; top row), only ER reporter cleavage (outcome 2; middle row) or cleavage of both FLRs (bottom row). Quantification of reporter cleavage (outcome 3; left panel). Representative snapshots show the reporter distribution of the intact reporter state and at 0 min (TOD). ER reporter = green, Mito reporter = red. Brightfield images show GrzB reporter cells and resting NK cells (blue arrows); orange arrows = cell debris/other non-NK cell particles; red arrows = NK92 cell in proximity of the killed GrzB reporter cell but do not contribute to the kill (right panel). Data include 5 independent experiments with N = 61 cells in total (N = 5 – 16 cells per experiment) and are shown as Mean ± SD. Images were acquired using the Axio Observer 7, 40 x magnification.

Table S3: ER and Mito reporter cleavage (mean at TOD, 0 min) from results of figure S9.

	ER reporter cleavage (mean at TOD)	Mito reporter cleavage (mean at TOD)
Outcome 1 (no reporter cleavage)	5.5 %	7.6 %
Outcome 2 (only ER reporter cleavage)	23.7 %	8.6 %
Outcome 3 (cleavage of both FLRs)	25.1 %	28.0 %

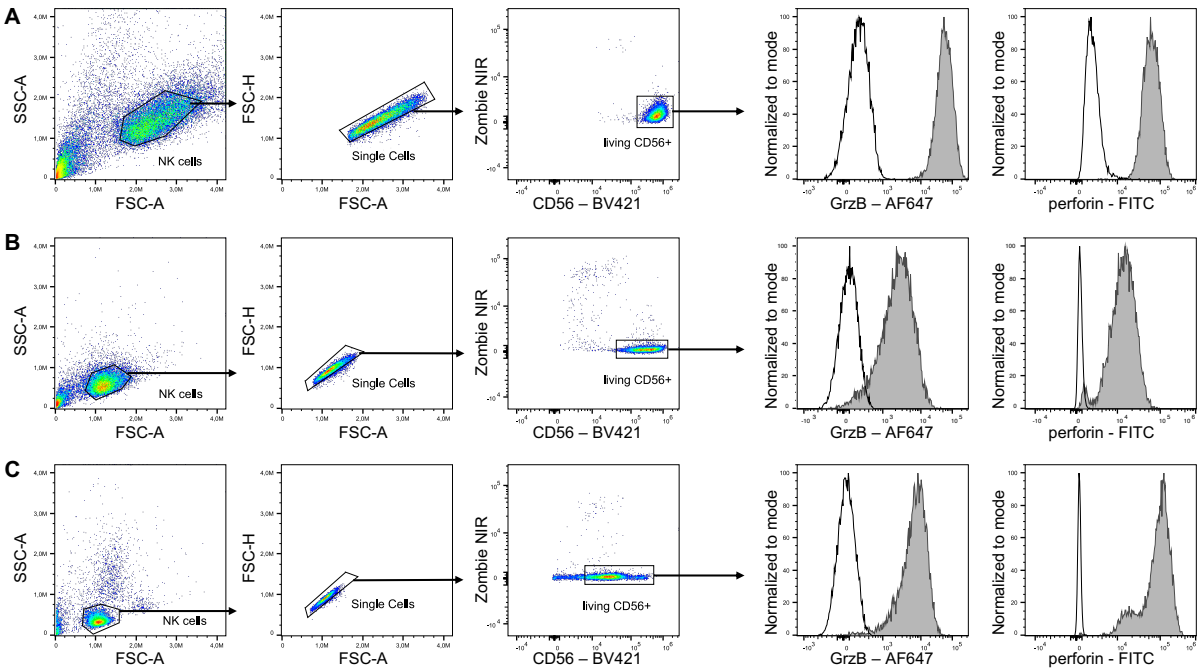

Figure S10: Gating strategy for flow cytometric analysis of GrzB and perforin levels in NK cells. First, it was gated on the NK cell population followed by single cell gating. From the single cell gate, a gate was drawn around the living CD56$^+$ cell population (Zombie NIR$^-$, CD56 – BV421$^+$). The GrzB and perforin levels of living CD56$^+$ NK cells were plotted as normalized histograms (normalized to mode) along with with an unstained control. **A** NK92 cells, **B** pre-activated NK cells, **C** resting NK cells.

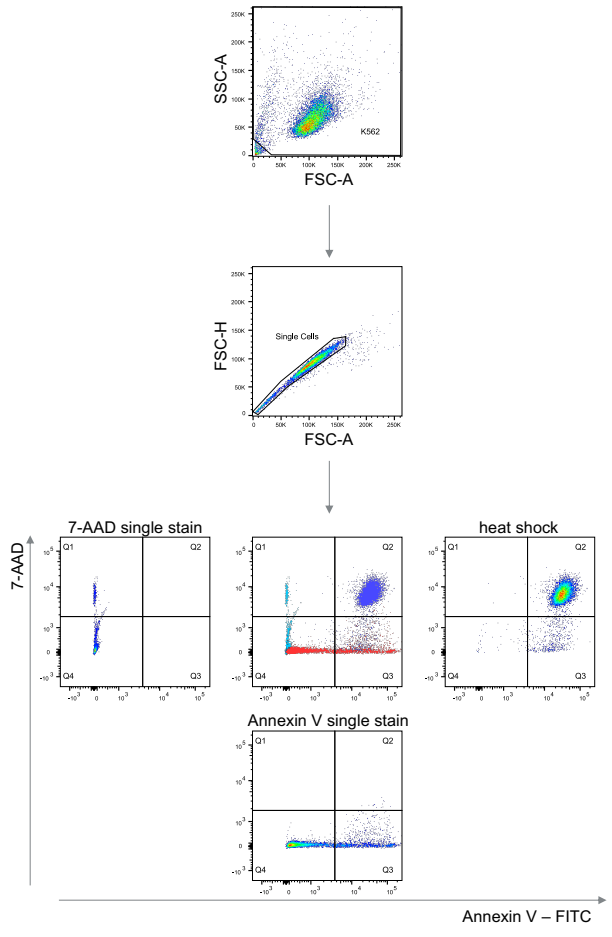

Figure S11: Gating strategy for flow cytometric analysis of lytic capacity of isolated granules.
The first gate includes all events except the smallest, followed by single cell gating. 7-AAD and Annexin V – FITC single stains of living K562 as well as heat shocked K562 (5 min, 70 °C) were used to define living, early apoptotic (Annexin V – FITC positive) and late apoptotic/necrotic cell populations (Annexin V – FITC and 7-AAD positive).

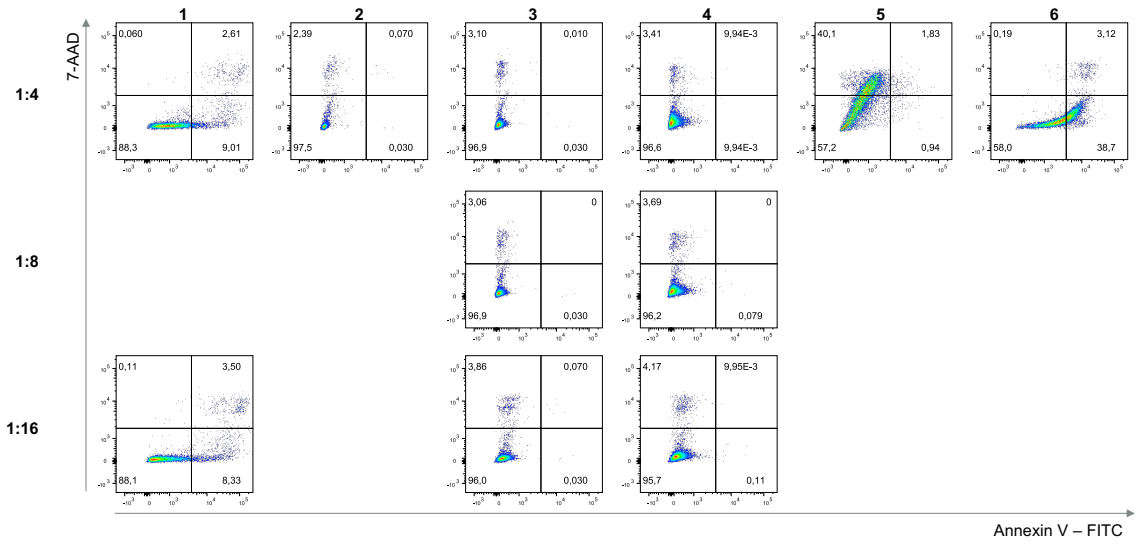

Figure S12: NKL derived lytic granules were isolated successfully, yet analysis of functionality led to inconclusive results. K562 CD48$^+$ were treated with HB buffer (solvent control) or NKL cell derived lytic granules from fractions 1 – 6 (dilution 1:4, 1:8, 1:16 (1:2 and 1:32 are shown in figure 21**C**)) for 2 h. Dot plots of late apoptotic/necrotic (7-AAD$^+$) and early apoptotic (Annexin V$^+$) flow cytometry staining. Fractions 1 – 6 (left to right) with 1:4 dilution of lytic granules (top row), 1:8 dilution (middle row) and 1:32 dilution (bottom row).

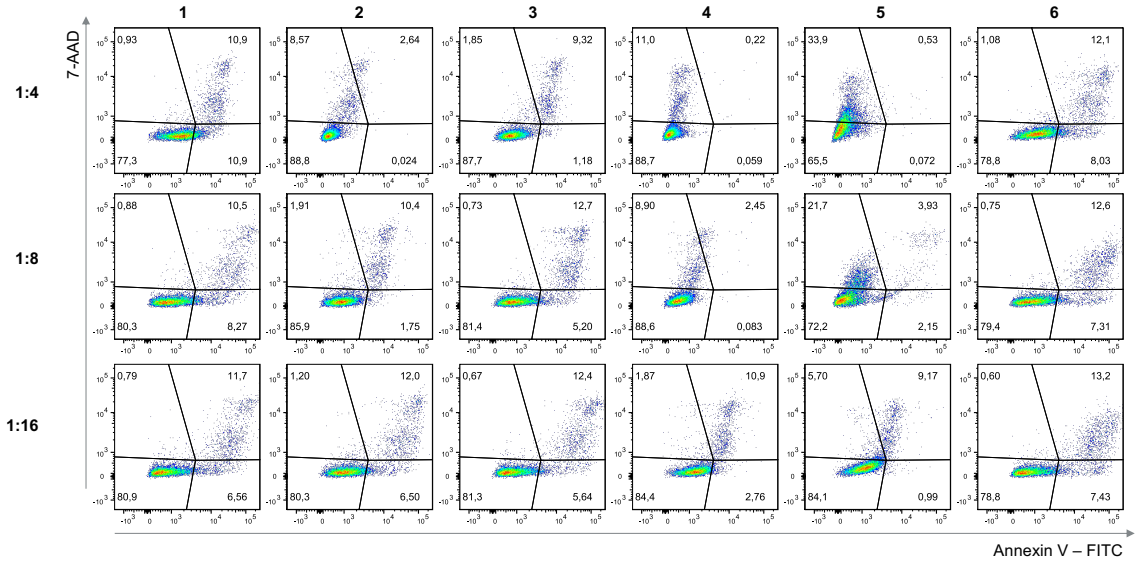

Figure S13: Pre-activated NK cell derived lytic granules demonstrate inconclusive results regarding functionality. K562 CD48$^+$ were treated with HB buffer (solvent control) or pre-activated NK cell derived lytic granules from fractions 1 – 6 (dilution 1:4, 1:8, 1:16 (1:2 and 1:32 are shown in figure 22**C**)) for 2 h. Dot plots of late apoptotic/necrotic (7-AAD$^+$) and early apoptotic (Annexin V$^+$) flow cytometry staining. Fractions 1 – 6 (left to right) with 1:4 dilution of lytic granules (top row), 1:8 dilution (middle row) and 1:32 dilution (bottom row).

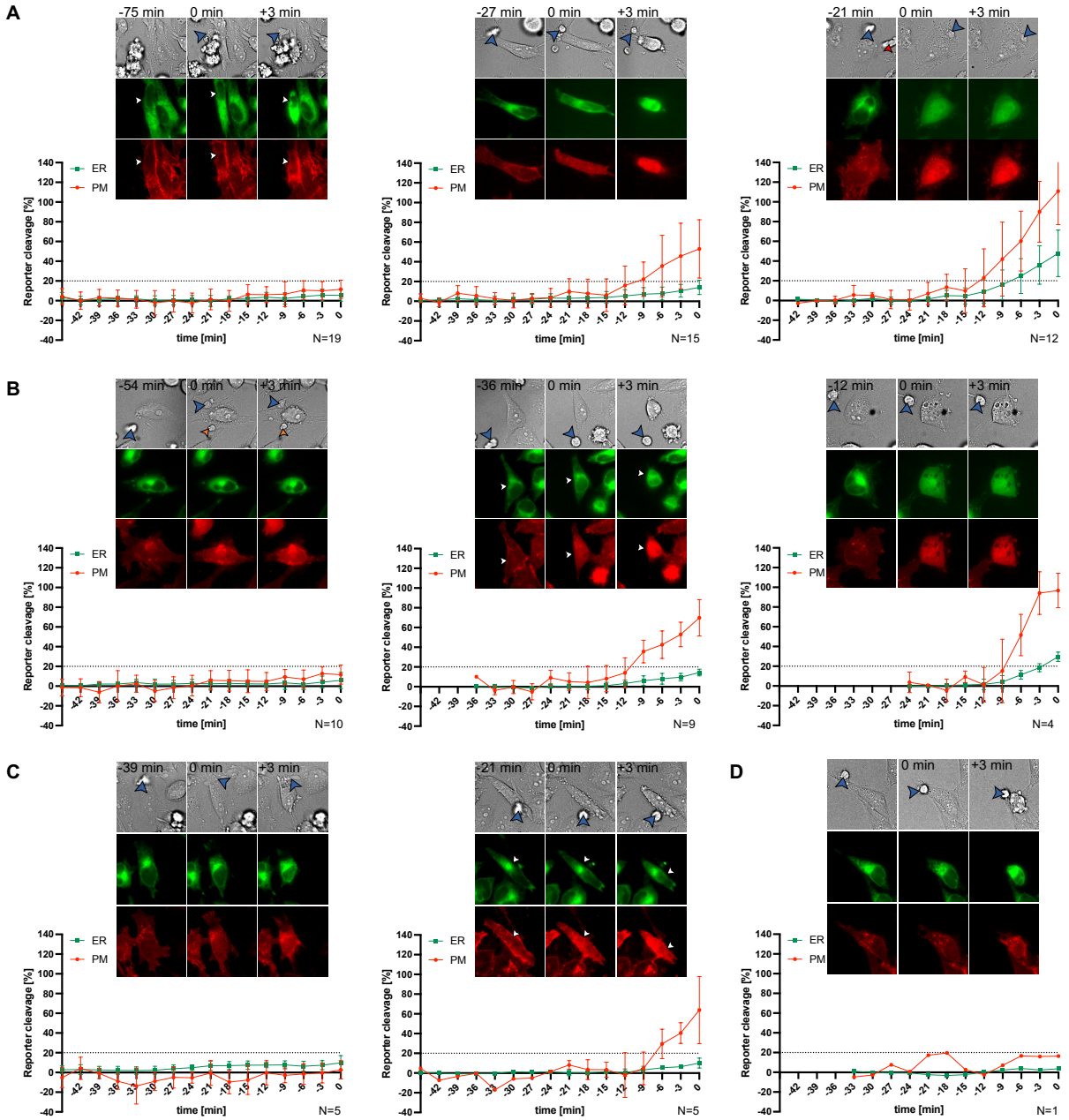

Figure S14: Pre-activated NK cells with less active perforin still induced GrzB activity predominantly at the PM. Pre-activated NK cells (isolated from whole blood and cultured for 3 – 4 weeks) were treated with DMSO (0.02 %; solvent control; 180 min; **A**) or CMA (50 nM) for 30 min (**B**), 60 min (**C**) and 180 min (**D**). Then, differently treated pre-activated NK cells were co-cultured with HeLa CD48^{+} PM^{mC}ER^{mGFP} GrzB reporter cells (E:T ratio of 1:1) for 3 h during live cell imaging. **A – D** Quantification of reporter cleavage display up to three different reporter cleavage outcomes: no reporter cleavage (outcome 1; **A – C** (left), **D**), only PM reporter cleavage (outcome 2; **A**, **B** (middle) and **C** (right)) or cleavage of both FLRs (outcome 3; **A, B** (right)). Representative snapshots show the reporter distribution of the intact reporter state, at 0 min (TOD) and 3 min after TOD. ER reporter = green, PM reporter = red. Brightfield images show GrzB reporter cells and treated pre-activated NK cells (blue arrows); orange arrows = cell debris/other non-NK cell particles; red arrows = pre-activated NK cell in proximity of the killed GrzB reporter cell but do not contribute to the kill. Data include 5 independent experiments with **A** N = 46 cells (N = 6 – 18 cells per experiment), **B** N = 23 cells (N = 2 – 7 cells per experiment), **C** N = 10 cells (N = 0 – 4 cells per experiment), **D** N = 1 cell. Data are shown as Mean ± SD. Images were acquired using the Axio Observer 7, 40 x magnification.

Table S4: PM and ER reporter cleavage (mean at TOD, 0 min) from results of figure S14.

DMSO (**A**)	PM reporter cleavage (mean at TOD)	ER reporter cleavage (mean at TOD)
Outcome 1 (no reporter cleavage)	11.5 %	5.4 %
Outcome 2 (only PM reporter cleavage)	53.1 %	14.0 %
Outcome 3 (cleavage of both FLRs, PM dominant)	110.8 %	47.9 %

CMA (30 min) (**B**)	PM reporter cleavage (mean at TOD)	ER reporter cleavage (mean at TOD)
Outcome 1 (no reporter cleavage)	11.7 %	5.8 %
Outcome 2 (only PM reporter cleavage)	69.8 %	14.4 %
Outcome 3 (cleavage of both FLRs, PM dominant)	96.8 %	29.6 %

CMA (60 min) (**C**)	PM reporter cleavage (mean at TOD)	ER reporter cleavage (mean at TOD)
Outcome 1 (no reporter cleavage)	2.7 %	9.8 %
Outcome 2 (only PM reporter cleavage)	63.9 %	10.1 %

CMA (180 min) (**D**)	PM reporter cleavage (mean at TOD)	ER reporter cleavage (mean at TOD)
Outcome 1 (no reporter cleavage)	16.4 %	3.6 %

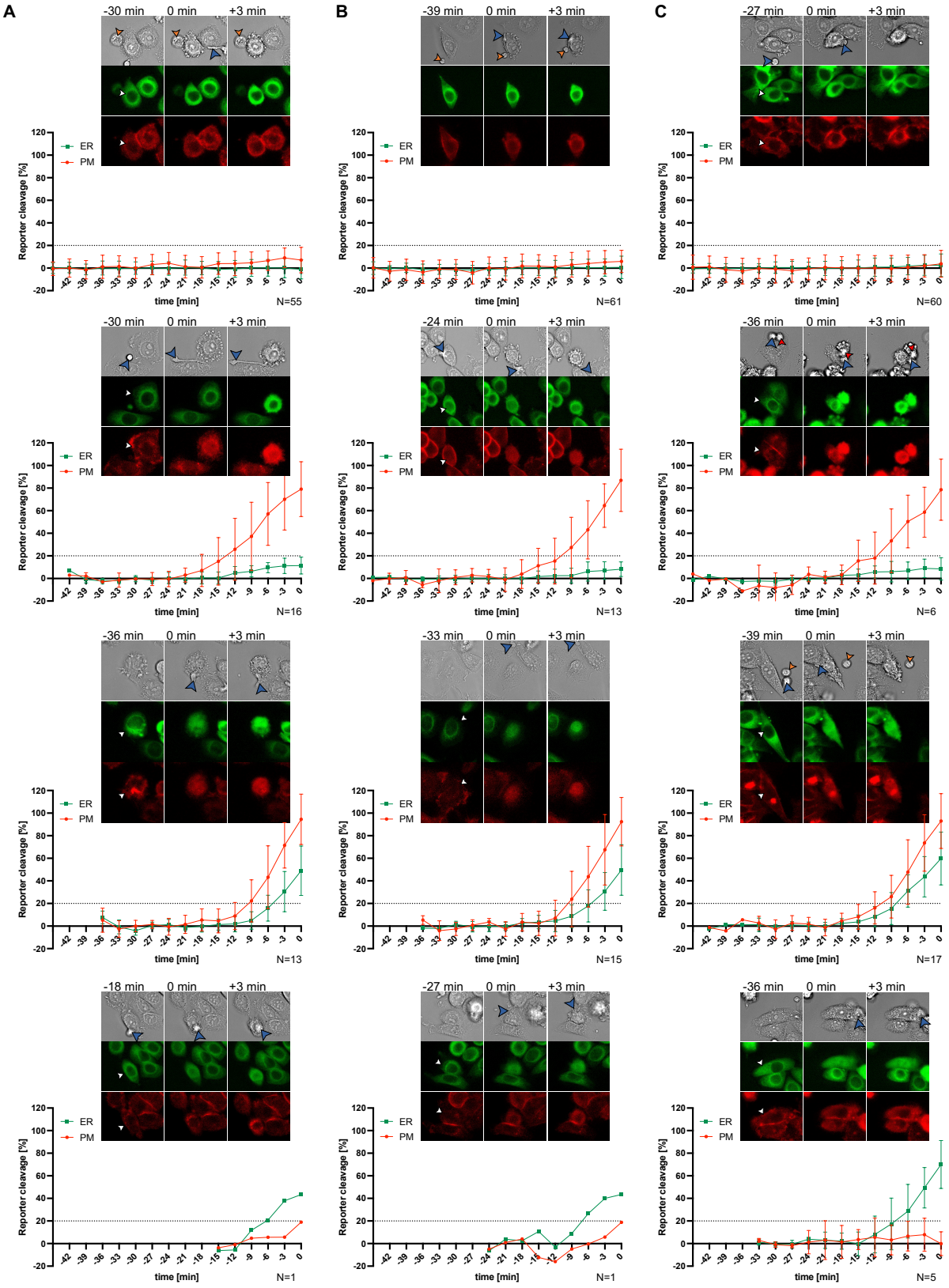
A
B
C
-30 min
0 min
+3 min
-39 min
-27 min
-24 min
-36 min
-33 min
-18 min
ER
PM
Reporter cleavage [%]
time [min]
N=55
N=61
N=60
N=16
N=13
N=6
N=13
N=15
N=17
N=1
N=1
N=5

Figure S15: (S)-4'-nitro-Blebbistatin treatment induced 4 outcomes with a tendency towards more events with a GrzB activity at the ER. MDA-MB #468 $PM^{mC}ER^{mGFP}$ GrzB reporter cells were pretreated with **A** DMSO, **B** medium or **C** 50 µM (S)-4'-nitro-Blebbistatin for 12 h in collagen coated slides. After 12 h, DMSO or (S)-4'-nitro-Blebbistatin were washed out and pre-activated NK cells (isolated from whole blood and cultured for 3 – 4 weeks; E:T of 1:2) were added (after additional 12 h) for 4 h during live cell imaging. **A – C** Quantification of reporter cleavage display four different reporter cleavage outcomes (from top to bottom): no reporter cleavage (outcome 1), only PM reporter cleavage (outcome 2), cleavage of both FLRs with dominant PM reporter cleavage (outcome 3) and dominant ER reporter cleavage (outcome 4). Quantification of reporter cleavage (left panel). Representative snapshots show the reporter distribution at the intact reporter state and at 0 min (TOD) and 3 min after TOD. ER reporter = green, PM reporter = red. Reporter cell of interest is marked by a white arrow. Brightfield images show GrzB reporter cells and pre-activated NK cells (blue arrows). orange arrows = cell debris/other non-NK cell particles; red arrows = pre-activated NK cell in proximity of the killed GrzB reporter cell but do not contribute to the kill. Data include 2 independent experiments (n = 4 donors in total, 2 per experiment) with **A** N = 85 cells in total (N = 11 – 33 cells per donor), **B** N = 90 cells in total (N = 13 – 31 cells per donor) and **C** N = 88 cells in total (N = 12 – 31 cells per donor) and are shown as Mean ± SD. Images were acquired using the MICA WideFocal, 40 x magnification.

Table S5: PM and ER reporter cleavage (mean at TOD, 0 min) from results of figure S15.

DMSO (**A**)	PM reporter cleavage (mean at TOD)	ER reporter cleavage (mean at TOD)
Outcome 1 (no reporter cleavage)	7.13 %	-1.13 %
Outcome 2 (only PM reporter cleavage)	79.08 %	11.39 %
Outcome 3 (cleavage of both FLRs, PM dominant)	94.53 %	49.02 %
Outcome 4 (cleavage of ER FLR dominant)	18.97 %	43.35 %

Medium (**B**)	PM reporter cleavage (mean at TOD)	ER reporter cleavage (mean at TOD)
Outcome 1 (no reporter cleavage)	5.94 %	0.65 %
Outcome 2 (only PM reporter cleavage)	86.85 %	8.19 %
Outcome 3 (cleavage of both FLRs, PM dominant)	92.38 %	49.66 %
Outcome 4 (cleavage of ER FLR dominant)	18.84 %	43.45 %

(S)-4'-nitro-Blebbistatin (**C**)	PM reporter cleavage (mean at TOD)	ER reporter cleavage (mean at TOD)
Outcome 1 (no reporter cleavage)	3.78 %	2.49 %
Outcome 2 (only PM reporter cleavage)	78.61 %	8.41 %
Outcome 3 (cleavage of both FLRs, PM dominant)	92.98 %	59.82 %
Outcome 4 (cleavage of ER FLR dominant)	-0.10 %	70.03 %